

# Design of Broadband Microwave Absorbers using Carbonyl Iron Filled Silicon Rubber Sheets in the Frequency Range of 1 to 8.2 GHz

by

**RAHUL VASHISTH**  
**201421006**

A Thesis Submitted in Partial Fulfilment of the Requirements for the Degree of

DOCTOR OF PHILOSOPHY

to

**Dhirubhai Ambani Institute of Information and Communication Technology**



January, 2022

## Declaration

I hereby declare that

- i) the thesis comprises of my original work towards the degree of Doctor of Philosophy at Dhirubhai Ambani Institute of Information and Communication Technology and has not been submitted elsewhere for a degree,
- ii) due acknowledgment has been made in the text to all the reference material used.

---

Rahul Vashisth

## Certificate

This is to certify that the thesis work entitled DESIGN OF BROADBAND MICROWAVE ABSORBERS USING CARBONYL IRON FILLED SILICON RUBBER SHEETS IN THE FREQUENCY RANGE OF 1 TO 8.2 GHZ has been carried out by RAHUL VASHISTH for the degree of Doctor of Philosophy at *Dhirubhai Ambani Institute of Information and Communication Technology* under my supervision.

---

Prof. Deepak K. Ghodgaonkar  
Thesis Supervisor

# Acknowledgments

First and foremost, I thank Almighty Supreme God for making this venture a success and also for giving me the opportunity to meet many talented personalities. Next to the God, I would like to thank Prof. K S Dasgupta, who insisted, motivated and permitted me to pursue Ph.D. I would express sincere gratitude to my supervisor Prof. Deepak K. Ghodgaonkar for his support and contribution throughout this PhD journey. By means of the courses and research projects, they introduced me to advance topics like Wireless Systems Design, Advanced Radio Wave Propagation and Metamaterials in microwave applications that laid a strong technical foundation of my research work. His philosophy of balanced life is an inspiration for me. He always motivated me whenever i feel down. He always encourage me to experiment new things. I would like to thank him for providing his precious time for discussions and problem solving.

I am very thankful to Prof. Sanjeev Gupta for their constructive questions and suggestions during research progress seminars. I sincerely thank to my Research Progress Seminar Committee members: prof Nabin Kumar Sahu, for channelizing my efforts and spending their valuable time. I would like to thank all professors of DA-IICT for their direct or indirect contribution to my PhD journey. I am very thankful to all unknown reviewers of my papers and book chapter.

I am very thankful to DA-IICT staff member Krunal Patel, Rameshbhai and help desk staff for their support. I am very thankful to all other staff members of DA-IICT who have directly or indirectly supported me during this journey.

I would like to thank PhD students Pankaj Chaudhary, Hardik Patel, Rishikant Rajdeepak, Madhu R. Kamble for their support. I would like to thank all PhD students who have directly or indirectly supported me in this journey. I would like

to thank all M.Tech students who have supported me during this journey.

I would like to thank my father JWO Rajvir Vashisth and mother Sunita Vashisth for their support and patience during this PhD journey. I am very thankful to my brother Krishna Kant Vashisth for encouraging me throughout the study. I would like to thank my wife Anuranjana Dwivdi for her support during this journey. I would like to thank all other family members who have supported directly or indirectly in this journey.

I would like to thank my school teachers and University professors for their direct or indirect contribution in this PhD journey.



# Contents

<b>Abstract</b>	<b>ix</b>
<b>List of Tables</b>	<b>x</b>
<b>List of Figures</b>	<b>xi</b>
<b>1 Introduction</b>	<b>1</b>
1.1 Introduction . . . . .	1
1.2 Problem Statement . . . . .	2
1.3 Contributions of the Proposed Research Work . . . . .	3
1.4 Organization of the thesis . . . . .	3
<b>References</b>	<b>5</b>
<b>2 Literature Survey</b>	<b>7</b>
2.1 Characterization of CISR Sheets . . . . .	7
2.2 Multilayered Microwave Absorbers . . . . .	10
2.3 FSS Microwave Absorbers . . . . .	13
2.4 Research gap . . . . .	19
<b>References</b>	<b>20</b>
<b>3 Fabrication of Carbonyl Iron filled Silicon Rubber Sheets</b>	<b>23</b>
3.1 Introduction . . . . .	23
3.2 Silicon Rubber . . . . .	23
3.2.1 Introduction . . . . .	23
3.2.2 Various Properties of silicon rubber . . . . .	24

3.2.2.1	Heat and Cold Resistance . . . . .	24
3.2.2.2	Thermal Property . . . . .	24
3.2.2.3	Mechanical Property . . . . .	25
3.2.3	Types of Silicon Rubber . . . . .	25
3.3	Carbonyl Iron Powder . . . . .	25
3.3.1	Chemical and Physical Property . . . . .	26
3.4	Fabrication of Carbonyl iron filled Silicon Rubber (CISR) Sheets . . .	27
<b>References</b>		<b>29</b>
<b>4</b>	<b>Characterization of CISR Sheets by using Coaxial Air Line Method, Rectangular Dielectric Waveguide Method</b>	<b>32</b>
4.1	Introduction . . . . .	32
4.2	Coaxial Air Line Method (1 to 4 GHz) . . . . .	33
4.3	RDWG Method (3.95 to 8.2 GHz) . . . . .	38
4.4	Measured results of CISR sheets . . . . .	42
4.4.1	Coaxial Air Line . . . . .	42
4.4.2	Rectangular Dielectric Waveguide (RDWG) . . . . .	46
4.5	Polynomial Approximation of $\epsilon_r$ and $\mu_r$ for intermediate concentration of CI Powder . . . . .	50
4.6	Conclusions . . . . .	53
<b>References</b>		<b>54</b>
<b>5</b>	<b>Design of broadband microwave absorber using multilayer carbonyl iron filled silicone rubber sheets</b>	<b>56</b>
5.1	Introduction . . . . .	56
5.2	Theory of multilayer microwave absorbers . . . . .	57
5.3	Design of multilayer microwave absorbers using genetic optimization .	59
5.4	Measured and simulated results of multilayer microwave absorber in 1 to 8.2 GHz frequency range . . . . .	62
5.4.1	Results for 2.5 to 8.2 GHz . . . . .	62
5.4.2	Results for 1.6 to 2.6 GHz . . . . .	64

5.5 Discussion and conclusions . . . . .	66
<b>References</b>	<b>67</b>
<b>6 Design of broadband microwave absorbers using frequency selective surface embedded in carbonyl iron filled silicone rubber sheets</b>	<b>68</b>
6.1 Introduction . . . . .	68
6.2 Characterization of CISR sheets . . . . .	70
6.3 Conventional Type FSS . . . . .	70
6.4 Pixelated FSS . . . . .	75
6.5 Comparison with other broadband microwave absorbers . . . . .	85
6.6 Conclusion . . . . .	87
<b>References</b>	<b>88</b>
<b>7 Conclusions and suggestions for future work</b>	<b>93</b>
<b>Appendix A FGM-40, FGM-125 and AN-series Data sheet [1,2]</b>	<b>95</b>
<b>Appendix References</b>	<b>100</b>
<b>Appendix B NRW Method</b>	<b>101</b>
<b>Appendix References</b>	<b>109</b>
<b>Appendix C NRL Arch Method (1 to 8.2 GHz)</b>	<b>110</b>
<b>Appendix References</b>	<b>113</b>
<b>Appendix D BASF CN Germany</b>	<b>114</b>
<b>Appendix References</b>	<b>115</b>
<b>Appendix E Matlab Code for Calculation of Reflectivity of Multilayer Microwave Absorbers</b>	<b>116</b>
<b>List of Publications</b>	<b>122</b>

# Abstract

For microwave absorber applications, carbonyl iron (CI) powder is a commonly used filler material in silicon rubber because of the high value of attenuation coefficients (50.56 dB/cm), high curie temperature, good temperature stabilization and the higher specific saturation magnetization intensity. Silicon rubber is preferred as the host material because of many desirable properties such as excellent weathering resistance, resistance to aging, chemical resistance, insulating properties and compatibility with many kinds of fillers. Microwave absorbers using carbonyl iron filled silicone rubber sheets (CISR) are widely used to attenuate electromagnetic interference, eliminating cavity resonances, isolating components via insertion loss, reducing harmonics and termination signals in waveguides. The fabrication accuracies in thicknesses and concentrations of CISR sheets are  $\pm 0.5$  mm and  $\pm 2\%$  of CI by volume, respectively. Multilayer microwave absorbers designed in this thesis have two layers because of inaccuracies in fabrication of CISR sheets. Broadband microwave absorbers are designed by using conventional type and pixelated type Frequency Selective Surface (FSS) layers embedded between two different concentrations of CISR sheets in the frequency range of 3.95 GHz to 8.2 GHz which are light in weight and small in thickness.

WR-187 (3.95 to 5.85 GHz) and WR-137 (5.85 to 8.2 GHz) rectangular dielectric waveguide (RDWG) systems are designed for non destructive testing of reflectivity,  $\epsilon_r$  and  $\mu_r$  of broadband microwave absorbers. RDWG systems consist of vector network analyzer (VNA), coaxial cables, coaxial to rectangular waveguide transitions, sections of metallic waveguides, standard gain horn antennas and sections of dielectric waveguides. For 1 to 8.2 GHz, NRL arch method is used for measuring reflectivity of microwave absorbers in the anechoic chamber at normal incidence and

20° in TE/TM polarizations. This method involves measurements with two double ridge horn antennas, two long coaxial cables, wooden board for holding 1 foot  $\times$  1 foot microwave absorbers and VNA. Reflectivity of microwave absorbers are measured in the far field using time domain gating of VNA.

Characterization ( $\epsilon_r$  and  $\mu_r$ ) of CISR sheets are carried out in coaxial air line system (1 to 4 GHz) and RDWG systems (3.95 to 8.2 GHz) for six CISR sheets (0%, 10%, 20%, 30%, 40% and 50% of CI in CISR sheets by volume). In RDWG systems, flexible CISR sheets are sandwich between two Teflon sheets which are quarter wavelength at mid band. Teflon sheets provide impedance matching and avoid sagging of CISR sheets. Coaxial air line system consists of coaxial air line fixture, sections of coaxial cables and the VNA. Toroidal shaped CISR sheets are prepared and used in the coaxial air line fixture for characterization. The Nicolson-Ross-Weir (NRW) method is used to extract  $\epsilon_r$  and  $\mu_r$  from measured  $S_{11}$  and  $S_{21}$  parameters of CISR sheets. For the design of microwave absorbers,  $\epsilon_r$  and  $\mu_r$  value are required for arbitrary volume fraction of CI in CISR sheets. The polynomial approximation method is used to get  $\epsilon_r$  and  $\mu_r$  at intermediate concentration of CI in CISR sheets by volume.

Multilayer microwave absorber in frequency range of 2.5 to 8.2 GHz is designed in this thesis using genetic optimization of concentrations and thicknesses of different layers of CISR sheets. Two layer broadband microwave absorber (7.35 mm of silicone rubber as first layer and 1.4 mm of 50% of CI powder in CISR sheet by volume as second layer) provides reflectivity better than -10 dB in the frequency range of 2.5 to 8.2 GHz. For frequency 1.6 GHz to 2.6 GHz range, single layer microwave absorber of thickness 3 mm is designed by 50% of CI powder in CISR sheet by volume.

Broadband microwave absorbers using conventional type FSS and pixelated type FSS are designed fabricated and tested by embedding them between two CISR sheets (24% and 33% of CI in CISR sheets by volume). Conventional type FSS layer were designed in CST microwave studio after performing large number of simulations. Pixelated FSS layer is designed with genetic algorithm optimization and geometry refinement method. The reflectivity of both broadband FSS microwave absorbers are tested in RDWG systems and found to be better than -11 dB at normal incidence in

the frequency range of 3.95 to 8.2 GHz. The two layer microwave absorber (without FSS layer) reflectivity is around -6 dB. But, by embedding FSS layer between two CISR layers increases its reflectivity to -11 dB which is low cost, light in weight. The broadband microwave absorber using pixelated FSS layer has better design methodology as it does not require human intuition, experience and a large number of simulations required in hit and trail methodology of conventional type FSS absorber. The analysis is performed at different incidence angle and TE / TM polarizations which shows reflectivity is generally insensitive to the incidence angles from 0° to 20°.

# List of Tables

2.1	Design of composite microwave absorber using genetic algorithm [6]	11
3.1	Carbonyl Iron powder Property [18]	27
4.1	Complex permittivity and complex permeability of CISR Sheets at 2.5 GHz	43
4.2	Complex permittivity and complex permeability of CISR Sheets at 6 GHz	47
6.1	Broadband microwave absorber are compared with other broadband microwave absorbers	86

# List of Figures

2.1	$\mu_r$ and $\epsilon_r$ of CISR sheet with 80% of CI powder by weight [1] . . . . .	8
2.2	(a) $\epsilon'$ and (b) $\epsilon''$ for RAM with volume fractions (0, 0.1, 0.2; 0.3, 0.4, and 0.45) [2] . . . . .	8
2.3	(a) $\mu'$ and (b) $\mu''$ for RAM with volume fractions (0, 0.1, 0.2, 0.3, 0.4, and 0.45) [2] . . . . .	9
2.4	$\epsilon_r$ and $\mu_r$ of CIP/SR composite, (a) $\epsilon_r$ (b) $\mu_r$ [5] . . . . .	10
2.5	The genetically optimized reflectivity of the composite microwave absorbers with variable thickness [6] . . . . .	11
2.6	Reflectivity of single layer microwave absorbers with different thicknesses [7] . . . . .	12
2.7	Reflectivity of double-layer absorber with $t_1$ (BF) of 0.9 mm and $t_2$ (BF-5CI) increased from 1.0 to 1.8 mm [7] . . . . .	12
2.8	Simulated and measured results of reflectivity of planar composite microwave absorbers [8] . . . . .	13
2.9	Reflectivity of FGM-40 and FGM-125 [9] . . . . .	14
2.10	Reflectivity of AN-series of microwave absorbers [10] . . . . .	14
2.11	Broadband microwave absorber embedded with FSS layer, $t_A = t_B = 2.7$ mm and FSS thickness is 0.92 mm [11] . . . . .	15
2.12	Simulated and measured result of broadband absorber and two layer absorber (without FSS) [11] . . . . .	15
2.13	(a) The composite microwave absorber embedded with a FSS layer. The thickness of each layer is $t_1=t_2=1$ mm, $t=0.2$ mm. (b) Geometry of FSS [12] . . . . .	16



2.14	The simulated (dotted curve) and measured (solid curves) reflectivity of samples [12] . . . . .	16
2.15	simulated and measured results for single layer FSS embedded microwave absorber and double layer FSS embedded microwave absorber.[14] . . . . .	17
2.16	(a) Simulated reflectivity of the RAM and the RAM with FSS and (b) the measured reflectivity of the RAM and the RAM with FSS [15]	17
2.17	the measured and simulated reflectivity curves of resistor loaded pixelated FSS (RPFSS) and pixelated FSS without resistors [16] . . . . .	18
2.18	(a) Pixelated FSS geometry and (b) The simulated (dotted curve) and measured (solid curves) reflectivity of pixelated FSS metamaterial absorber [17] . . . . .	18
3.1	Silicon rubber Structure . . . . .	24
3.2	Carbonyl Iron Powder [19] . . . . .	26
3.3	Internal mixture used for mixing Silicon rubber and CI powder . . . . .	28
3.4	Fabrication process of CISR sheets on two-roll mill assembly . . . . .	28
4.1	Photograph of coaxial air line system . . . . .	33
4.2	Schematic diagram of coaxial air line fixture [5] . . . . .	34
4.3	Components of coaxial air line fixture . . . . .	34
4.4	The photograph of coaxial air line fixture . . . . .	35
4.5	Photograph of toroidal shape sleeve CISR. . . . .	35
4.6	$T_1$ , $T_2$ and $T_3$ parameters inside the coaxial air line fixture . . . . .	36
4.7	Sample inside the coaxial air line fixture [1] . . . . .	36
4.8	Schematic diagram of sample inside the coaxial airline fixture . . . . .	37
4.9	Photograph of WR-137 RDWG system for 5.85 to 8.2 GHz frequency range . . . . .	38
4.10	Photograph of WR-187 RDWG system for 3.95 to 5.85 GHz frequency range . . . . .	39
4.11	Photograph of tapered dielectric waveguide section for WR-137 frequency bands . . . . .	39

4.12 Through Calibration Standard . . . . .	40
4.13 Reflect calibration standard . . . . .	40
4.14 Line Calibration standard . . . . .	40
4.15 Toroidal-shaped CISR sleeves for coaxial air line . . . . .	42
4.16 Complex permittivity and Complex permeability of CISR sheets (0% of CI by volume) . . . . .	44
4.17 Complex permittivity and Complex permeability of CISR sheets (10% of CI by volume) . . . . .	44
4.18 Complex permittivity and Complex permeability of CISR sheets (20% of CI by volume) . . . . .	44
4.19 Complex permittivity and Complex permeability of CISR sheets (30% of CI by volume) . . . . .	45
4.20 Complex permittivity and Complex permeability of CISR sheets (40% of CI by volume) . . . . .	45
4.21 Complex permittivity and Complex permeability of CISR sheets (50% of CI by volume) . . . . .	45
4.22 Photograph of Fabricated CISR sheets (a) 0% (b) 10% (c) 20% (d) 30% (e) 40% (f) 50% of CI in CISR sheets by volume. . . . .	46
4.23 Complex permittivity and Complex permeability of Silicon Rubber (0% of CI by volume) . . . . .	48
4.24 Complex permittivity and Complex permeability of CISR sheets (10% of CI by volume) . . . . .	48
4.25 Complex permittivity and Complex permeability of CISR sheets (20% of CI by volume) . . . . .	48
4.26 Complex permittivity and Complex permeability of CISR sheets (30% of CI by volume) . . . . .	49
4.27 Complex permittivity and Complex permeability of CISR sheets (40% of CI by volume) . . . . .	49
4.28 Complex permittivity and Complex permeability of CISR sheets (50% of CI by volume) . . . . .	49
4.29 Polynomial approximation of $\epsilon'$ at 2.5 GHz . . . . .	51

4.30	Polynomial approximation of $\mu'$ at 2.5 GHz . . . . .	51
4.31	Polynomial approximation of $\mu''$ at 2.5 GHz . . . . .	52
4.32	Polynomial approximation of $\epsilon'$ at 6 GHz . . . . .	52
4.33	Polynomial approximation of $\mu'$ at 6 GHz . . . . .	52
4.34	Polynomial approximation of $\mu''$ at 6 GHz . . . . .	53
5.1	Transmission line model of multilayer microwave absorber . . . . .	57
5.2	Flow Chart of Genetic Optimization . . . . .	61
5.3	Measured results of two layer microwave absorber at normal incidence by NRL arch method and RDWG method . . . . .	62
5.4	Measured reflectivity of two layer microwave absorber at angle of in- cidences ( $0^\circ$ , $10^\circ$ and $20^\circ$ ) for TE waves in 1 to 8.2 GHz frequency range . . . . .	63
5.5	Simulated reflectivity of two layer microwave absorber at angle of incidences ( $0^\circ$ , $10^\circ$ and $20^\circ$ ,) for TE waves in 1 to 8.2 GHz frequency range . . . . .	63
5.6	Measured reflectivity of two layer microwave absorber at angle of in- cidences ( $0^\circ$ , $10^\circ$ and $20^\circ$ ) for TM waves in 1 to 8.2 GHz frequency range . . . . .	64
5.7	Simulated reflectivity of two layer microwave absorber at angle of incidences ( $0^\circ$ , $10^\circ$ and $20^\circ$ ,) for TM waves in 1 to 8.2 GHz frequency range . . . . .	64
5.8	Measured and simulation result of single layer microwave absorber for normal incidence . . . . .	65
5.9	Simulation result of single layer microwave absorber at angle of in- cidences ( $0^\circ$ , $10^\circ$ and $20^\circ$ ) for TE waves in 1 to 8.2 GHz frequency range . . . . .	65
5.10	Simulation result of single layer microwave absorber at angle of in- cidences ( $0^\circ$ , $10^\circ$ and $20^\circ$ , ) for TM waves in 1 to 8.2 GHz frequency range . . . . .	66
6.1	Schematic diagram of broadband microwave absorber . . . . .	69

6.2	Measured $\epsilon_r$ and $\mu_r$ value for CISR sheets 24% of CI in CISR sheet by volume . . . . .	70
6.3	Measured $\epsilon_r$ and $\mu_r$ value for CISR sheets 33% of CI in CISR sheet by volume . . . . .	71
6.4	Geometry of FSS unit cell (a) Top view (b) Side view . . . . .	72
6.5	Photograph of Fabricated FSS . . . . .	72
6.6	$\epsilon_r$ and $\mu_r$ value of FSS . . . . .	73
6.7	Calculated impedance of FSS . . . . .	73
6.8	Simulated and measured results of microwave absorbers . . . . .	74
6.9	TE polarization of broadband microwave absorber at various incidence angles . . . . .	75
6.10	TM polarization of broadband microwave absorber at various incidence angles . . . . .	75
6.11	Flow chart of optimized pixelated FSS layer . . . . .	76
6.12	Flow chart of optimized pixelated FSS layer . . . . .	77
6.13	Photograph of optimized pixelated FSS layer . . . . .	78
6.14	Reflection and Transmission of optimized pixelated FSS layer (Magnitude) . . . . .	79
6.15	Reflection and Transmission of optimized pixelated FSS layer (Phase)	79
6.16	Reflectivity of optimized pixelated FSS layer in TE polarization . . .	80
6.17	Reflectivity of optimized pixelated FSS layer in TM polarization . . .	80
6.18	Measured reflectivity of broadband microwave absorber by RDWG system . . . . .	81
6.19	Vector plot of the surface current density in metallic plate at resonance frequency of 4 GHz . . . . .	82
6.20	Vector plot of the surface current density in pixelated FSS layer at resonance frequency of 4 GHz . . . . .	83
6.21	Vector plot of the surface current density in metallic layer at resonance frequency of 7.5 GHz . . . . .	84
6.22	Vector plot of the surface current density in pixelated FSS layer at resonance frequency of 7.5 GHz . . . . .	84

6.23	Reflectively in TE-polarization at different incident angle . . . . .	85
6.24	Reflectively in TM-polarization at different incident angle . . . . .	85
B.1	Schematic diagram of CISR sheet . . . . .	101
B.2	Schematic diagram of Teflon sheet-CISR sheet-Teflon sheet assembly	104
C.1	Measurement system for NRL arch method . . . . .	111
C.2	$S_{21}$ of metallic plate and microwave absorber. . . . .	112

# Chapter 1

## Introduction

### 1.1 Introduction

High loss microwave absorbers are used to attenuate electromagnetic interference. Absorbers are used in a wide range of applications to eliminate stray or unwanted electromagnetic radiation that could interfere with a system's operation. Also, absorbers have become a critical element in some systems to reduce interference between circuit components [1-4]. The design of a microwave absorbers essentially requires two important conditions to help suppress electromagnetic radiations. First, minimal reflection at the air-absorber interface and, second, sufficient attenuation of the incident within the different layer of microwave absorbers. The first condition of microwave absorber can be acheive by impedance matching at the air-absorber interface. Another property can be achieved by attenuation within the absorber matrix using lossy material. These two properties depend on complex permittivity ( $\epsilon_r$ ) and complex permeability ( $\mu_r$ ) of absorbing material at the desired frequency [5-9].

Absorbers can take many different physical forms including flexible elastomers, foam, rigid epoxy and plastics. The design of planner microwave absorber is carried out by composite layers, Frequency Selective Surface (FSS) layers [10-12]. Composite materials use different host materials like rubber (silicon rubber, polyvinyl rubber, etc), epoxy resin, etc which are filled with filler materials like Carbonyl Iron (CI) powders, carbon nanotube, graphite powder, etc. These types of microwave absorbers are either single layer or multilayer. FSS layer type of absorber are of two types. These are metallic and resistive. FSS types of absorber gives flexibility in choosing frequency response.

CI powder is a commonly used filler materials in silicon rubber because of the high value of attenuation coefficients (50.56 dB/cm) [1], high Curie temperature, good temperature stabilization and the higher specific saturation magnetization intensity [2]. Silicon rubber is preferred as the host material because of many desirable properties such as excellent weathering resistance, resistance to aging, chemical resistance, insulating properties and compatibility with many kinds of fillers [2]. CI powder is a ferromagnetic material and it is expected that carbonyl iron filled silicone rubber (CISR) sheets will be magnetic material with ( $\mu_r$ ) values greater than  $1 - j0.0$  [1,2].  $\epsilon_r$  and  $\mu_r$  value are measured in 1 to 4 GHz frequency range by using coaxial air line method and in 3.95 to 8.2 GHz frequency range by using rectangular dielectric waveguide (RDWG) methods. 0%, 10%, 20%, 30%, 40% and 50% of CI in CISR sheets by volume are fabricated and used for characterization of CISR sheets. Polynomial approximation is used to calculate  $\epsilon_r$  and  $\mu_r$  values at intermediate concentration of CI in CISR sheets.

In this thesis, multilayer microwave absorbers were designed in 1.6 to 8.2 GHz frequency range. Metallic FSS are designed which are conventional type [11] and pixelated type [12] . These FSS layer are embedded in two different concentrations of CISR sheets to get broadband microwave absorbers.

## 1.2 Problem Statement

To develop high loss microwave absorbers in sheet form that attenuate electromagnetic interference. These sheets are used for reducing or eliminating cavity resonances, isolating components via insertion loss, reducing harmonics and termination signals in waveguides. The operating frequency is 1 to 8.2 GHz with reflection better than -10 dB. The base materials should be iron filled silicone rubber with hardness of 73 (Shore A). The specific gravity is between 2.1 to 5.1. Its tensile strength is  $9.8 \text{ Kg/cm}^2$ . Total Mass Loss (TML) and Collected Volatile Condensate Material (CVCM) values should be less than 1.0% and 0.1%, respectively.

## 1.3 Contributions of the Proposed Research Work

- Pixelated FSS microwave absorber is designed, fabricated and tested in 3.95 to 8.2 GHz range. Pixelated FSS is designed by using genetic optimization and geometry refinement technique.
- Microwave absorber is designed in 3.95 to 8.2 GHz range by using three conductive concentric square loops FSS (metamaterial).
- Multilayer microwave absorber is design, fabricated and tested in 2.5 to 8.2 GHz frequency range. Polynomial approximation method is used to get  $\epsilon_r$  and  $\mu_r$  values at intermediate concentrations of CI in CISR sheets. Genetic optimization is performed to get concentration of CI and thickness of CISR sheets. This absorber should work in the space environment. TML and CVCM testing was performed at SAC, ISRO.
- For 3.95 to 8.2 GHz range, non-destructive method (RDWG) is used to measure reflectivity of microwave absorbers and characterize ( $\epsilon_r$  and  $\mu_r$ ) CISR sheets.

## 1.4 Organization of the thesis

In chapter 2, literature survey of characterization of CISR sheets, multilayer microwave absorbers and FSS microwave absorbers are discussed.  $\epsilon_r$  and  $\mu_r$  values of CISR sheets, reflectivity of multilayer microwave absorbers and FSS microwave absorbers reported by different researchers are given in this chapter.

Chapter 3 describe materials used and fabrication process of CSIR sheets. Material properties of silicon rubber as matrix material and carbonyl iron powder as filler material are presented. Fabrication of CISR sheets are carried out on two roll mill assembly and molding under  $150 \text{ Kg/cm}^2$  pressure.

Chapter 4 discuss about coaxial air line method and rectangular dielectric waveguide method (RDWG) for characterization of CISR sheets. CISR sheets of different concentrations of CI powder were fabricated and used for characterization. Polyno-



mial approximation is used to calculate  $\epsilon_r$  and  $\mu_r$  values at intermediate concentrations of CI powder in CISR sheets.

Chapter 5 presents theory of multilayer microwave absorbers and design of multilayer microwave absorbers by using genetic optimization. In this chapter, microwave absorbers are designed and tested for 1.6 to 8.2 GHz frequency range.

The design of microwave absorbers are presented in chapter 6 by embedding FSS layer in two different concentrations of CISR sheets. These FSS are designed either by using conventional type or by using pixelated type in 3.95 to 8.2 GHz frequency range in 1 to 10 GHz frequency range. Genetic optimization technique was used in pixelated type FSS design.

Chapter 7 describes conclusions and suggestions for future work.

Appendix A gives data sheets of commercially available microwave absorbers (FGM-40, FGM-125 and AN-73).

Appendix B describes Nicolson-Ross-Weir (NRW) method for calculation of  $\epsilon_r$  and  $\mu_r$  and gives Matlab code.

Appendix C presents NRL Arch method in 1 to 8.2 GHz frequency range.

Appendix D gives data sheets of CI powder manufactured by BASF CN Germany.

Appendix E gives Matlab Code for calculation of reflectivity of multilayer microwave absorbers.

## References

- [1] D.K. Ghodgaonkar, V.K. Varadan and V.V. Varadan,"Microwave Dielectric and Magnetic Properties of Carbonyl Iron Powder Loaded Silicon Rubber Sheets," *Journal of Wave Material Interaction*, Vol. 8, pp.171-184,1994.
- [2] Yuping Duan, Guofang Li, Lidong Liu and Shunhua Liu,"Electromagnetic properties of carbonyl iron and their microwave absorbing characterization as filler in silicone rubber," *Indian Academy of Sciences Bull. Material Science*, Vol. 33, No. 5, October 2010, pp. 633–636.
- [3] D. K. Ghodgaonkar, V. V. Varadan and V. K. Varadan,"Free Space Measurement of Complex Permittivity and Complex Permeability of Magnetic Materials at Microwave Frequencies," *IEEE Transactions on Instrumentation and Measurements*, Vol. 39, pp. 398-394, April 1990.
- [4] R. Vashisth, D. Ghodgaonkar and S. Gupta,"Permittivity and Permeability Measurements of CISR sheets for Microwave Absorber Applications," *2018 IEEE International RF and Microwave Conference (RFM)*, Penang, Malaysia,17-18 Dec 2018, pp. 359-362.
- [5] Luiza de C. Folgueras, Mauro A. Alves Mirabel C. Rezende,"Microwave absorbing paints and sheets based on carbonyl iron and polyaniline measurement and simulation of their properties," *Journal of Aerospace Technology and Management*, vol 2, no 1, April 2010.
- [6] E.Michielsen, J.Sajer, S.Ranjithan and R. Mittra,"Design of lightweight, broadband microwave absorbers using genetic algorithms," *IEEE Transactions on Microwave Theory and Techniques*, vol. 41, no. 6, pp. 1024-1031, June-July 1993.

- [7] D.S.Weile, E. Michielssen and D.E. Goldberg, "Genetic algorithm design of Pareto optimal broadband microwave absorbers," *IEEE Transactions on Electromagnetic Compatibility*, vol.38, no.3, pp.518-525, August 1996.
- [8] S.Roy, S.D. Roy, J.Tewary, A.Mahanti, and G.K.Mahanti, "Particle Swarm Optimization for Optimal Design of Broadband Multilayer Microwave Absorber for Wide Angle of Incidence," *Progress In Electromagnetics Research B*, Vol. 62, pp.121-135, 2015.
- [9] Somayyeh Chamaani, Seyed Abdullah and Mirtaheri, Mahdi Aliyari and Shooreldeli, "Design of very thin wide band absorbers using modified local best particle swarm optimization," *AEU-International Journal of Electronics and Communications*, Volume 62, Issue 7, 2008, pp. 549-556.
- [10] Ahmed I. Imran, Taha A. Elwi, "A cylindrical wideband slotted patch antenna loaded with Frequency Selective Surface for MRI applications," *Engineering Science and Technology, an International Journal*, Volume 20, Issue 3, 2017, pp. 990-996,
- [11] R. Vashisth, D. Ghodgaonkar and S. Gupta, "Design and Fabrication of Broadband Microwave Absorber using FSS embedded in CISR sheets," *2018 IEEE MTT-S International Microwave and RF Conference (IMaRC)*, Kolkata, India, Dec 2018, pp. 1-4.
- [12] Vashisth Rahul, Ghodgaonkar Deepak, Gupta Sanjeev, " Broadband Microwave-Absorber using Pixelated FSS Embedded in CISR Sheets in Frequency Range of 3.95 to 8.2 GHz". *Journal of Electromagnetic Waves and Applications*, Taylor Francis, 1569-3937. doi: 10.1080/09205071.2021.1947899

## Chapter 2

# Literature Survey

In this chapter, literature is reviewed for characterization of complex permittivity ( $\epsilon_r$ ) and complex permeability ( $\mu_r$ ) for Carbonyl Iron filled Silicone Rubber (CISR) sheets, design of the multi-layer microwave absorbers and design of frequency selective surface (FSS) layer embedded in sheets.

### 2.1 Characterization of CISR Sheets

Myung-Jun Park et al [1] have presented the design of pyramidal absorbers in 1 to 18 GHz frequency range with -20 dB reflectivity. They have used two kind of filler magnetic materials namely, Ni-Zn ferrite and Carbonyl iron powder. Silicone rubber is used as matrix material. The complex permeability and complex permittivity were measured by using the standard coaxial air line in frequency range from 50 MHz –18 GHz. In case of silicone rubber composite using CI powder, they observed broad loss spectrum ( $\mu''$ ) in 2 to 18 GHz range as shown in Figure 2.1.  $\mu'$  varies from 4.8 at 1 GHz to 1.2 at 18 GHz.  $\epsilon'$  value remains constant at 12 over entire the frequency range.  $\epsilon''$  is close to 0 over the entire frequency range. In this silicone rubber composite using CI powder, the weight fraction of CI powder is 80% (approximately 36% by volume).

Yong-Bao Feng et al [2] have fabricated rubber (Ethylene–Propylene–Diene Monomer) radar absorbing material (RAM) with various carbonyl iron volume fractions (0, 0.1, 0.2, 0.3, 0.4, and 0.45) and calculated its  $\epsilon_r$  and  $\mu_r$  value by using the transmission/reflection method. They have used APC-7 coaxial line system for measurement of  $S_{11}$  and  $S_{21}$  in 2 to 18 GHz frequency range. As shown in Figures 2.2 and 2.3,

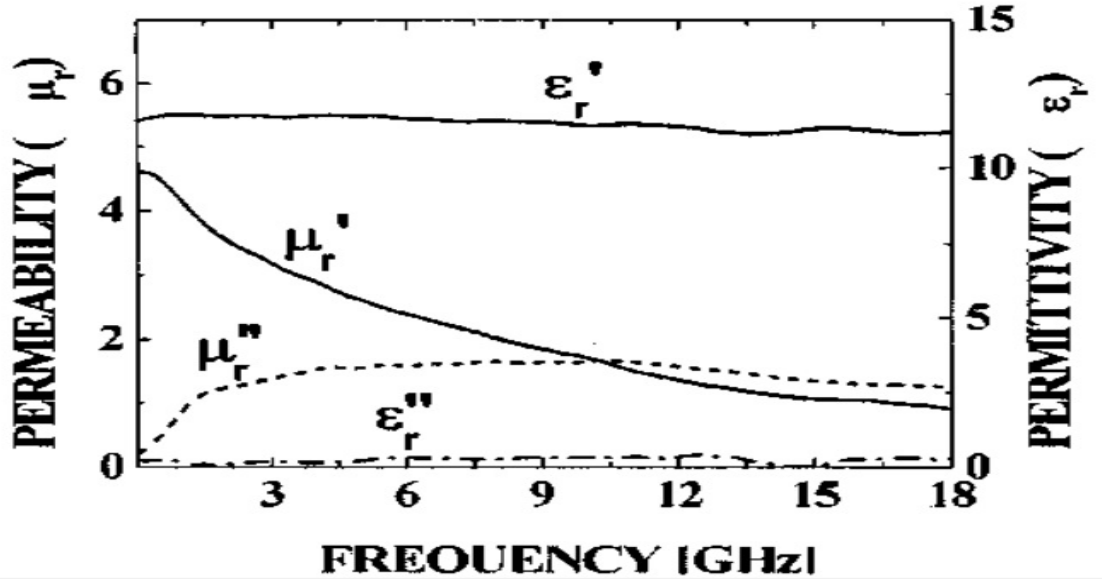


Figure 2.1:  $\mu_r$  and  $\epsilon_r$  of CISR sheet with 80% of CI powder by weight [1]

the value of  $\epsilon'$  varies from 2.5 to 15 and  $\mu''$  varies from 0 to 1.7 with increasing concentrations of CI powder.  $\epsilon''$  is nearly 0 over entire frequency range.

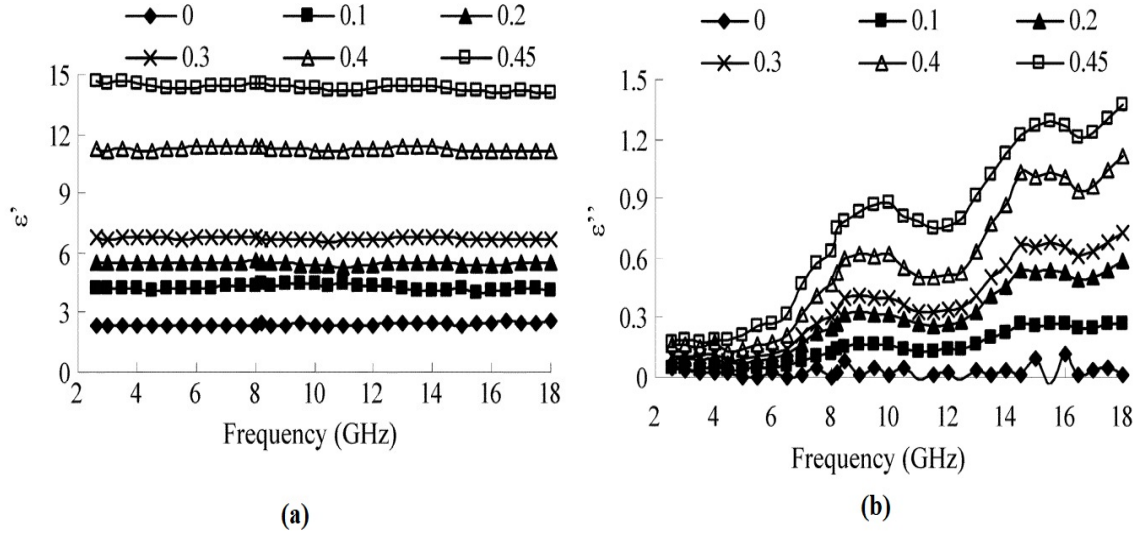


Figure 2.2: (a)  $\epsilon'$  and (b)  $\epsilon''$  for RAM with volume fractions (0, 0.1, 0.2; 0.3, 0.4, and 0.45) [2]

R. Vashisth et al [3] have calculated  $\epsilon_r$  and  $\mu_r$  of 0%, 19%, 24%, 33%, and 43% of CI powder by volume in CISR sheets by using transmission/reflection method. They used two RDWG systems, WR-137 for 5.85 to 8.2 GHz frequency range and WR-187 for 3.95 to 5.85 GHz frequency range. They are used for measurement of  $S_{11}$  and  $S_{21}$  of CISR sheets. rectangular dielectric waveguide (RDWG) is a non-destructive

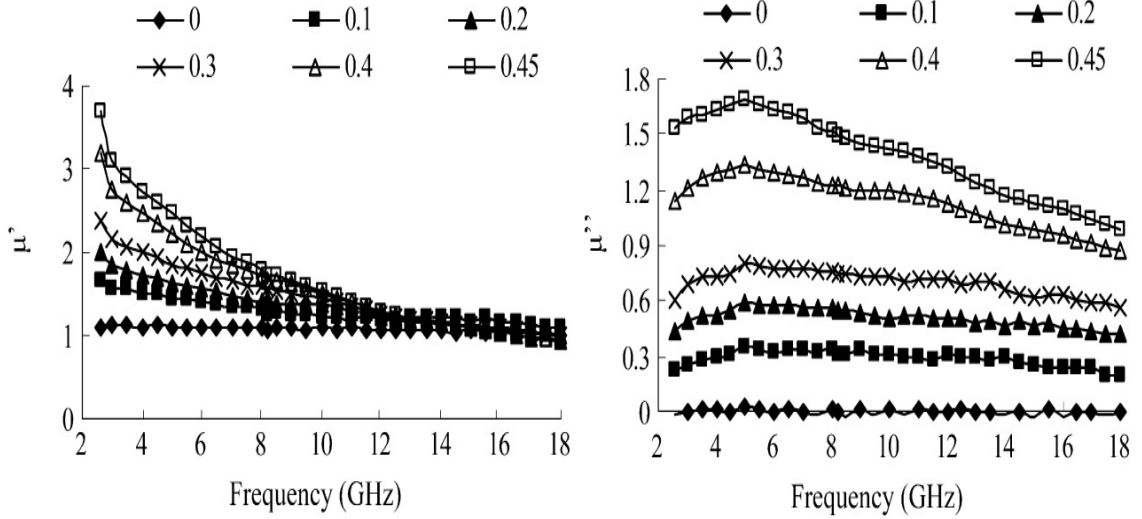


Figure 2.3: (a)  $\mu'$  and (b)  $\mu''$  for RAM with volume fractions (0, 0.1, 0.2, 0.3, 0.4, and 0.45) [2]

measurement method.  $\epsilon_r$  and  $\mu_r$  at 6 GHz are given in Table 2.1. From Table 2.1, it is observed that values of  $\epsilon'$ ,  $\mu'$  and  $\mu''$  increase with increasing volume fraction of CI powder. The negative value of  $\epsilon''$  and  $\mu''$  are due to measurement errors.  $\epsilon''$  values are close to 0 over 3.95 to 8.2 GHz frequency range.

D.K. Ghodgaonkar et al [4] have fabricated carbonyl iron loaded silicone rubber sheets and calculated its  $\epsilon_r$  and  $\mu_r$  values by measuring  $S_{11}$  and  $S_{21}$  using a free space method. The measurement of  $S_{11}$  and  $S_{21}$  are carried out in 8.6 GHz to 13.4 GHz. Five CSIR sheets were prepared for measurement with 0%, 20%, 30%, 40% and 50% of CI by volume in RTV silicone rubber. The value of  $\epsilon'$  of CI powder composite decreases with increase in frequency from 8.6 GHz to 13.4 GHz frequency range.  $\mu'$  and  $\mu''$  value decreases with increase in frequency with concentration higher than 20%.  $\epsilon'$  and  $\mu''$  value increases with increase in concentration of CI upto 50% by volume in composite. Expected values of  $\epsilon''$  is nearly equal to zero.

X. T. Ma and Z. P. Jiang et al [5] calculated  $\epsilon_r$  and  $\mu_r$  of silicone rubber filled with carbonyl iron powder (CIP/SR) sheets by using coaxial air line method. They have fabricated CIP/SR composite with CIP of 78% by weight (33.33% by volume).  $\epsilon_r$  and  $\mu_r$  values of CIP/SR are calculated from measured  $S_{11}$  and  $S_{21}$  in the frequency range of 2 to 18 GHz as shown in Fig. 2.4.  $\epsilon'$  is 9.8 at 2 GHz and 10.25 at 18 GHz.  $\epsilon''$  value is 0.1 at 2 GHz and 1.75 at 18 GHz.  $\mu'$  value is 2.6 at 2 GHz and 1.1 at 18

GHz.  $\mu''$  is 1 at 2 GHz and 0.6 at 18 GHz.

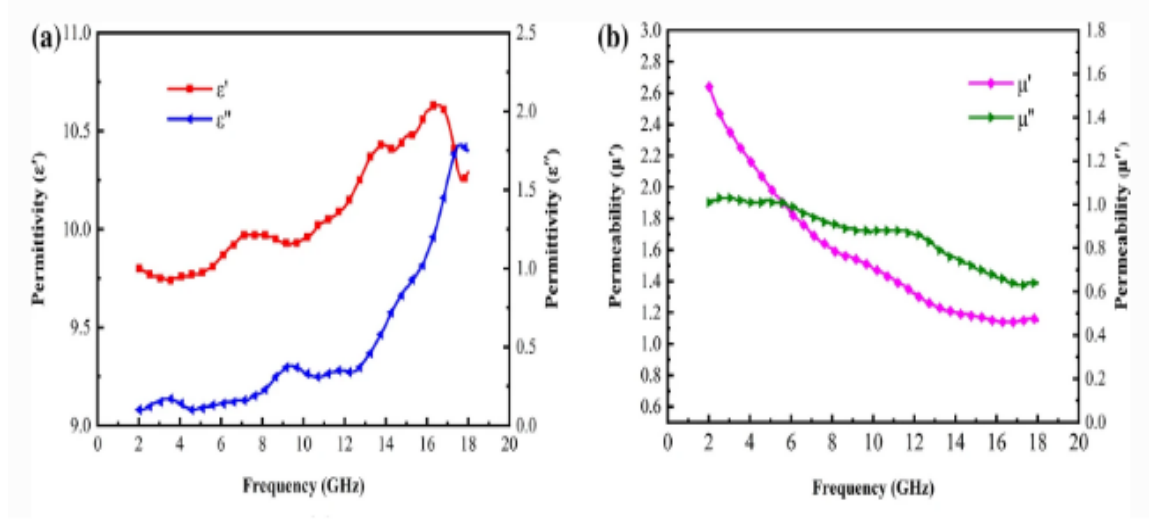


Figure 2.4:  $\epsilon_r$  and  $\mu_r$  of CIP/SR composite, (a)  $\epsilon_r$  (b)  $\mu_r$  [5]

## 2.2 Multilayered Microwave Absorbers

Yonggang Xu et al [6] have fabricated a multilayer microwave absorber using CI powder as a filler in Methylvinyl silicon rubber. They have reported the reflectivity of multilayer composite microwave absorber to be better than -10 dB in 8 - 18 GHz frequency band. Genetic algorithm is used to find optimized layer characteristics and thickness of absorbing materials. Table 2.1 gives design of composite microwave absorber using genetic algorithm. In this table, F means flaky shaped CI powder and S means spherical shaped CI powder. The genetically optimized reflectivity of the composite microwave absorbers are shown in Figure 2.5.

Xiaohu Ren et al [7] have prepared the single and multi-layer microwave absorbers by filling  $BaCo_{0.4}Zn_{1.6}Fe_{16}O_{27}$  and carbonyl iron powder into epoxy matrix material.  $BaCo_{0.4}Zn_{1.6}Fe_{16}O_{27}$  powder is mixed with CI powder forming four different concentrations. In figure 2.6, BF means 70% of ferrite by volume in epoxy matrix, BF-1CI means 63% of ferrite and 7% of CI by volume in epoxy matrix, BF-3CI means 49% of ferrite and 21% of CI powder by volume in epoxy matrix and BF-5CI means 35% of ferrite and 35% of CI by volume in epoxy matrix. They have reported a single layer absorber with BF-5CI material with a bandwidth of 4 GHz in

Sr. No	1 <sup>st</sup> Layer Thickness Type-Conc.	2 <sup>st</sup> Layer Thickness Type-Conc.	3 <sup>st</sup> Layer Thickness Type-Conc.	4 <sup>st</sup> Layer Thickness Type-Conc.	Total Thickness	Mutation Coefficient
1	0.47 mm, F-38%	0.16 mm, S-5%	0.50 mm, S-18%	0.50 mm, F-22%	1.63 mm	0.4
2	0.40 mm, F-43%	0.77 mm, S-19%	0.43 mm, F-2%	—	1.60 mm	0.5
3	0.40 mm, F-44%	0.43 mm, S-22%	0.50 mm, S-12%	0.23 mm, F-39%	1.56 mm	0.6
4	0.30 mm, F-44%	0.30 mm, F-39%	0.40 mm, S-4%	0.50 mm, F-19%	1.50 mm	0.7
5	0.47 mm, F-42%	0.67 mm, S-18%	0.33 mm, F-42%	—	1.47 mm	0.8

Table 2.1: Design of composite microwave absorber using genetic algorithm [6]

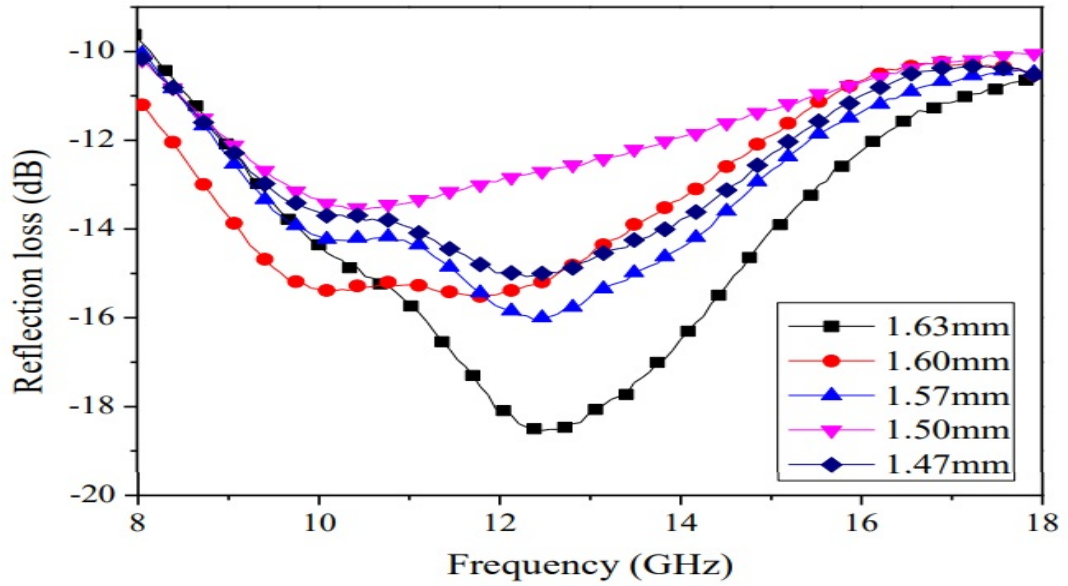


Figure 2.5: The genetically optimized reflectivity of the composite microwave absorbers with variable thickness [6]

the frequency range of 3.8 to 7.8 GHz as shown in Figure 2.6. Double-layer absorber consist of 0.9 mm BF as matching layer and 1.4 mm BF-5CI as absorption layer as shown in Figure 2.7.

Saichao Dang et al [8] have designed triple-layered planar microwave absorber using flaky carbonyl iron powder (FCIPs) as filler in paraffin wax matrix material. Six composite materials were prepared with 20%, 30%, 50%, 60%, 70% and 75% of flaky CI powder in paraffin wax by weight. With these composites, particle swarm optimization was used to optimize the thickness of triple-layer planner microwave



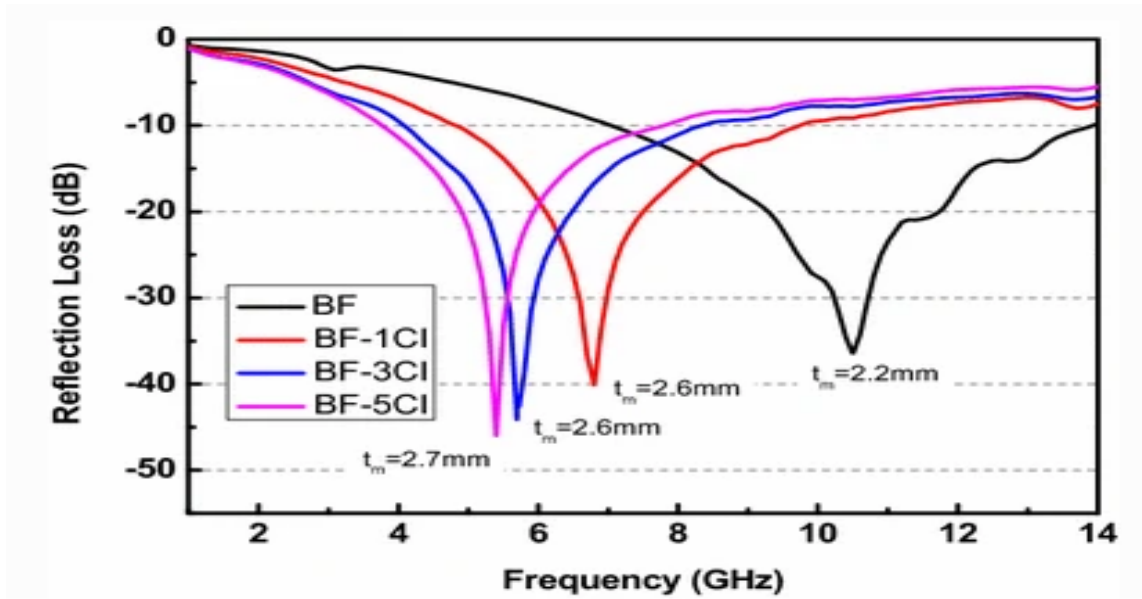


Figure 2.6: Reflectivity of single layer microwave absorbers with different thicknesses [7]

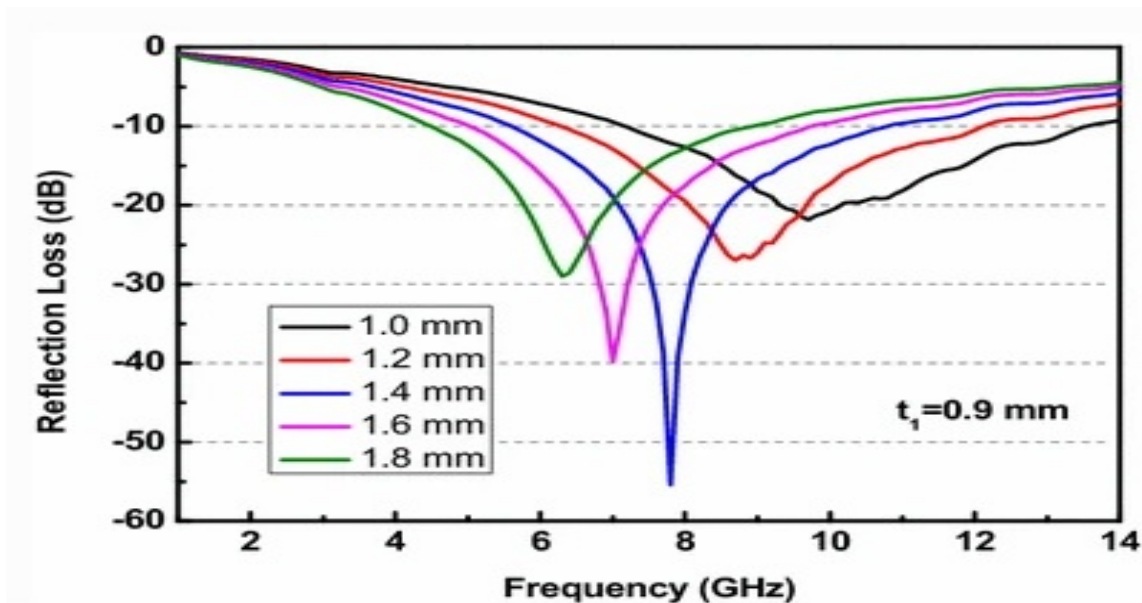


Figure 2.7: Reflectivity of double-layer absorber with  $t_1$  (BF) of 0.9 mm and  $t_2$  (BF-5CI) increased from 1.0 to 1.8 mm [7]

absorber. The thicknesses of the three layers were 4.16 mm, 0.92 mm and 1.08 mm with the FCIPs contents of 20%, 60% and 75%, respectively. Figure 2.8 shows the simulated and measured results of reflectivity of planner composite microwave absorber with total thickness of 6.16 mm. Bandwidth of planner composite microwave absorber is from 3.1 to 18 GHz and 26.1 to 40 GHz. Results of absorber with uniform

75% by weight (25.71% by volume) of FCIP with 6.16 mm thickness is also shown in Figure 2.8.

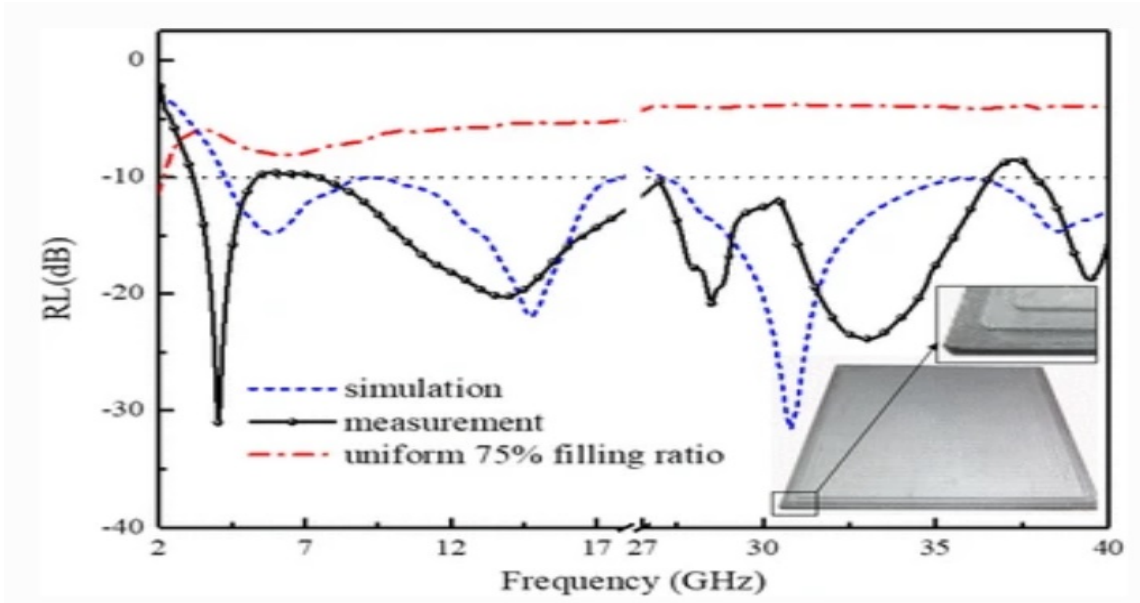


Figure 2.8: Simulated and measured results of reflectivity of planar composite microwave absorbers [8]

Reflectivity of FGM-40 and FGM-125 microwave absorbers manufactured by Laird Technology, Inc are shown in Figure 2.9 [9]. Thickness of FGM-40 is 40 mills (1mm) and FGM-125 is 125 mills (3.2mm). The bandwidth of FGM-40 is from 5.5 GHz to 8.5 GHz and bandwidth of FGM-125 is from 2.5 GHz to 12.5 GHz. These are thin, flexible, magnetically loaded silicene broadband microwave absorber. The data sheet of FGM-40 and FGM-125 is given in appendix A.

Reflectivity of An-series of broadband microwave absorbers manufactured by Laird Technology, Inc as shown in Figure 2.10 [10]. These microwave absorbers are lightweight, flexible and polyurethane foam sheets. Reflectivity of Data sheet of AN-series of absorber is given in appendix A.

## 2.3 FSS Microwave Absorbers

R. Vashisth et al [11] designed and fabricated broadband microwave absorber having reflectivity better than -10 dB in the frequency range of 3.95 to 8.2 GHz. They realized microwave absorber by embedding the FSS layer between two CISR sheets

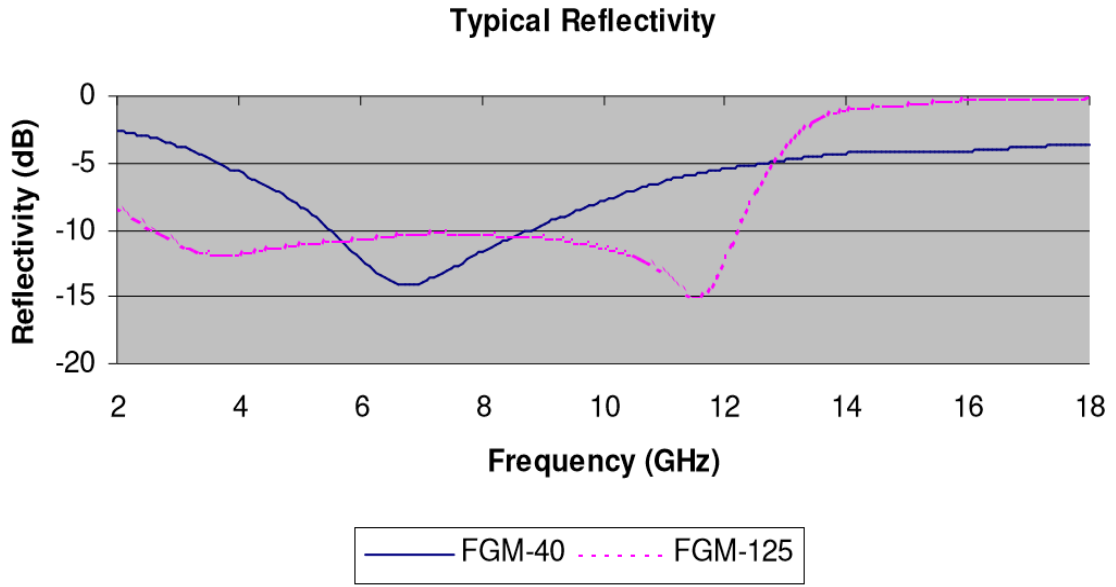


Figure 2.9: Reflectivity of FGM-40 and FGM-125 [9]

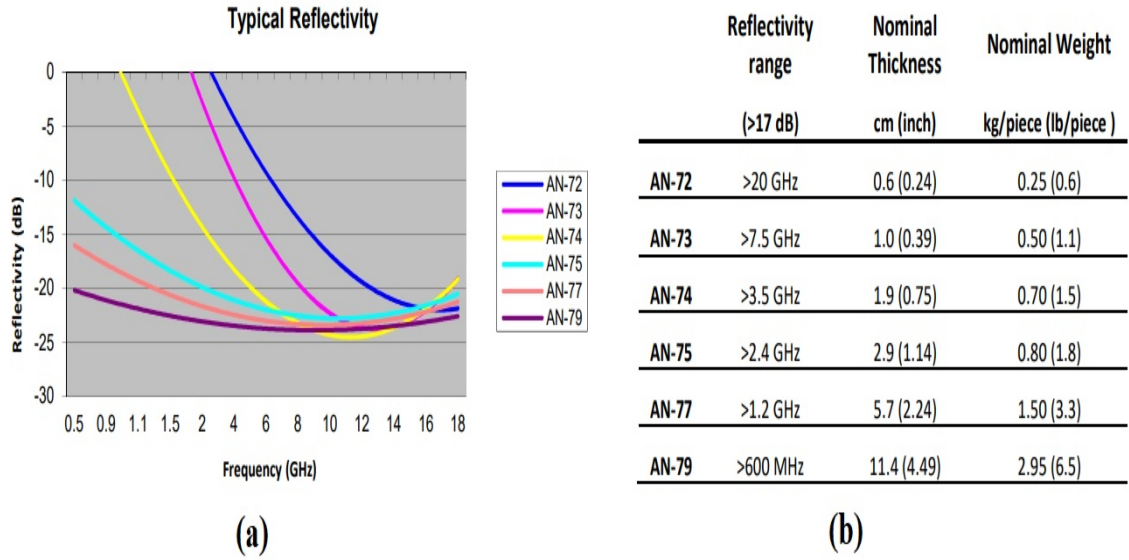


Figure 2.10: Reflectivity of AN-series of microwave absorbers [10]

as shown in Figure 2.11. Two CISR sheets were fabricated with 24% and 33% of CI powder by volume and their  $\epsilon_r$  and  $\mu_r$  values are calculated by RDWG method. The FSS layer consists of three consecutive conducting loops on FR4 substrate of thickness of 0.02 mm which is printed on 0.9 mm FR4. Figure 2.12 shows simulated and measured reflectivity of microwave absorber and two layer absorber without FSS. The bandwidth of composite microwave absorber is better than -11 dB from 3.95 to 8.2 GHz.

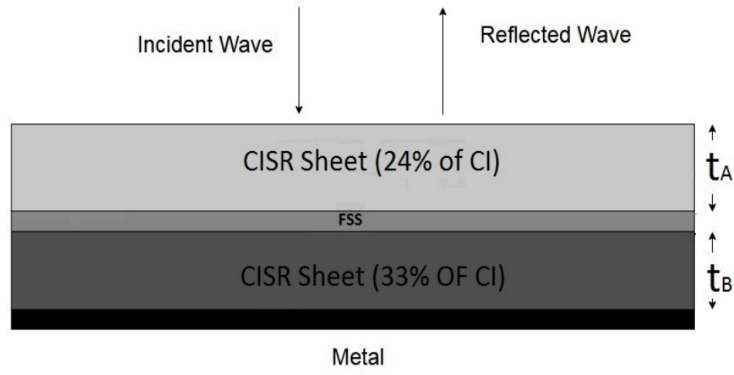


Figure 2.11: Broadband microwave absorber embedded with FSS layer,  $t_A = t_B = 2.7$  mm and FSS thickness is 0.92 mm [11]

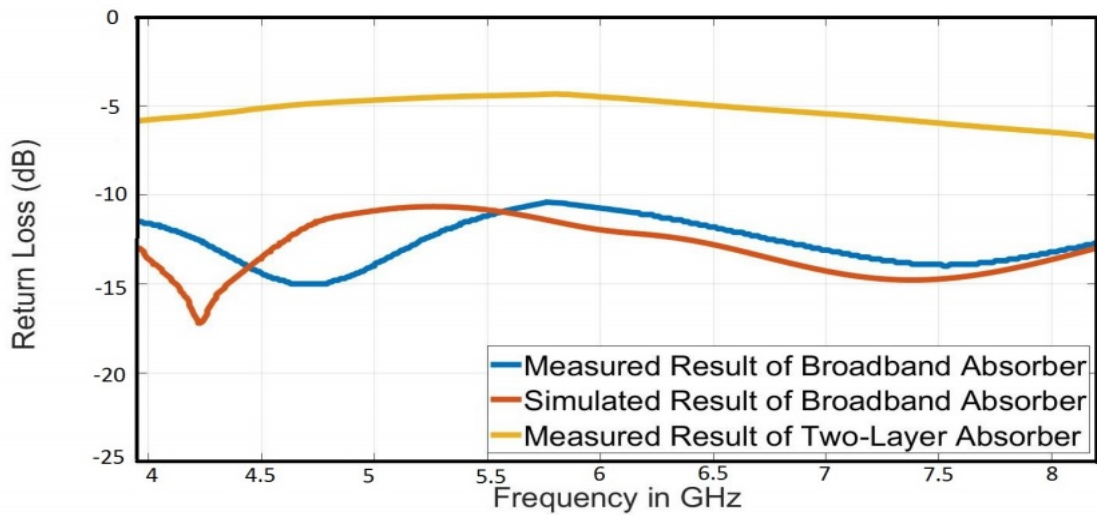


Figure 2.12: Simulated and measured result of broadband absorber and two layer absorber (without FSS) [11]

Wei Yuan et al [12] reported a microwave absorber which consists of edge-split square-loop FSS embedded in two sheets of silicon rubber filled with carbonyl iron (magnetic sheet). Two different magnetic sheets are prepared and  $\epsilon_r$  and  $\mu_r$  are calculated by coaxial air line method from measuring S-parameters. Figure 2.12 shows layers of composite microwave absorber and geometry of FSS. In Figure 2.13 (b),  $P=15$ mm,  $L=13$ mm,  $W=2$ mm and  $S=3.25$ mm. Reflectivity of composite microwave absorber is better than -10 dB over frequency range of 4 to 18 GHz as shown in Figure 2.14. Sample 1 is two layer microwave absorber without FSS and sample 2 is FSS embedded in two magnetic sheets.

Hai-Yan Chen et al [14] have designed absorbers which involve single-layer FSS and double-layer FSS embedded in polymer composites filled with carbonyl iron and

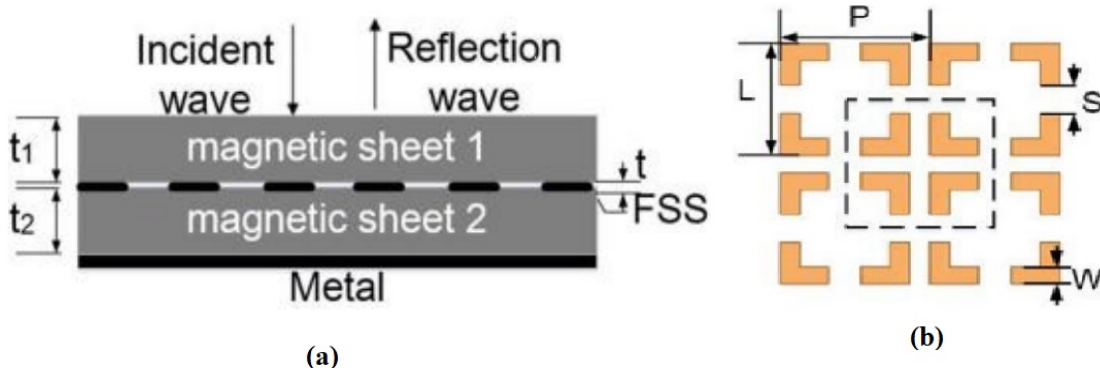


Figure 2.13: (a) The composite microwave absorber embedded with a FSS layer. The thickness of each layer is  $t_1=t_2=1\text{mm}$ ,  $t=0.2\text{mm}$ . (b) Geometry of FSS [12]

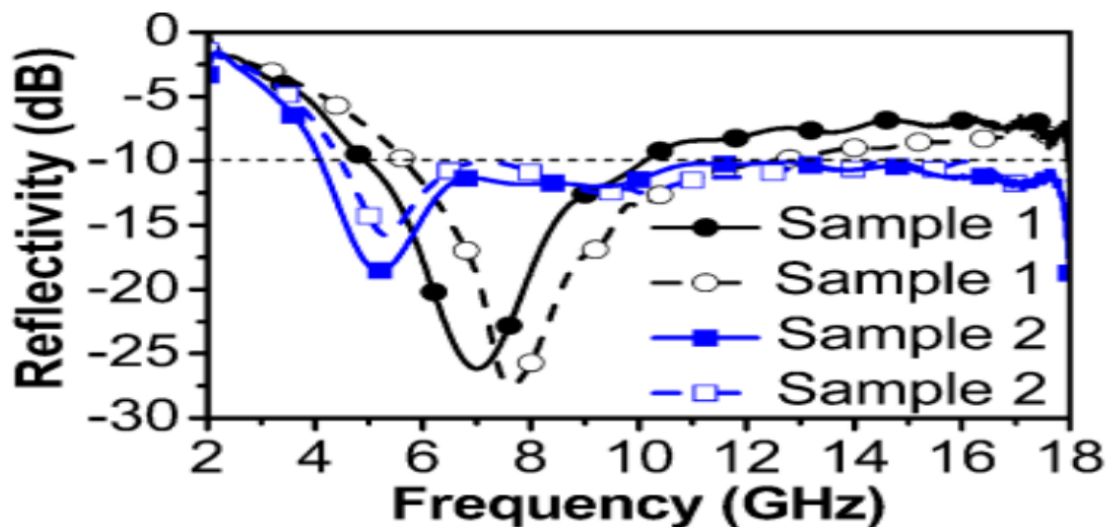


Figure 2.14: The simulated (dotted curve) and measured (solid curves) reflectivity of samples [12]

$CO_2Z$  ferrite. Figure 2.15 shows simulated and measured results for single layer FSS embedded microwave absorber and double layer FSS embedded microwave absorber. The thickness for both absorbers are 2 mm and thickness of all FSS are 0.017 mm. They reported operating bandwidth of 1.08 to 3.02 GHz by double-layer FSS case for microwave absorbers.

H. Xu et al [15] have embedded a conductor square loop FSS between layers of EW (a type of CI powder) and flaky CI powder in silicon rubber matrix to fabricate metamaterial absorber. Silicone rubber has 70% EW by weight (25% EW by volume) and 60% flaky CI powder by weight (17.5% flaky CI powder by volume). The thickness of both the layers are 1 mm and that of FSS is 0.017 mm. Figure 2.16 shows the simulated and measured reflectivity of the radar absorbing material (RAM)

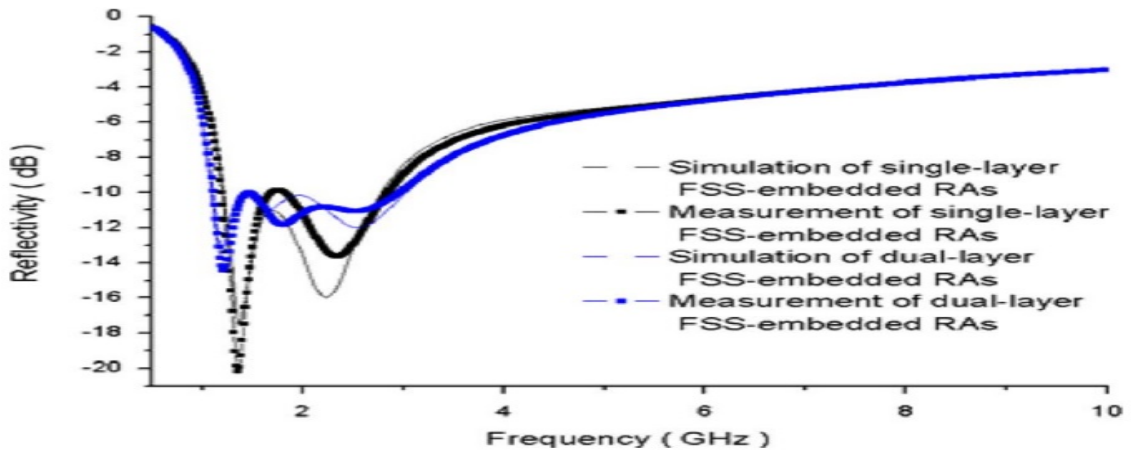


Figure 2.15: simulated and measured results for single layer FSS embedded microwave absorber and double layer FSS embedded microwave absorber.[14]

with and without the FSS. They reported reflectivity of RAM better than -10 dB over frequency range of 5.35 to 18 GHz.

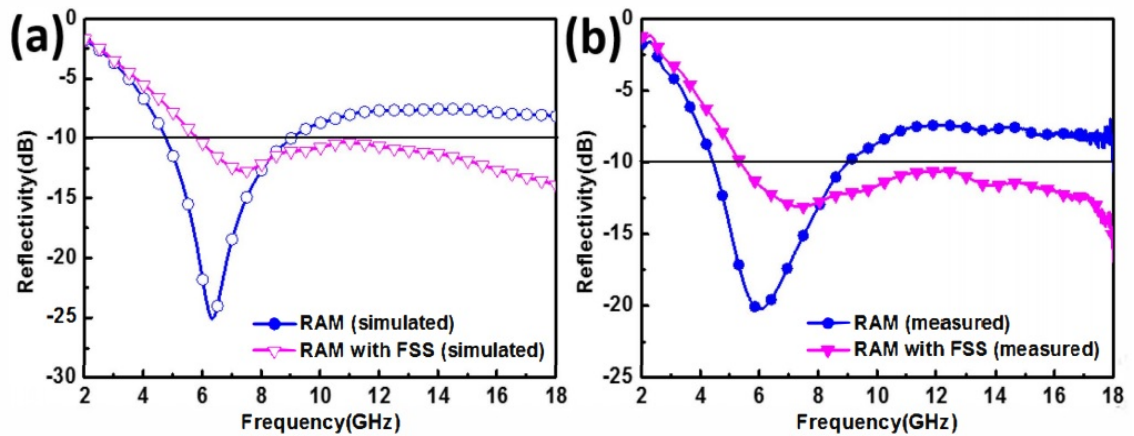


Figure 2.16: (a) Simulated reflectivity of the RAM and the RAM with FSS and (b) the measured reflectivity of the RAM and the RAM with FSS [15]

M. Zhao et al [16] have fabricated and measured performance of metallic pixelated FSS without resistors ( $100 \Omega$ ) and with resistors. Figure 2.17 shows the measured and simulated reflectivity curves of resistor loaded pixelated FSS (RPFSS) and pixelated FSS without resistors. They observed two strong absorption peaks below -6 dB in pixelated FSS with resistors in 3.08 to 6 GHz band.

P. Ranjan et al [17] have reported a pixelated FSS metamaterial absorber with six discrete bands of absorptions at 7.6, 10.1, 13.3, 14.7, 15.8 and 16.7 GHz. They have designed and fabricated the pixelated structure on FR4 substrate with thickness of



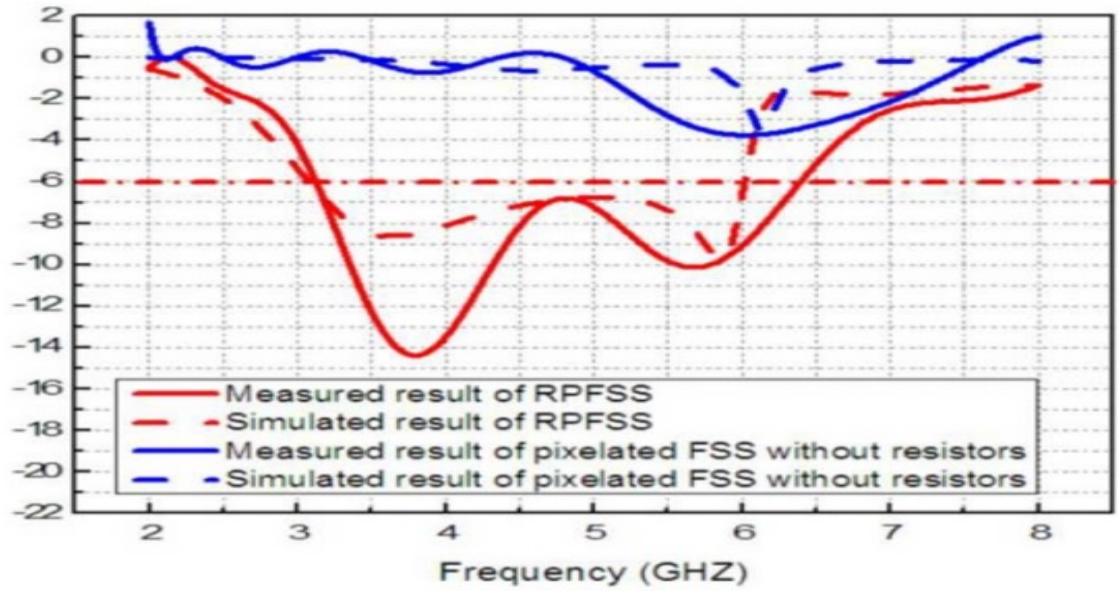


Figure 2.17: the measured and simulated reflectivity curves of resistor loaded pixelated FSS (RPFSS) and pixelated FSS without resistors [16]

3.2 mm which has more than 90% absorptivity at six discrete bands under normal incidence as shown in Figure 2.18.

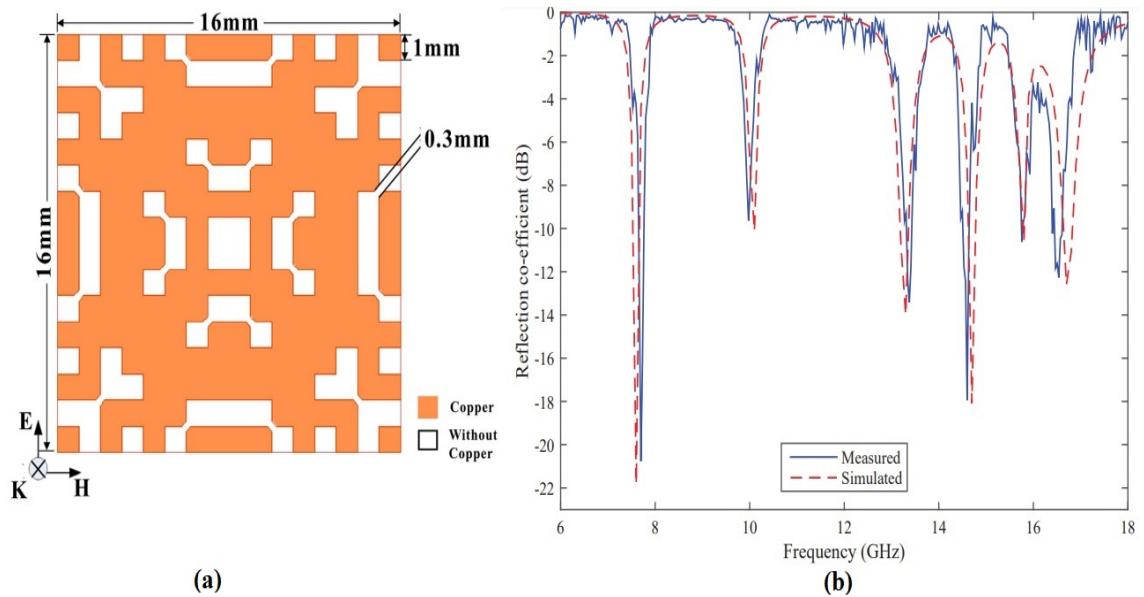


Figure 2.18: (a) Pixelated FSS geometry and (b) The simulated (dotted curve) and measured (solid curves) reflectivity of pixelated FSS metamaterial absorber [17]

## 2.4 Research gap

A very thin and light in weight microwave absorber are required in many applications where physical space is limited. These absorbers should be polarization-insensitive. In the first approach, the number of layers and their thickness must be increased to obtain ultra-wideband absorption using optimization technique. The second approach which reduced the structure thickness drastically by incorporating FSS structure. These structure should be either conventional type or pixelated type FSS.

The existing design technique using multilayer microwave absorber reported in the literature have various limitations such as they do not cover lower frequency (L and S band) bands. These multilayer absorber should work fine in space environment. For it, the Total Mass Loss (TML) and Collected Volatile Condensable Material (CVCM) values of designed multilayer microwave absorber should be less than 1.0% and 0.1%, respectively.

Microwave absorber using conventional type and pixelated FSS are discussed in the literature survey. The reflectivity of pixelated microwave absorber is not better than -6 dB which is very less. Even the authors [16] used resistance in between pixels to get broadband absorption. The reflectivity is quite less for many applications. The design complexity of conventional type FSS microwave absorber is quite high. The reflectivity of these absorber may vary with slight variation in dimension of either FSS or thickness of microwave absorber. The design of less sensitive microwave absorber is needed for many applications.



## References

- [1] Myung-Jun Park, Jaeho Choi and Sung-Soo Kim, "Wide bandwidth pyramidal absorbers of granular ferrite and carbonyl iron powders," *IEEE Transactions on Magnetics*, vol. 36, no. 5, pp. 3272-3274, Sept 2000.
- [2] Yong-Bao Feng, Tai Qiu, Chun-Ying Shen and Xiao-Yun Li, "Electromagnetic and absorption properties of carbonyl iron/rubber radar absorbing materials," *IEEE Transactions on Magnetics*, vol. 42, no. 3, pp. 363-368, March 2006.
- [3] R. Vashisth, D. Ghodgaonkar and S. Gupta, "Permittivity and Permeability Measurements of CISR sheets for Microwave Absorber Applications," *2018 IEEE International RF and Microwave Conference (RFM)*, 2018, pp. 359-362.
- [4] D.K. Ghodgaonkar, V.K. Varadan and V.V. Varadan, "Microwave Dielectric and Magnetic Properties of Carbonyl Iron Powder Loaded Silicon Rubber Sheets," *Journal of Wave Material Interaction*, Vol. 8, pp.171-184,1994.
- [5] Ma, X.T., Jiang, Z.P., Wang, F.S.D. H. Wang, Y. Li B. Xu."Numerical study of thermal effect in silicone rubber filled with carbonyl iron powder under microwave radiation." *Journal of Materials Science* volume 56, pp. 10264–10281 (2021).
- [6] Yonggang Xu, Liming Yuan, Xiaobing Wang, Deyuan Zhang, "Two-step milling on the carbonyl iron particles and optimizing on the composite absorption, " *Journal of Alloys and Compounds*, Vol 676, 2016, pp. 251-259.
- [7] X. Ren, H.Fan, Y.Cheng, "Microwave absorption properties of double-layer absorber based on carbonyl iron/barium hexaferrite composites, " *Applied Physics A* 122, Article number 506 , 2016. <https://link.springer.com/article/10.1007%2Fs00339-016-0041-8>.

- [8] Saichao Dang, Yang Lin, Xuezhong Wei Hong Ye, "Design and preparation of an ultrawideband gradient triple-layered planar microwave absorber using flaky carbonyl iron as absorbent." *Journal of Materials Science: Materials Electron* 29, 17651–17660 (2018).
- [9] <https://www.laird.com/products/microwave-absorbers/microwave-absorbing-elastomers-and-films/eccosorb-fgm>
- [10] <https://www.laird.com/products/microwave-absorbers/microwave-absorbing-foams/eccosorb-an>
- [11] R. Vashisth, D. Ghodgaonkar and S. Gupta, "Design and Fabrication of Broadband Microwave Absorber using FSS embedded in CISR sheets," *2018 IEEE MTT-S International Microwave and RF Conference (IMaRC)*, Kolkata, India, Dec 2018, pp. 1-4.
- [12] W. Yuan, Q. Chen, Y. Xu, H. Xu, S. Bie and J. Jiang, "Broadband Microwave Absorption Properties of Ultrathin Composites Containing Edge-Split Square-Loop FSS Embedded in Magnetic Sheets," *IEEE Antennas and Wireless Propagation Letters*, vol.16, pp. 278-281, 2017.
- [13] Linbo Zhang, Peiheng Zhou, Huibin Zhang, Lijuan Lu, Guorui Zhang, Haiyan Chen, Haipeng Lu, Jianliang Xie, and Longjiang Deng, "A Broadband Radar Absorber Based on Perforated Magnetic Polymer Composites Embedded With FSS," *IEEE Transactions on Magnetics*, vol. 50, no. 5, pp. 1-5, May 2014.
- [14] H. Chen, H. Zhang and L. Deng, "Design of an Ultra-Thin Magnetic-Type Radar Absorber Embedded With FSS," *IEEE Antennas and Wireless Propagation Letters*, vol. 9, pp. 899-901, 2010.
- [15] Haibing Xu, Shaowei Bie and Jianjun Jiang, "Ultra-broadband and polarization-insensitive metamaterial absorber based on frequency selective surface," *2016 10th International Congress on Advanced Electromagnetic Materials in Microwaves and Optics (METAMATERIALS)*, China, 2016, pp. 400-402.

- [16] Mengyun Zhao, Xiaowei Yu, Qiao Wang, Peng Kong, Yun He, Ling Miao, Jianjun Jiang, "Novel Absorber Based on Pixelated Frequency Selective Surface Using Estimation of Distribution Algorithm," *IEEE Antennas and Wireless Propagation Letters*, vol. 14, pp. 1467-1470, 2015.
- [17] P. Ranjan, A. Choubey, Santosh Kumar Mahto, Rashmi Sinha, "A six-band ultra-thin polarization-insensitive pixelated metamaterial absorber using a novel binary wind driven optimization algorithm," *Journal of Electromagnetic Waves and Applications*, vol. 32, pp. 2367-2385, August 2018.

## Chapter 3

# Fabrication of Carbonyl Iron filled Silicon Rubber Sheets

### 3.1 Introduction

Various matrix materials like silicone rubber[1-7], natural rubber[8,9], epoxy resin[10,11] etc. are studied for designing planar microwave absorbers. Materials such as Carbonyl Iron (CI) powder[1-4][6-7][12], carbon black [9], graphite powder[13], Multi Wall carbon Nano Tube (MWCNT) [11][14] etc are used as filler materials in microwave absorbers. Composite materials with desired electromagnetic property are obtained by varying filler concentration in matrix materials and thickness.

CI powder is cheaper and has more saturation magnetism. Silicone rubber is a material which is stable against most chemicals and have wide operating temperature range (-100°to 315°) [13]. Carbonyl Iron Filled silicon Rubber (CISR) sheets are fabricated by mixing silicon rubber and carbonyl iron (CI) powder in two roll mill assembly [1-4][6-7].

### 3.2 Silicon Rubber

#### 3.2.1 Introduction

Silicone rubber is an elastomer (rubber-like material) composed of mostly silicone along with carbon, hydrogen, and oxygen. The silicon rubber structure is shown in Figure 3.1. Silicon rubber molecule has higher binding energy. The siloxane

bond (-Si-O-Si-) that form backbone of silicone are highly stable. At 433 KJ/mol, their binding energy is higher than that of carbon bonds (C-C), at 355 KJ/mol. Thus, compare to common organic polymer, silicon rubber have high heat resistance, chemical resistance and provide better electric insulation. These properties helps in making it the best matrix material for microwave absorber application. The matrix material is the component that holds the functional filler together to form the bulk of the composite. High elasticity, high compressibility and excellent resistance to cold temperatures are due to lower inter molecular force and helical molecular structure of silicon rubber. Methyl group in silicone rubber structure is located on the outside of coil structure that can rotate freely. This is the reason for its distinctive interfacial properties such as water repellency and good releasability [15].

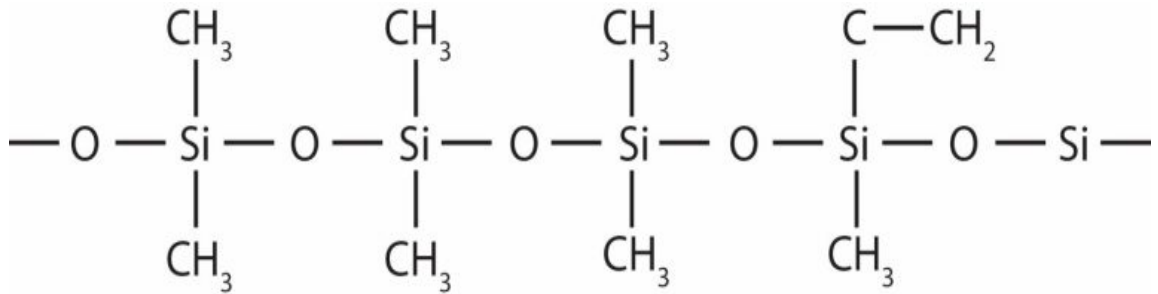


Figure 3.1: Silicon rubber Structure

## 3.2.2 Various Properties of silicon rubber

### 3.2.2.1 Heat and Cold Resistance

Silicon rubber withstand high and cold temperatures far better than other organic rubber. Silicon rubber can withstand 150°C temperature indefinitely with almost no change in its properties. It can survive temperature of 200°C for 20,000 hours and some products can survive temperature of 350°C for short period. It also has excellent resistance to cold temperatures [15].

### 3.2.2.2 Thermal Property

Thermal expansion coefficient of silicon rubber is very high. Volumetric and linear thermal expansion coefficients are in the ranges  $5.9$  to  $8 \times 10^{-4}/^{\circ}\text{C}$  and  $2$  to

$3 \times 10^{-4}/^{\circ}C$  respectively. Additions of fillers lower thermal expansion coefficients. Thermal conductivity of silicon rubber increases with increase in filler concentration. Silicon rubber is having good flame resistance property [15].

### **3.2.2.3 Mechanical Property**

Silicon rubber is a resilient material which can store more mechanical energy than any other commonly used materials. Ultimate tensile strength of silicon rubber varies from few hundreds to 1500 psi. Ultimate elongation of silicon rubber varies from 100% to 1000%. The Specific gravity of silicon rubber is in range of 1.1 to 1.6  $g/cm^3$

The shore A hardness range of silicon rubber is from 25 to 75. Very broad range of hardness is achieved through combination of molecular structure of silicon rubber and inert fillers. The value of coefficient of friction is in the range of 0.25 to 0.75. Surface of silicon rubber becomes very slippery when in contact with fluids [15].

### **3.2.3 Types of Silicon Rubber**

There are mainly two types of silicone rubber, namely, high consistency rubber (HCR) and liquid silicone rubber (LSR). Viscosity of HCR is higher than that of LSR. HCR contains polymers with a high molecular weight and long polymer chains. LSR consists of liquid silicone material that has very low viscosity, which allows the material to be cast into rubber sheets. Very low viscosity of LSR allows to cast into rubber sheets [16].

## **3.3 Carbonyl Iron Powder**

Carbonyl iron powder is widely used in the field of electromagnetic shielding and absorbing materials [1-4] over a wide frequency range because it has high curie temperature, good temperature stabilization, higher specific saturation magnetization intensity, high value of microwave permeability and high dielectric constant. CI powder is produced from normal scrap iron, which is finely ground and reacted with carbon monoxide at increased temperatures under high pressure. This process yields iron pentacarbonyl, an oily yellow fluid [17]. At this stage, the impurities present in

the scrap iron can be easily removed. Iron pentacarbonyl is distilled and obtained in very high purity. The compound is then heated until it decomposes again into its constituents. Carbon monoxide released during this treatment can be recycled for the synthesis of iron pentacarbonyl. The iron, however, is deposited in the form of high purity, microscopically small spherical particles of exactly defined structure and size.

### 3.3.1 Chemical and Physical Property

Chemical composition of CI powder is minimum 99.5% of Iron, maximum 0.04% of Carbon, maximum 0.01% of Nitrogen and maximum 0.3% of Oxygen. The CI powder is gray in color, fine-grained powder with mechanically soft and spherical in shape with particle size of 6  $\mu\text{m}$  to 10  $\mu\text{m}$  in diameter[3-4]. The picture of CI powder is shown in Figure 3.2. Chemical and physical properties of CI powder are given in Table 3.1 as well as in appendix D.



Figure 3.2: Carbonyl Iron Powder [19]

Sr. No	Property	Value
1	Molecular Weight	55.85
2	Appearance	Gray powder
3	Melting Point	1535°C
4	Boiling Point	2750
5	Density	7.86 g/cm <sup>3</sup> (25°C)
6	Electrical Resistivity	9.71 $\mu \cdot \text{cm}$ (20°C)
7	Heat of Fusion	3.56 Cal/gm-mole
8	Heat of Vaporization	84.6 KCal/gm atom at 2750°C
9	Poisson's Ratio	0.29
10	Specific Heat	0.106 Cal/g/K @ 25°C
11	Thermal Conductivity	0.804 W/cm/K (298.2 K)
12	Thermal Expansion	(25 °C) 11.8 $\mu\text{m} \cdot \text{m}^{-1} \cdot \text{K}^{-1}$

Table 3.1: Carbonyl Iron powder Property [18]

### 3.4 Fabrication of Carbonyl iron filled Silicon Rubber (CISR) Sheets

Fabrication of CISR sheets requires two most common machines used in rubber industry for mixing shore A 40 HCR silicon rubber and CI powder. These machine are internal mixer and two-roll mill as shown in Figures 3.3 and 3.4. The internal mixer produces complex flow paths and high shear forces, ensuring a uniform dispersion of CI powder and the breakdown of particulate filler additives. A consequence of the high shear forces is the rapid rise in material temperature during mixing. The rubber mix is discharged from the internal mixer on to the two-roll mill as shown



in Figure 3.4. Two rollers are rotating in opposite direction and mixture are put on top in between them. Distance between two roller varies with the thickness of sheets. A sheet is formed at the bottom of the two-roll mill when the roller rotates. This process is carried out at ambient temperature with RPM (Revolution Per Minutes) of 10-15 as per standard practice in the rubber industry as shown in Figure 3.4. Molding of CISR sheets is carried out with the pressure of  $150 \text{ kg/cm}^2$  in a hydraulic press under the temperature of  $160^\circ\text{C}$ . The vulcanising ingredients name peroxide are added at this stage without the danger of premature vulcanisation occurring in rubber sheets. Vulcanization of CISR sheets is carried out at Ami Polymer Pvt Ltd, Silvassa, Dadar and Nagar Haveli, India [3-4]. Vulcanised rubber is tough, strong and highly elastic. Density of CI powder is  $7.8 \text{ g/cm}^3$  and density of HCR silicon rubber is  $1.1 \text{ g/cm}^3$ . CISR sheets are formed by mixing CI powder(0 to 57 % by volume)[20] in silicone rubber. Specific gravity of CISR sheets are in the range of  $1.1\text{g/cm}^3$  to  $4.45\text{g/cm}$  as the CI powder concentration changes from 0% to 50% by volume.

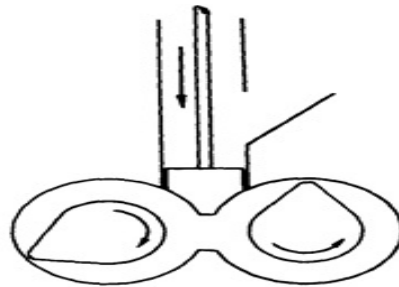


Figure 3.3: Internal mixture used for mixing Silicon rubber and CI powder

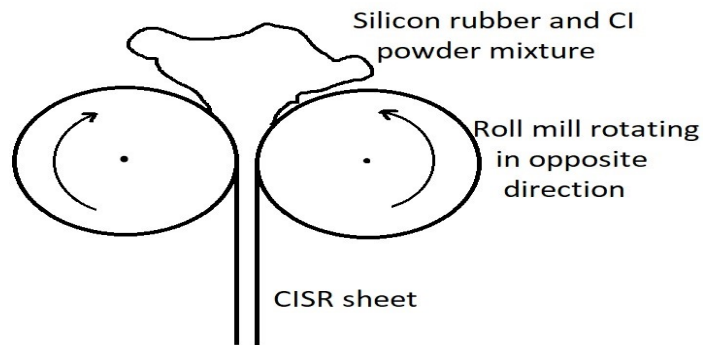


Figure 3.4: Fabrication process of CISR sheets on two-roll mill assembly

## References

- [1] Yuping Duan, Guofang Li, Lidong Liu and Shunhua Liu, "Electromagnetic properties of carbonyl iron and their microwave absorbing characterization as filler in silicone rubber," *Indian Academy of Sciences Bull. Material Science*, Vol. 33, No. 5, October 2010, pp. 633–636.
- [2] Yonggang Xu, Deyuan Zhang, Jun Cai, Liming Yuan, Wenqiang Zhang, "Microwave absorbing property of silicone rubber composites with added carbonyl iron particles and graphite platelet", *Journal of Magnetism and Magnetic Materials*, Volume 327, 2013, Pages 82-86.
- [3] R. Vashisth, D. Ghodgaonkar and S. Gupta, "Design and Fabrication of Broadband Microwave Absorber using FSS embedded in CISR sheets," *2018 IEEE MTT-S International Microwave and RF Conference (IMaRC)*, 2018, pp. 1-4.
- [4] R. Vashisth, D. Ghodgaonkar and S. Gupta, "Permittivity and Permeability Measurements of CISR sheets for Microwave Absorber Applications," *2018 IEEE International RF and Microwave Conference (RFM)*, 2018, pp. 359-362.
- [5] Hua Zou, Shuhuan Li, Liqun Zhang, Shani Yan, Hanguang Wu, Shuai Zhang, Ming Tian, "Determining factors for high performance silicone rubber microwave absorbing materials", *Journal of Magnetism and Magnetic Materials*, Volume 323, Issue 12, 2011, Pages 1643-1651.
- [6] Yonggang Xu, Deyuan Zhang, Jun Cai, Liming Yuan, Wenqiang Zhang, "Microwave absorbing property of silicone rubber composites with added carbonyl iron particles and graphite platelet", *Journal of Magnetism and Magnetic Materials*, Volume 327, 2013, Pages 82-86.

- [7] Duan, Y., Li, G., Liu, L. et al. "Electromagnetic properties of carbonyl iron and their microwave absorbing characterization as filler in silicone rubber". *Bull Material Science* 33, 633–636 (2010).
- [8] Kiadtisak Salayong, Titipong Lertwiriayaprapa, Kittisak Phaebua, Prayoot Akkaraekthalin, Hsi-Tseng Chou, "Electromagnetic Absorber Made by Natural Rubber", *IEICE Transactions on Communications*, 2019, Volume E102.B, Issue 2, Pages 189-196.
- [9] Ahmed A. Al-Ghamdi, Omar A. Al-Hartomy, Falleh R. Al-Solamy, Nikolay Dishovsky, Petrunka Malinova, Gabriela Atanasova, Nikolay Atanasov, "Conductive carbon black/magnetite hybrid fillers in microwave absorbing composites based on natural rubber", *Composites Part B: Engineering*, Volume 96, 2016, Pages 231-241.
- [10] Yu Liu, Delong He, Olivier Dubrunfaut, Anne Zhang, Hanlu Zhang, "GO-CNTs hybrids reinforced epoxy composites with porous structure as microwave absorbers". *Composites Science and Technology*, Elsevier, 2020, 200, pp.108450.
- [11] Wei Chen, Xiangnan Zheng, Xingyang He, Ying Su, Jun Wang, Jin Yang, Shun Chen, Zhengqi Zheng, "Achieving full effective microwave absorption in X band by double-layered design of glass fiber epoxy composites containing MWCNTs and Fe<sub>3</sub>O<sub>4</sub> NPs", *Polymer Testing*, Volume 86, June 2020, 106448.
- [12] Mingxun Yu, Xiangcheng Li, Rongzhou Gong, Yanfei He, Huahui He, Peixiang Lu, "Magnetic properties of carbonyl iron fibers and their microwave absorbing characterization as the filler in polymer foams", *Journal of Alloys and Compounds*, Volume 456, Issues 1–2, 2008, Pages 452-455.
- [13] Azizurrahman Ansari and Mohammad Jaleel Akhtar, "Co/graphite based light weight microwave absorber for electromagnetic shielding and stealth applications", *2017 Material Research. Express* Volume 4, Number 1, 016304.
- [14] Patrizia Savi, Mario Miscuglio, Mauro Giorcelli, and Alberto Tagliaferro, "Analysis of Microwave Absorbing Properties of Epoxy MWCNT Composites," *Progress In Electromagnetics Research Letters*, Vol. 44, 63-69, 2014.

- [15] Wilfred Lynch, " Hand book on Silicon Rubber Fabrication", ISBN-10 : 0442249624 ISBN-13 : 978-0442249625.
- [16] HM Royal Materials distribution. An internet resource regarding HCR and LSR silicone rubber. Website at <https://hmroyal.com/blog/rtv-vs-hcr-vs-lsr-injection-molding/>
- [17] Iron powder of North Amreica. An internet resource regarding Fabrication of CI powder. Website at <https://iron-powder.com/types-of-iron-powder/cipms-carbonyl-iron-powder/>
- [18] American element, UK. An internet resource regarding property of CI powder. Website at <https://www.americanelements.com/carbonyl-iron-powder-7439-89-6>.
- [19] BASF.CN, Germany.An internet resource regarding CI powder. Website at <https://aerospace.basf.com/carbonyl-iron-powder.html>

## Chapter 4

# Characterization of CISR Sheets by using Coaxial Air Line Method, Rectangular Dielectric Waveguide Method

### 4.1 Introduction

For the design of microwave absorbers, it is necessary to measure the complex permeability and complex permittivity of materials used. Coaxial Air Line (coaxial airline)[1-4] method and Rectangular Dielectric Waveguide (RDWG) [5-8] are used to measure complex permittivity ( $\epsilon_r$ ) and complex permeability ( $\mu_r$ ) of CISR sheets. Coaxial airline method is used in the frequency range of 1 to 4 GHz and RDWG method is used in the frequency range of 3.95 to 8.2 GHz. For arbitrary concentration of CI powder in CISR sheets, polynomial approximate method is used for intermediate concentrations. Physical and mechanical properties such specific gravity is in the range of  $1.1 \text{ g/cm}^3$  to  $4.45 \text{ g/cm}^3$ , tensile strength is  $110.43 \text{ Kg/cm}^2$ , hardness is 61 shore A, elongation at breakdown is 352%, etc of CISR sheets are measured by Ami Polymer Pvt. Ltd, Dadar and Nagar Haweli, India. Total Mass Loss (TML) and Collected Volatile Condensable Material (CVCM) values is less than 1.0% and 0.1%, respectively. This test is performed in SAC, ISRO.

## 4.2 Coaxial Air Line Method (1 to 4 GHz)

The coaxial air line is used for calculation of  $\epsilon_r$  and  $\mu_r$  values from measured  $S_{11}$  and  $S_{21}$  of toroidal shaped samples. Coaxial air line measurement system consists of coaxial air line fixture, sections of coaxial cables and the VNA as shown in Figure 4.1 [1-4].

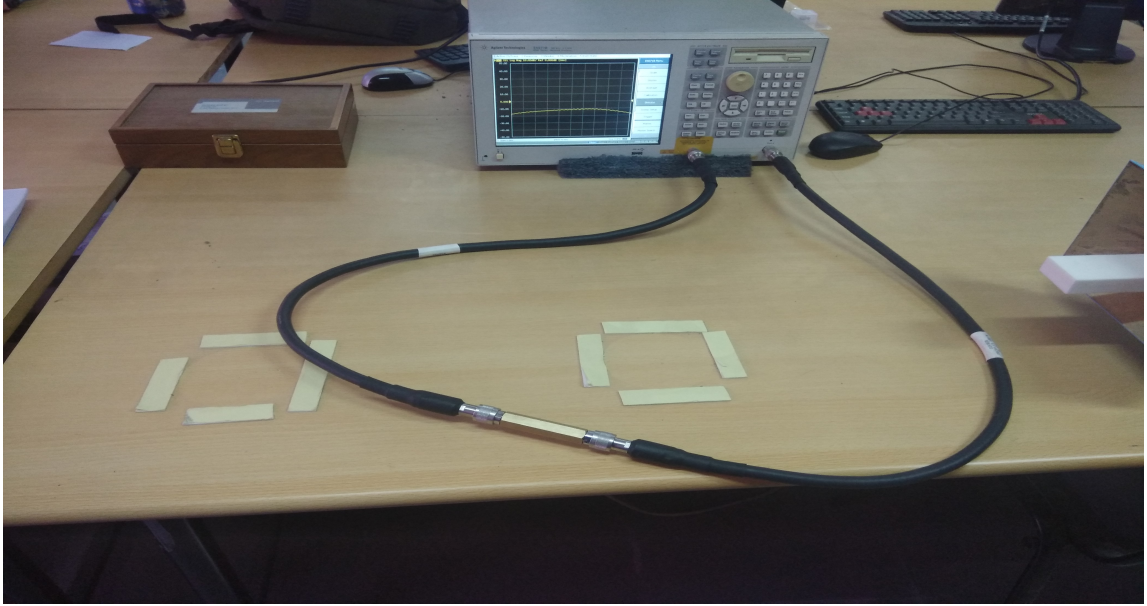


Figure 4.1: Photograph of coaxial air line system

The schematic diagram of coaxial air line fixture is shown in Figure 4.2. Figure 4.3 shows outer conductor, inner conductor, input/output N-type connectors and Teflon sleeve which are used in coaxial air line fixture. The photograph of coaxial air line fixture is shown in Figure 4.4. Photograph of toroidal shaped sleeve of CISR is shown in Figure 4.5.

Electronic calibration kit (N4690D E-Cal module DC-18GHz) of VNA is used for full-two calibration of coaxial air line measurement system using Open, short, load and through option [11]. The N4690D is a precision 2-port E-Cal module that supports 50-ohm N-type connectors. It is available in male/male (option M0M), female/female (option F0F), and male/female (option M0F) connector configurations.

For measurement of  $\epsilon_r$  and  $\mu_r$ , it is necessary to shift calibration planes from  $A$  to  $A'$  ( $T_1$ ) and  $B$  to  $B'$  ( $T_2$ ).  $T_3$  is the length of sample as shown in Figure 4.6. The

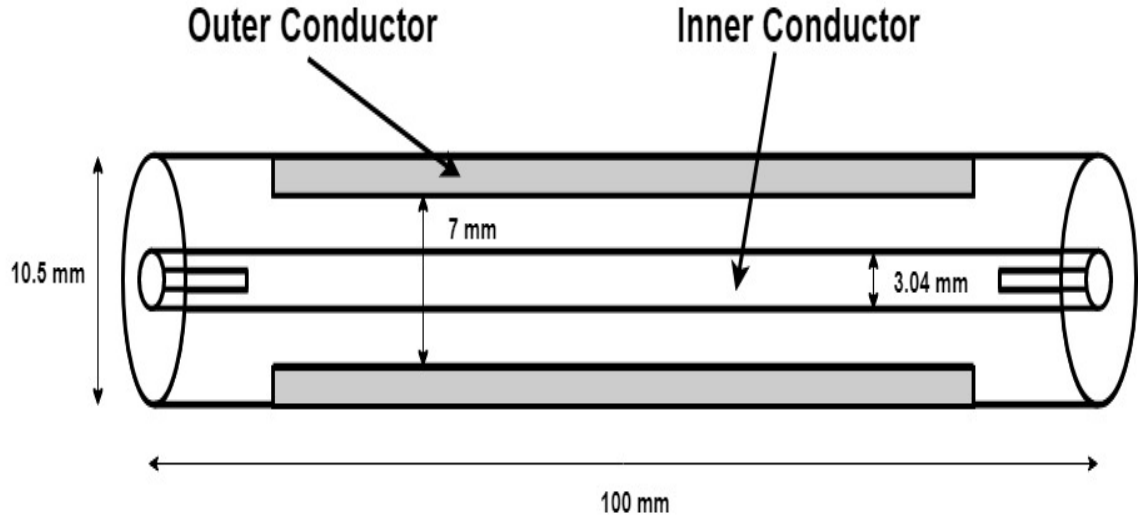


Figure 4.2: Schematic diagram of coaxial air line fixture [5]

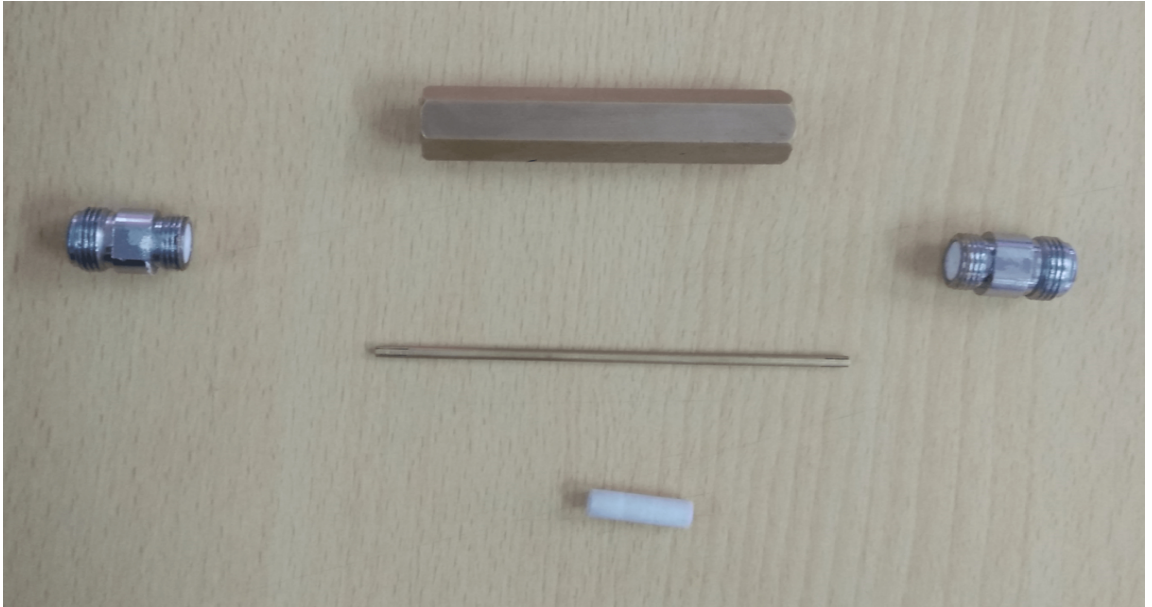


Figure 4.3: Components of coaxial air line fixture

calibration plane shifting equations are given in equations 4.1 and 4.2 [1].

$$S_{11\_A'} = S_{11\_A} e^{j2\beta T_1} \quad (4.1)$$

$$S_{21\_A',B'} = S_{21\_A,B} e^{j\beta(T_1+T_2)} \quad (4.2)$$

Where A and B are port 1 and port 2 of calibrated coaxial air line.

By assuming 20 mm long toroidal-shaped Teflon sleeve or air line,  $T_1$  and  $T_2$  are



Figure 4.4: The photograph of coaxial air line fixture



Figure 4.5: Photograph of toroidal shape sleeve CISR.

estimated by optimization. It is assume value of  $\epsilon_r$  for Teflon is  $2.08 - j0.08$  [12].

From  $S_{11A'}$  and  $S_{21A'B'}$ ,  $\epsilon_r$  measured and  $\mu_r$  measured values are calculated by using NRW method as shown in appendix B. The amplitude and phase of  $S_{21}$  (or  $S_{12}$ ) was within  $0.00 \pm 0.06$  dB and  $0.0 \pm 0.8^\circ$ , respectively. The amplitude and phase of  $S_{11}$  (or  $S_{22}$ ) were  $0.00 \pm 0.06$  dB and  $180.0 \pm 1.9^\circ$ , respectively. For materials such as CISR sheets using NRW method, the maximum error in  $\epsilon'$ ,  $\mu'$ ,  $\tan\delta_\epsilon (= \epsilon''/\epsilon')$  and  $\tan\delta_\mu (= \mu''/\mu')$  are 3.7%, 9.9%, 0.048 and 0.11, respectively [12].

Insert the toroidal shaped sample inside the coaxial air line as shown in Figure 4.7. The thickness of the toroidal shaped sample should be equal to or slightly less



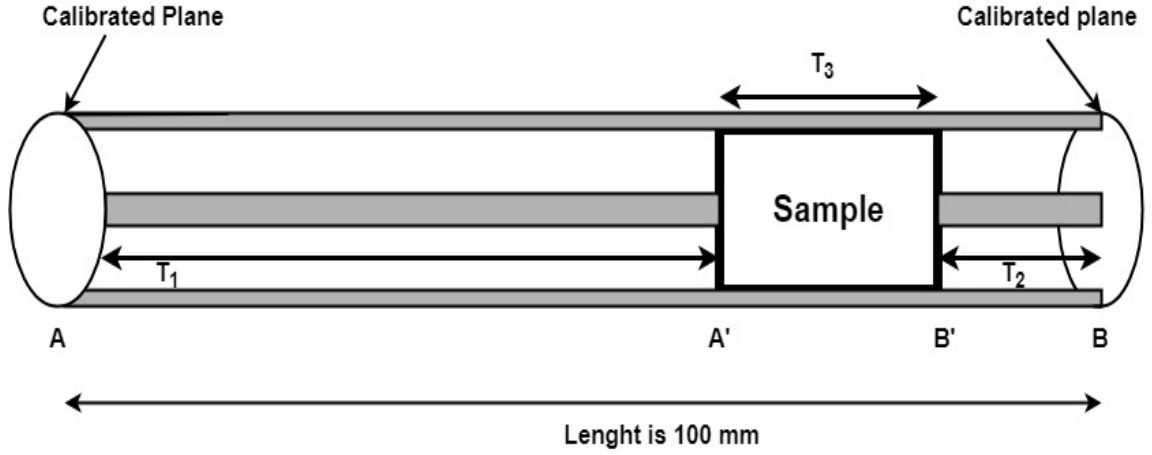


Figure 4.6:  $T_1$ ,  $T_2$  and  $T_3$  parameters inside the coaxial air line fixture

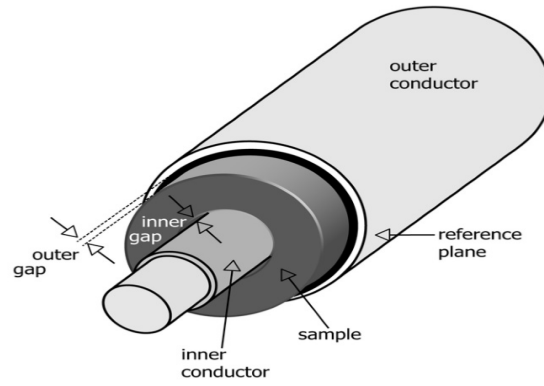


Figure 4.7: Sample inside the coaxial air line fixture [1]

than the size of a coaxial air line so that sample can slide without difficulty inside the coaxial air line. The air gap will be created between the sample and coaxial air line because of dimensional mismatch as shown in Figure 4.8.  $D_1$  and  $D_2$  are diameters of inner conductor and outer conductor of coaxial air line.  $d_1$  and  $d_2$  are the inner and outer diameter of toroidal-shaped sample. Air gap correction method must be used to avoid anomalies in the calculated values of  $\epsilon_r$  and  $\mu_r$  [1,2,4].  $\epsilon'$  corrected,  $\epsilon''$  corrected,  $\mu'$  corrected and  $\mu''$  corrected are given [1].

$$\epsilon'_{corrected} = \epsilon'_{measured} \frac{L_3(1 + \tan^2 \delta_\epsilon)[L_3 - L_1 \epsilon'_{measured}(1 + \tan^2 \delta_\epsilon)]}{L_2[L_3 - L_1 \epsilon'_{measured}(1 + \tan^2 \delta_\epsilon)]^2 + L_3^2 \tan^2 \delta_\epsilon} \quad (4.3)$$

$$\epsilon''_{corrected} = \epsilon'_{measured} \frac{L_3 \tan \delta_\epsilon}{L_3 - L_1 \epsilon'_{measured}(1 + \tan^2 \delta_\epsilon)} \quad (4.4)$$

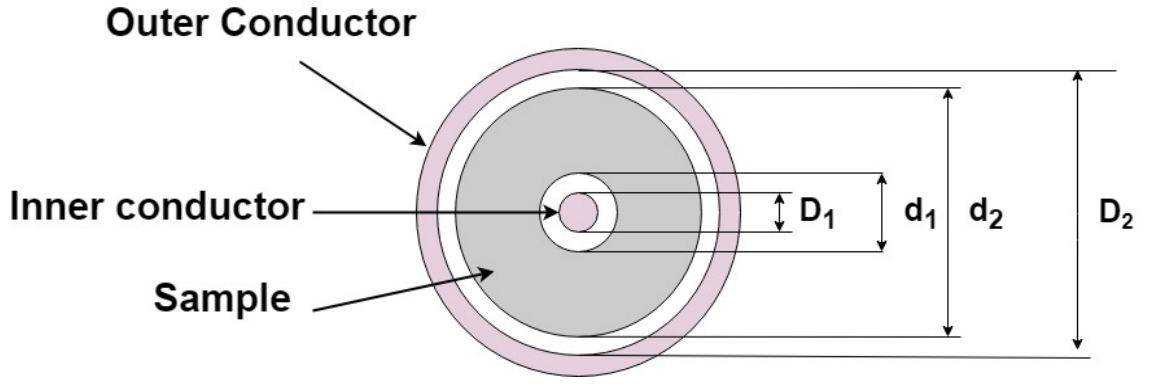


Figure 4.8: Schematic diagram of sample inside the coaxial airline fixture

$$\mu'_{corrected} = \frac{\mu'_{measured} L_3 - L_1}{L_2} \quad (4.5)$$

$$m\mu''_{corrected} = \mu''_{measured} \frac{L_3}{L_2} \quad (4.6)$$

Where :-

$$L_1 = \ln \frac{d_1}{D_1} + \ln \frac{D_2}{d_2} \quad (4.7)$$

$$L_2 = \ln \frac{d_2}{d_1} \quad (4.8)$$

$$L_3 = \ln \frac{D_2}{D_1} \quad (4.9)$$

These air gap correction formula are only valid for isotropic solid sample like Teflon. But for flexible materials like CISR sleeves, the effect of air gap can be removed only by careful design of CISR sleeves and calibrations with Teflon as the standard material. For accurate values of  $\epsilon_r$  and  $\mu_r$  of toroidal-shaped sleeves, the length should be close to odd multiple of  $\lambda/4$  [1]. In case of CISR sleeves, length should be between 4 mm to 6 mm for frequency range of 1 to 4 GHz.

### 4.3 RDWG Method (3.95 to 8.2 GHz)

Complex permittivity ( $\epsilon_r$ ), complex permeability ( $\mu_r$ ) and reflectivity of CISR sheets are measured using RDWG systems which are non-destructive in nature. Two RDWG systems have been designed, namely, WR-137 for 5.85 to 8.2 GHz and WR-187 for 3.95 to 5.85 GHz which are shown in Figure 4.9 and 4.10.

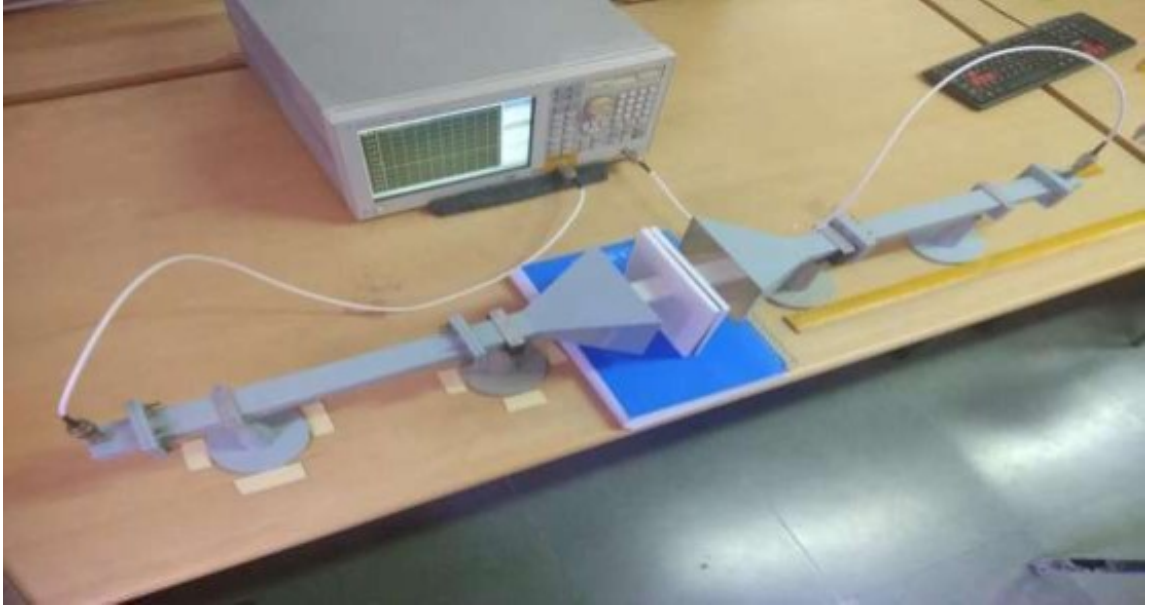


Figure 4.9: Photograph of WR-137 RDWG system for 5.85 to 8.2 GHz frequency range

RDWG systems consists of vector network analyzer (VNA), coaxial cables, coaxial to rectangular waveguide transitions, sections of metallic waveguides, standard gain horn antennas and section of dielectric waveguides. Agilent E5071 B model used as VNA. Section of metallic waveguide should be of more than few wavelength long. Standard gain horn antenna is used which act as a launcher for microwave signal and provide mechanical support. Teflon is used as a material for dielectric waveguides. A portion of dielectric waveguide (1.3 wavelengths in Teflon at center frequency) which is inserted into metallic rectangular waveguide is tapered for conversion of  $TE_{10}$  mode to  $E_{11}^y$  mode in dielectric waveguide as shown in Figure 4.11. The length of tapered dielectric waveguide section beyond the horn antenna is approximately 2 to 5 wavelengths at the center frequency. This length is required to avoid surface waves in dielectric waveguide [7].

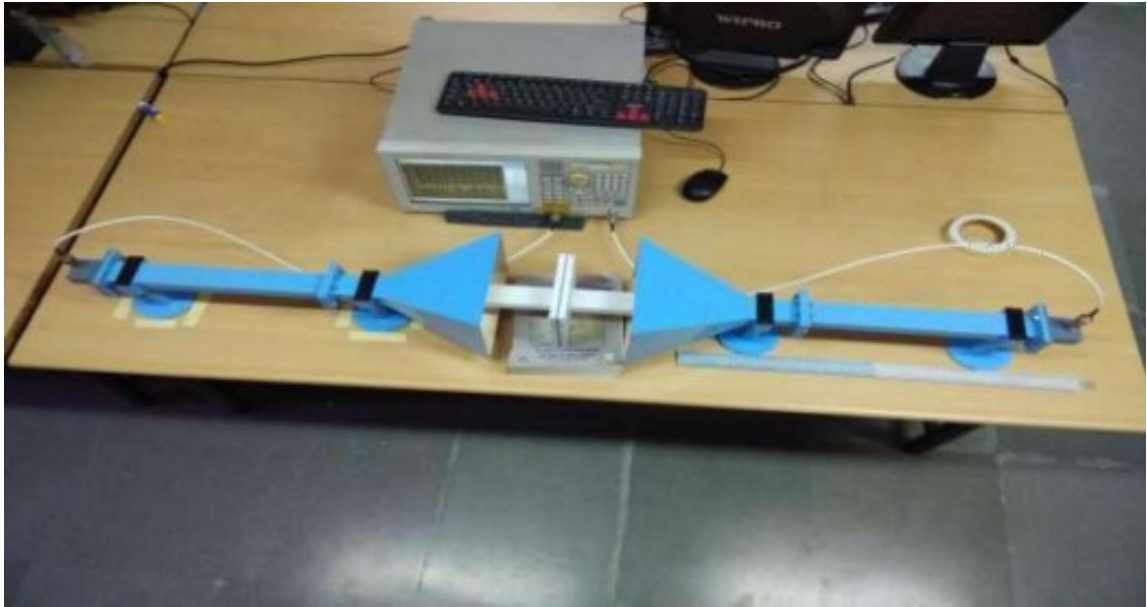


Figure 4.10: Photograph of WR-187 RDWG system for 3.95 to 5.85 GHz frequency range



Figure 4.11: Photograph of tapered dielectric waveguide section for WR-137 frequency bands

The TRL (Through, Reflect, Line) calibration method [5-8] and time domain gating in VNA are used to calibrate and remove all measurement errors associated with the RDWG systems due to multiple reflections. TRL calibration model of VNA is used for RDWG systems. The through standard is realized by keeping the distance between two tip's of dielectric waveguides equal to zero as shown in Figure 4.12. The reflect standard is realized by placing a 2.5 mm copper sheet between two tip's of dielectric waveguides as shown in Figure 4.13. The line standard is obtained by separating the tip's of dielectric waveguides by a distance of  $\lambda/4$  at

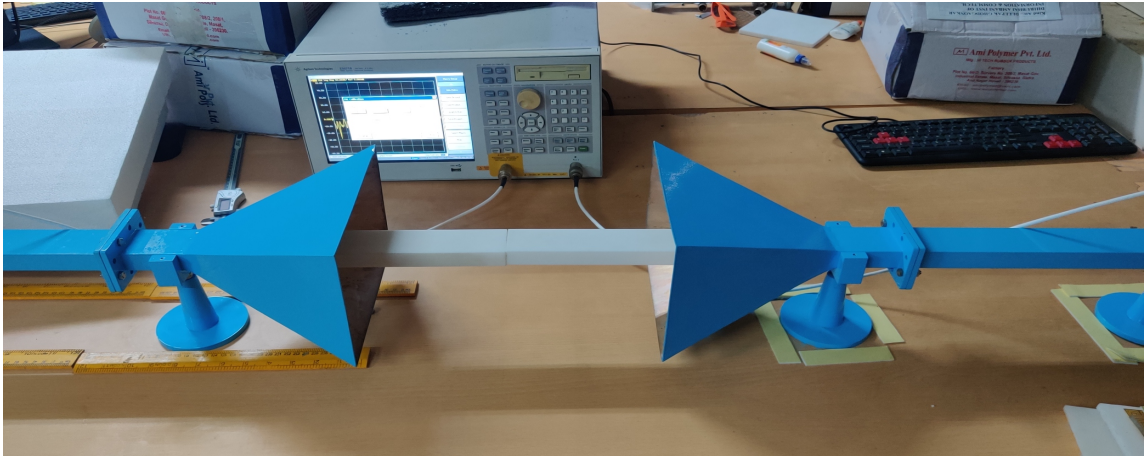


Figure 4.12: Through Calibration Standard

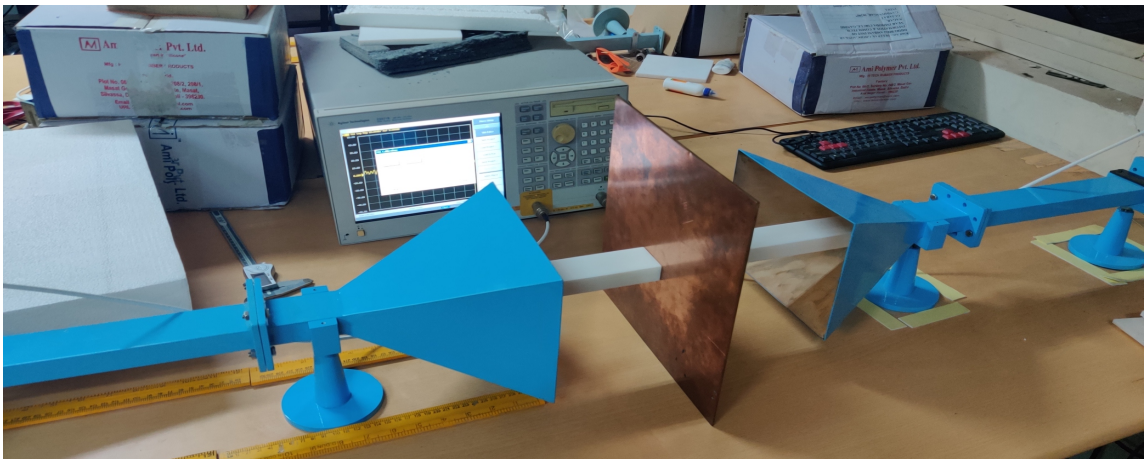


Figure 4.13: Reflect calibration standard

the mid band as shown in Figure 4.14.. The TRL calibration kit of the VNA is

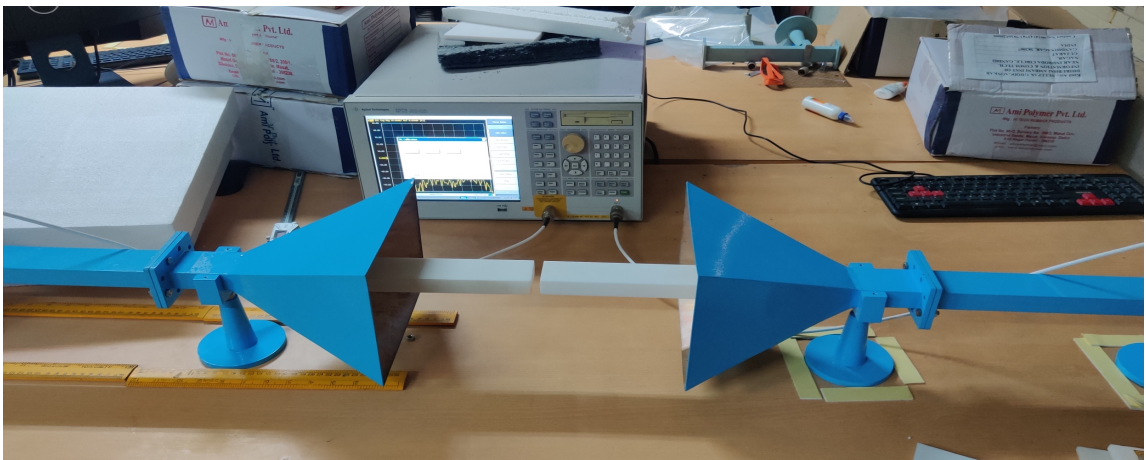


Figure 4.14: Line Calibration standard

modified by defining these calibration standards regarding characteristic impedance



and electrical delay. The full 2-port calibration is performed in dielectric waveguide by using these calibration standards.

After TRL calibration, A ripple is observed during S-parameter measurement of the sample. The reason for this is residual load and source mismatch. Time domain gating (feature of VNA) is performed on S-parameters to remove residual load and source mismatch [5-8]. The time-domain S-parameter response is obtain from frequency domain-response data by taking inverse Fourier transform. The gated window of pass band is applied over main path S-parameter response. Measured data with time domain gating is obtained by taking the Fourier transform of gated S-parameter response. After gating, through standard was measured. The amplitude and phase of  $S_{21}$  (or  $S_{12}$ ) was within  $0.00 \pm 0.06$  dB and  $0.0 \pm 0.8$  °, respectively. For the metal plate, the amplitude and phase of  $S_{11}$  (or  $S_{22}$ ) were  $0.00 \pm 0.06$  dB and  $180.0 \pm 1.9$ °, respectively [5-6]. All the abrasions and reflection arising because of bend in coaxial cable and imperfect coaxial to waveguide transitions and abrupt change in impedance value in waveguide have been successfully eliminated. Full 2 port TRL calibration with time domain gating can be applied to any load placed between two tip's of dielectric waveguides. Care must be taken that the setup should not be disturbed once calibration is done. If any change in RDWG systems happens due to insertion of samples between two tip's of dielectric waveguides, calibration must be performed again.

For characterization of CISR sheets,  $\epsilon_r$  and  $\mu_r$  values are calculated from measured  $S_{11}$  and  $S_{21}$  data using Reflection/Transmission method given by Ghodgaonkar et al [12] as shown in appendix B. For materials such as CISR sheets, the maximum error in  $\epsilon'$ ,  $\mu'$ ,  $\tan\delta_\epsilon$  ( $= \epsilon''/\epsilon'$ ) and  $\tan\delta_\mu$  ( $= \mu''/\mu'$ ) are 3.7%, 9.9%, 0.048 and 0.11, respectively [12].

CISR sheets are placed in good contact between two tip's of dielectric waveguides. This method is also called as Nicolson Weir ross method. Accuracy of reflection and transmission method for RDWG system was verified by measuring dielectric properties of sheets of standard materials such as Teflon, PVC, polycarbonate, plexiglass and nylon.

To avoid effect of sagging of thin and flexible CISR sheets, they are sandwich

between two teflon sheets. These Teflon sheets are quarter wavelength at mid-band for impedance matching of CISR sheets [5,6]. Thickness of Teflon sheets are 7.4 mm and 10.3 mm for WR-137 and WR-187 waveguide bands, respectively. It is placed in direct mechanical contact between two RDWGs as shown in Figures 4.10 and 4.11.

## 4.4 Measured results of CISR sheets

### 4.4.1 Coaxial Air Line

Toroidal-shaped CISR sleeves with 0%, 10%, 20%, 30%, 40%, and 50% of CI powder by volume were fabricated as shown in Figure 4.15.



Figure 4.15: Toroidal-shaped CISR sleeves for coaxial air line

$\epsilon_r$  and  $\mu_r$  values of toroidal-shaped CISR sleeves are given in Figures 4.16 to 4.21 and in Table 4.1. The value of  $\epsilon'$  for silicon rubber varies from 2.95 to 2.9 in 1 to 4 GHz range. The negative values of  $\epsilon''$  and  $\mu''$  are due to measurement errors in coaxial air line measurement system. The value of  $\mu'$  remains close to 1.  $\epsilon'$  values varies from 2.95 to 24 at 1 GHz and 2.9 to 17 at 4 GHz, with change in concentration from 0 % to 50% in CI powder by volume.  $\epsilon''$  remains close to 0 in 1 to 4 GHz range for all concentrations of CI powder by volume.  $\mu'$  varies from 1 to 5 at 1 GHz and 1

to 2.4 at 4 GHz as concentration changes from 0% to 50% of CI powder by volume. As concentration of CI powder changes from 0 % to 50% in CI powder by volume, the value of  $\mu''$  changes from 0 to 1.8 at 1 GHz and 0 to 2.4 at 4 GHz. At 2.5 GHz, values of  $\epsilon'$ ,  $\epsilon''$ ,  $\mu'$  and  $\mu''$  for toroidal-shaped CISR sleeves are given in Table 4.1. From Table 4.1 and Figures 4.17 to 4.22, it is observed that the values of  $\epsilon'$ ,  $\mu'$  and  $\mu''$  increase with increase in volume fraction of CI powder. Silicon rubber (0% of CI powder by volume) is nonmagnetic. So, the expected value for  $\mu'$  and  $\mu''$  are exactly 1 and 0.0, respectively. The negative values of  $\epsilon''$  and  $\mu''$  are due to measurement errors in coaxial air line system.

CISR Sheets	$\epsilon'$	$\epsilon''$	$\mu'$	$\mu''$
Silicon Rubber sheet	2.95	0.04	1.09	0.09
CISR Sheet (10% of CI powder by volume)	4.2	0.05	1.56	0.25
CISR Sheet (20% of CI powder by volume)	7.09	-0.08	1.75	0.44
CISR Sheet (30% of CI powder by volume)	11.30	-0.12	2.25	1.02
CISR Sheet (40% of CI powder by volume)	17.06	-0.8	2.45	1.62
CISR Sheet (50% of CI powder by volume)	23.06	0.2	2.51	1.86

Table 4.1: Complex permittivity and complex permeability of CISR Sheets at 2.5 GHz



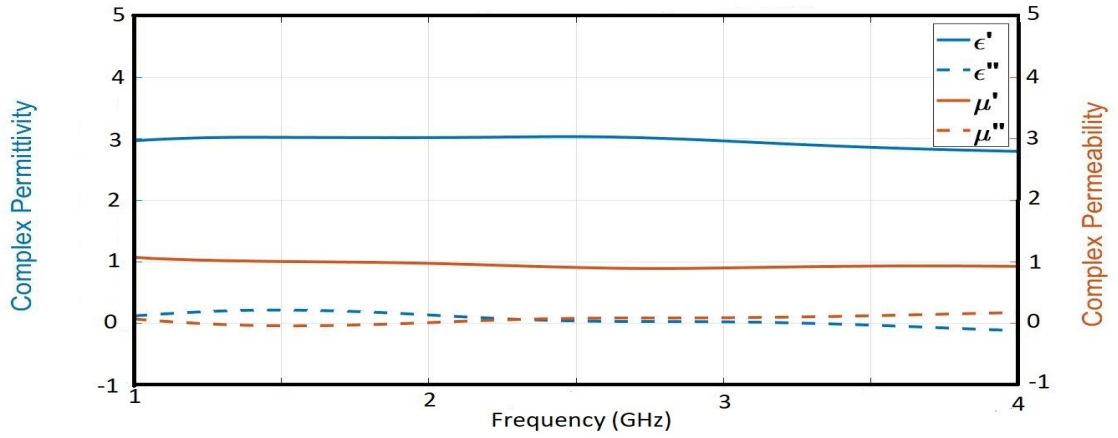


Figure 4.16: Complex permittivity and Complex permeability of CISR sheets (0% of CI by volume)

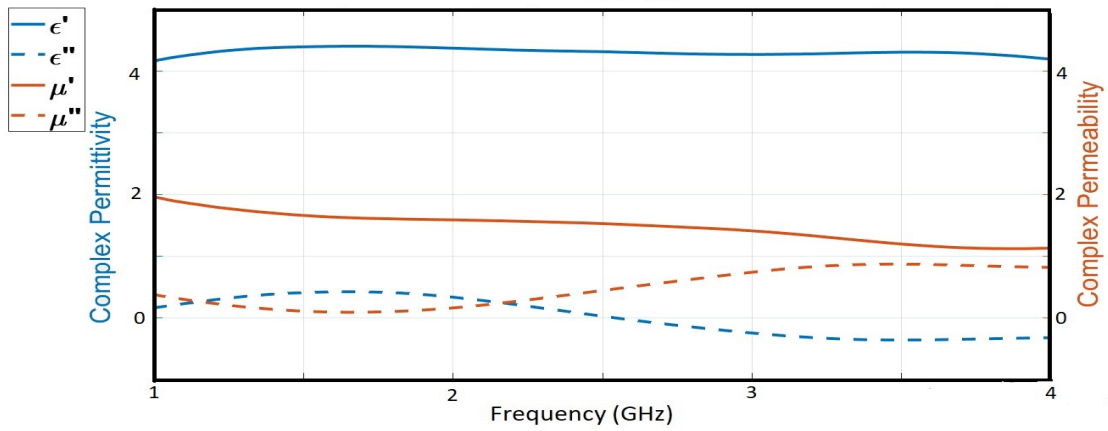


Figure 4.17: Complex permittivity and Complex permeability of CISR sheets (10% of CI by volume)

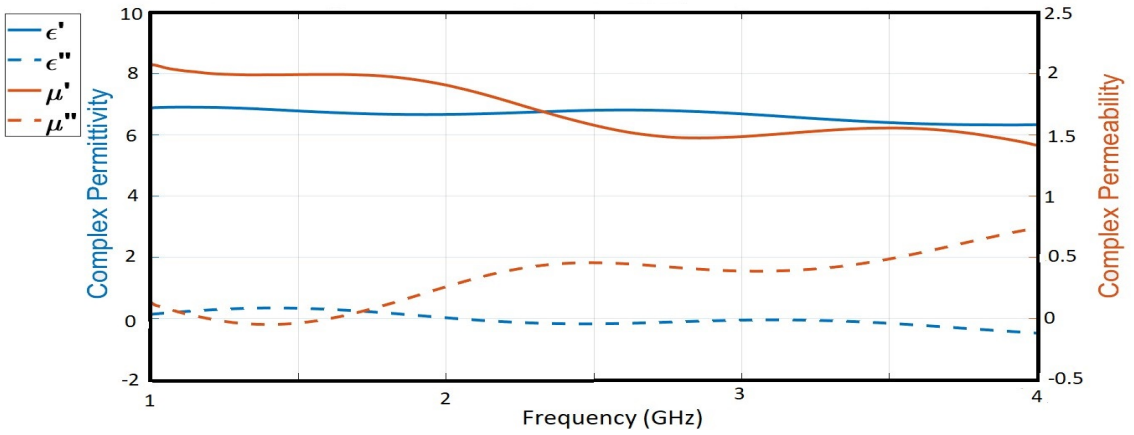


Figure 4.18: Complex permittivity and Complex permeability of CISR sheets (20% of CI by volume)

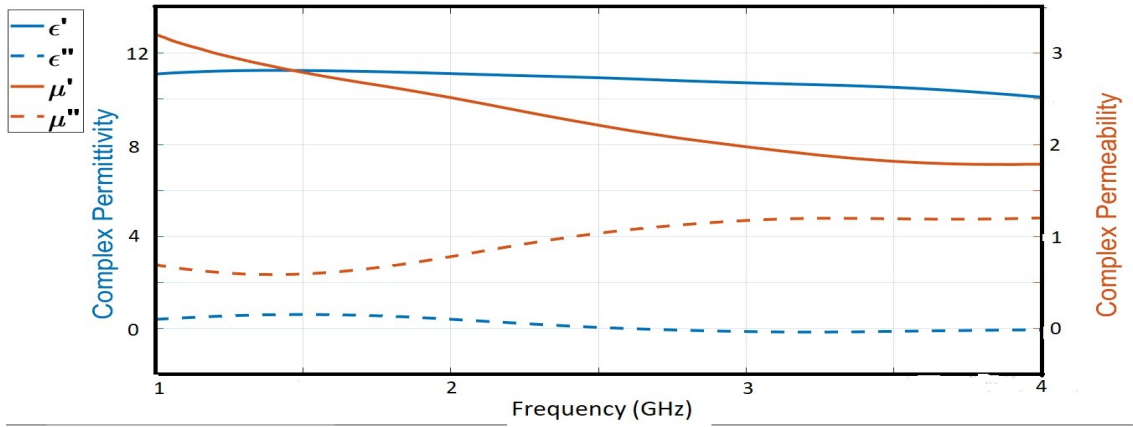


Figure 4.19: Complex permittivity and Complex permeability of CISR sheets (30% of CI by volume)

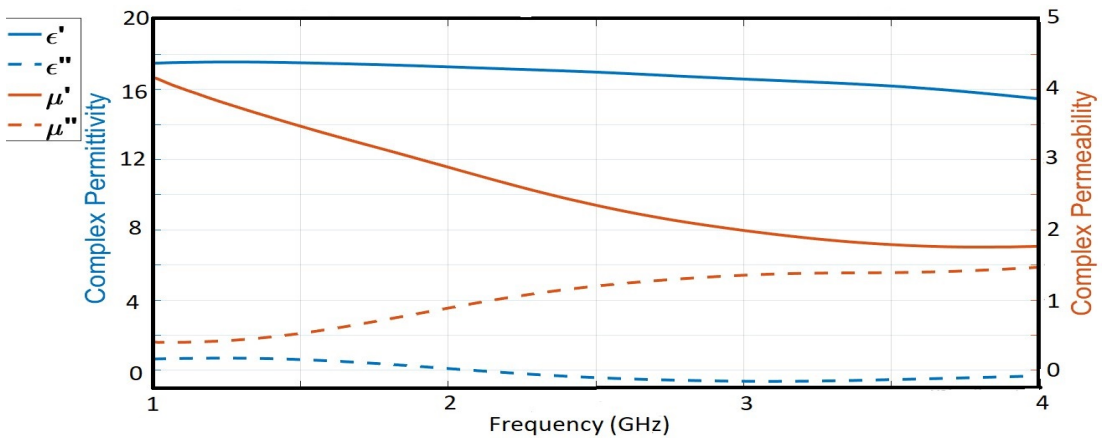


Figure 4.20: Complex permittivity and Complex permeability of CISR sheets (40% of CI by volume)

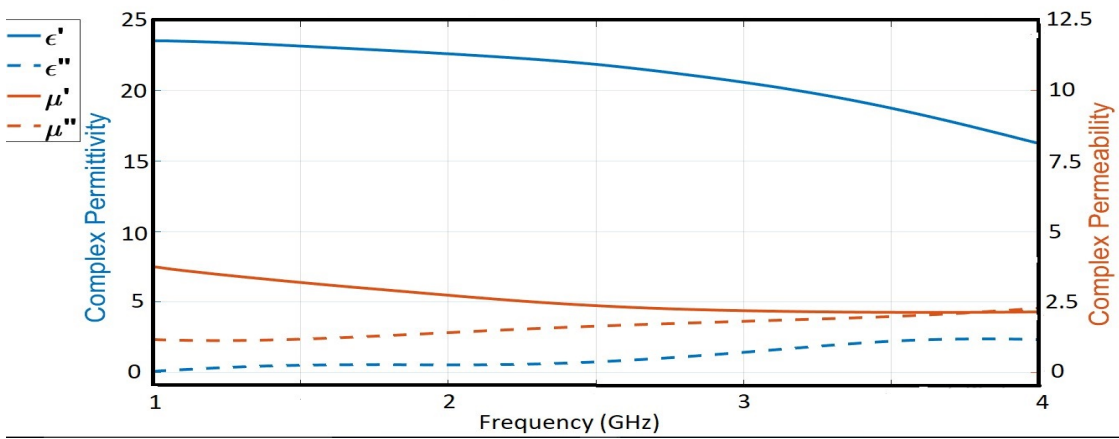


Figure 4.21: Complex permittivity and Complex permeability of CISR sheets (50% of CI by volume)

#### 4.4.2 Rectangular Dielectric Waveguide (RDWG)

0%, 10%, 20%, 30%, 40%, and 50% of CI powder in CISR sheets by volume are fabricated with dimension of 300 mm x 300mm x 3 mm. It is then sliced into 150 mm x 150 mm for use in the RDWG system as shown in Figures 4.22. The aperture of horn antenna is approximately equal to the slice size of CISR sheets. The maximum energy is within the dielectric waveguide  $\epsilon_r$  and  $\mu_r$  values of CISR sheets having 0%,

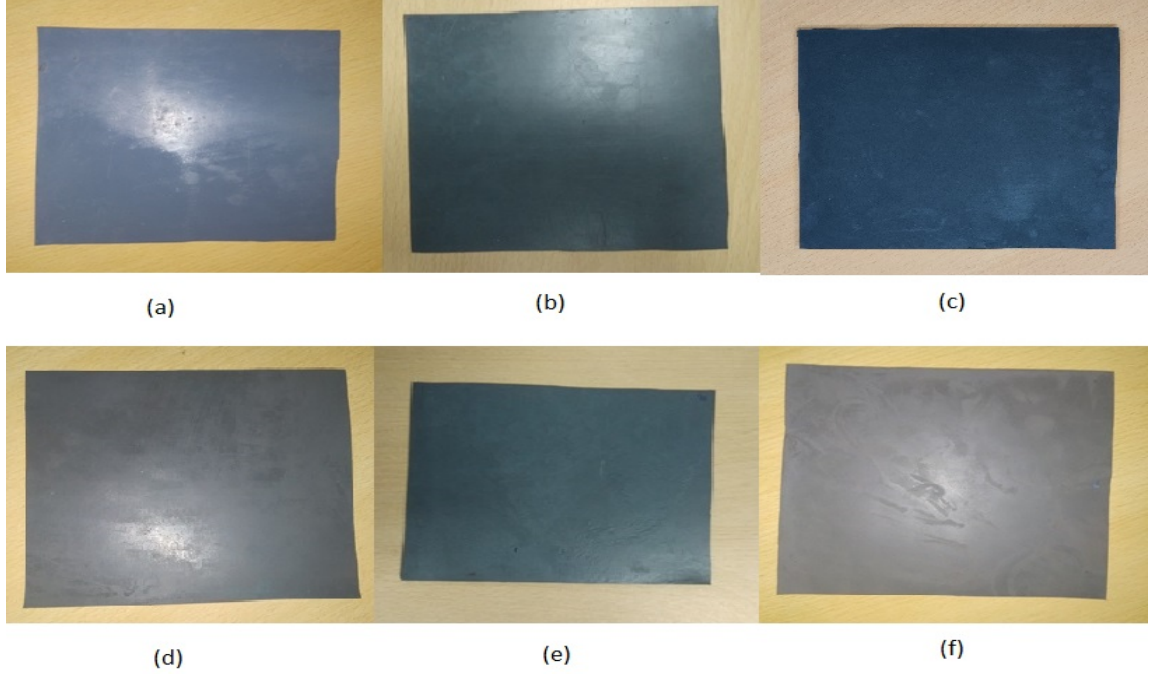


Figure 4.22: Photograph of Fabricated CISR sheets (a) 0% (b) 10% (c) 20% (d) 30% (e) 40% (f) 50% of CI in CISR sheets by volume.

10%, 20%, 30%, 40% and 50% of CI powder by volume are plotted in Figures 4.23 to 4.28.

For CISR sheets, the maximum errors in  $\epsilon'$ ,  $\mu'$ ,  $\tan\delta_\epsilon$  ( $= \epsilon''/\epsilon'$ ) and  $\tan\delta_\mu$  ( $= \mu''/\mu'$ ) are 3.7%, 9.9%, 0.048 and 0.11, respectively [5,6,12]. In Figures 4.23, it is observed that the value of  $\epsilon'$  for silicon rubber varies from 2.75 to 2.6 in 3.95 to 8.2 GHz range of frequency. The negative values of  $\epsilon''$  and  $\mu''$  are due to measurement errors in RDWG measurement system. The value of  $\mu'$  remains close to 1. From Figure 4.24 to 4.28,  $\epsilon'$  values varies from 4.1 to 21 at 3.95 GHz and 3.98 to 23 at 8.2 GHz, with change in concentration from 0 % to 50% in CI powder by volume.  $\epsilon''$  remains close to 0 at the frequency range of 3.95 to 8.2 GHz for all concentrations

CISR Sheets	$\epsilon'$	$\epsilon''$	$\mu'$	$\mu''$
Silicon Rubber sheet	2.75	0.04	0.996	-0.01
CISR Sheet (10% of CI by volume)	4.18	0.15	1.16	0.25
CISR Sheet (20% of CI by volume)	7.12	0.21	1.57	0.74
CISR Sheet (30% of CI by volume)	10.60	-0.12	1.77	1.12
CISR Sheet (40% of CI by volume)	18.06	-0.08	1.74	1.62
CISR Sheet (50% of CI by volume)	24.06	-0.08	1.84	1.82

Table 4.2: Complex permittivity and complex permeability of CISR Sheets at 6 GHz

of CI by volume.  $\mu'$  varies from 1.2 to 2.1 at 3.95 GHz and 1.1 to 1.5 at 8.2 GHz with change in concentration from 0% to 50% of CI by volume. The value of  $\mu''$  varies from 0.1 to 1.95 at 3.95 GHz and from 0.25 to 1.5 at 8.2 GHz with change in concentration from 0 % to 50% in CI powder by volume. At 6 GHz, values of  $\epsilon'$ ,  $\epsilon''$ ,  $\mu'$  and  $\mu''$  for CISR sheets are given in Table 4.2. From Table 4.2 and Figures 4.23 to 4.28, it is observed that the values of  $\epsilon'$ ,  $\mu'$  and  $\mu''$  increase with increase in volume fraction of CI powder. The values of  $\epsilon'$ ,  $\mu'$  and  $\mu''$  increase with increasing volume fraction of CI powder.

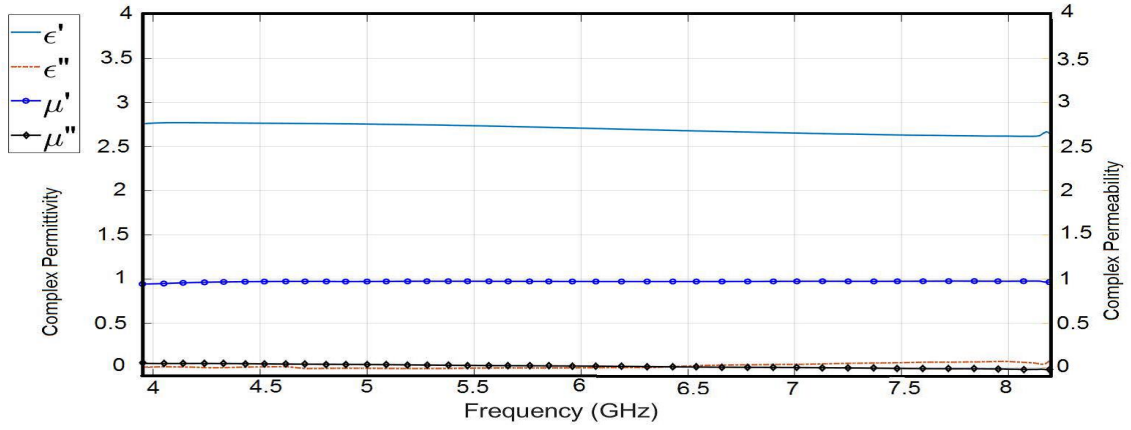


Figure 4.23: Complex permittivity and Complex permeability of Silicon Rubber (0% of CI by volume)

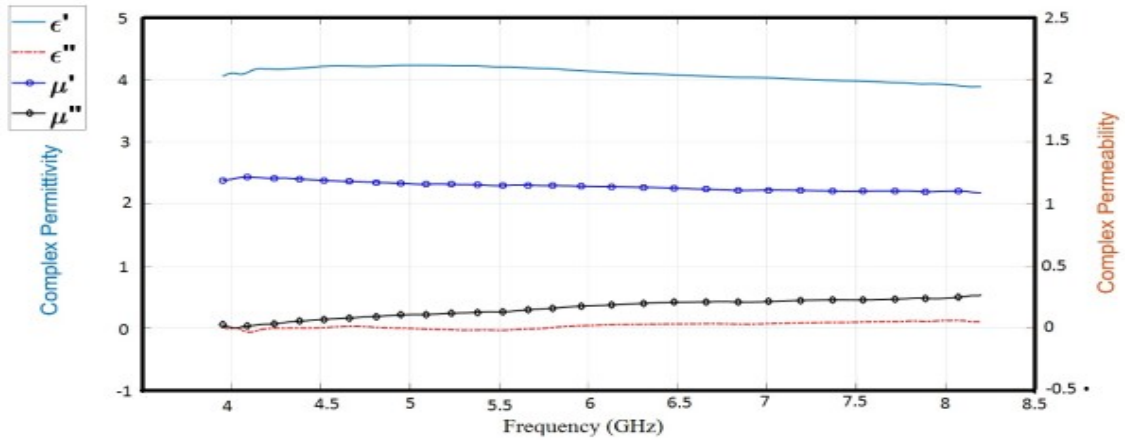


Figure 4.24: Complex permittivity and Complex permeability of CISR sheets (10% of CI by volume)

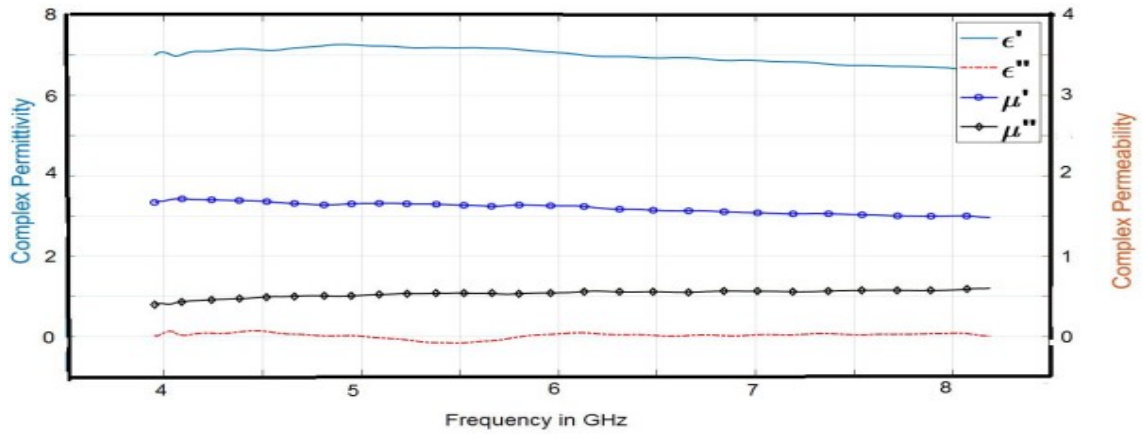


Figure 4.25: Complex permittivity and Complex permeability of CISR sheets (20% of CI by volume)

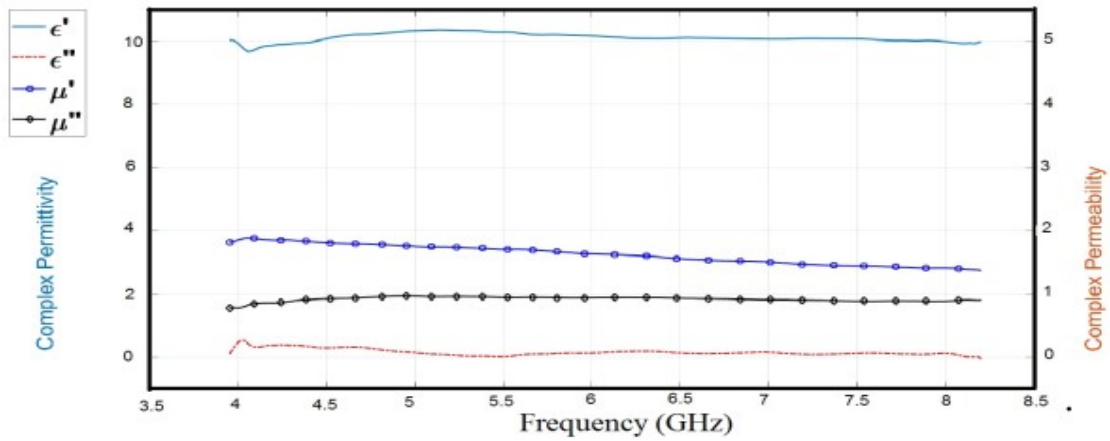


Figure 4.26: Complex permittivity and Complex permeability of CISR sheets (30% of CI by volume)

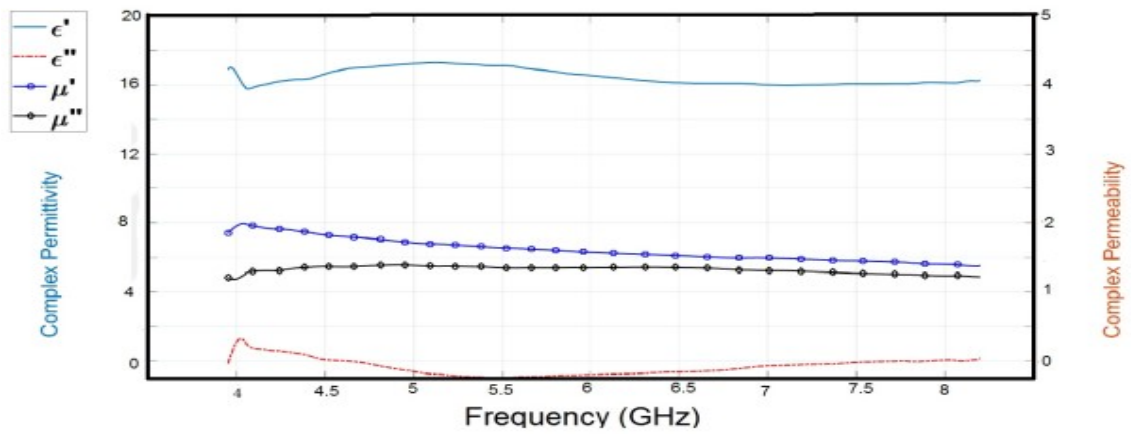


Figure 4.27: Complex permittivity and Complex permeability of CISR sheets (40% of CI by volume)

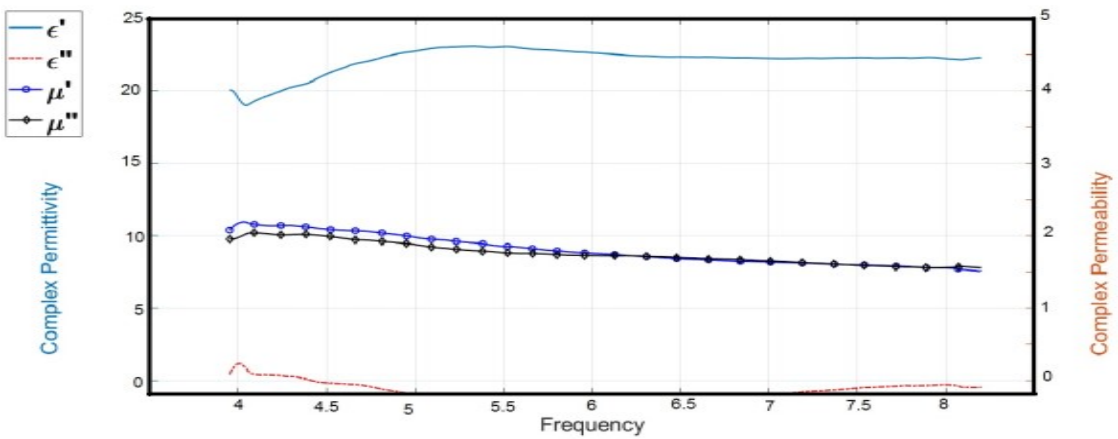


Figure 4.28: Complex permittivity and Complex permeability of CISR sheets (50% of CI by volume)

## 4.5 Polynomial Approximation of $\epsilon_r$ and $\mu_r$ for intermediate concentration of CI Powder

For the design of microwave absorbers,  $\epsilon_r$  and  $\mu_r$  values are required for arbitrary volume fraction of CI in CISR sheets. Six CISR sheets were fabricated with 0%, 10%, 20%, 30%, 40% and 50% of CI powder by volume to cover possible range of concentrations from 0 to 50%[13].

For intermediate values of CI powder by volume in CISR sheets,  $\epsilon'$  can be obtained by exponential dielectric mixture theory because of high contrast in dielectric and magnetic properties of silicon rubber and CI powder [13, 14, 15]. For  $\mu'$  and  $\mu''$ , linear interpolation is a good approximation because of small changes as a function of concentration [14, 15].  $\epsilon''$  can be assumed to be close to zero for intermediate concentrations of CI powder in CISR sheets. The exponential dielectric mixture equation is given by following equation .

$$(\epsilon_{eff})^a = f \cdot (\epsilon_{ci})^a + (1 - f)(\epsilon_s)^a \quad (4.10)$$

Where  $\epsilon_{eff}$ ,  $\epsilon_{ci}$ ,  $\epsilon_s$  and  $f$  are dielectric constant of CISR sheets, dielectric constant of CI powder in silicon rubber, dielectric constant of silicon rubber and concentration of CI in CISR sheets by volume, respectively. Using this equation for  $a = 0.4$ , calculated value of  $\epsilon_{ci}$  varies from 54 to 74 for change in CI concentration from 10% to 50%. Change in  $\epsilon_{ci}$  will cause errors in estimation of  $\epsilon'$ .

In our design of microwave absorbers, it was found that  $\epsilon'$ ,  $\mu'$  and  $\mu''$  can be estimated by polynomial approximation method which is superior to dielectric mixture theory for  $\epsilon'$  and linear interpolation for  $\mu'$ ,  $\mu''$ . In order to minimize errors in estimation of  $\epsilon'$  for intermediate concentrations, the exponential dielectric mixture formula works well with small changes in concentrations like 0% to 20%, not 0% to 50%. In our experience in design of microwave absorber, polynomial approximation works well as it approximates the curve equation with points at different concentrations of CI by volume at a fixed frequency. The function "basic fitting" is available in Matlab which is used.

Figures 4.29 to 4.31 for 2.5 GHz and Figures 4.32 to 4.34 for 6 GHz show results from polynomial approximation technique for  $\epsilon'$ ,  $\mu'$  and  $\mu''$ , respectively. For any frequencies in 1 to 8.2 GHz frequency range, similar polynomial approximation results can be obtained.

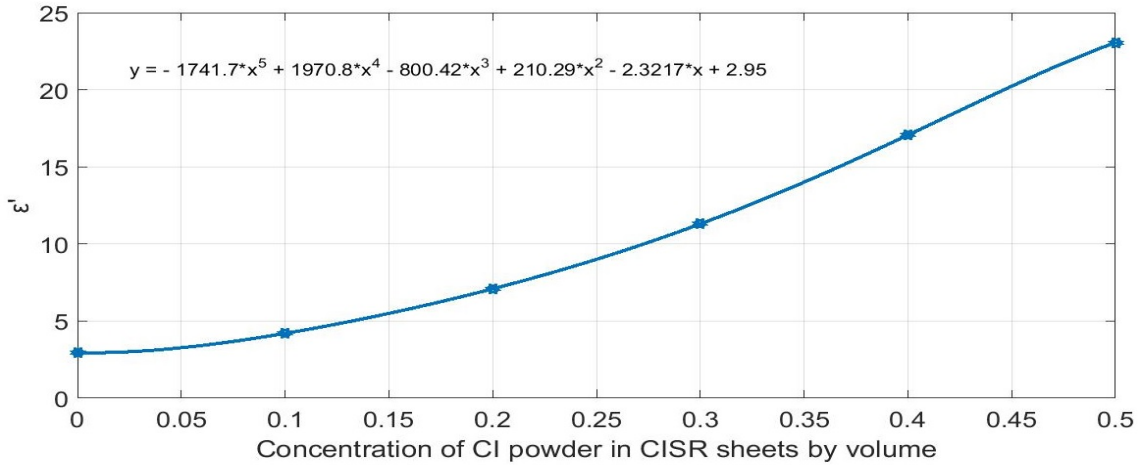


Figure 4.29: Polynomial approximation of  $\epsilon'$  at 2.5 GHz

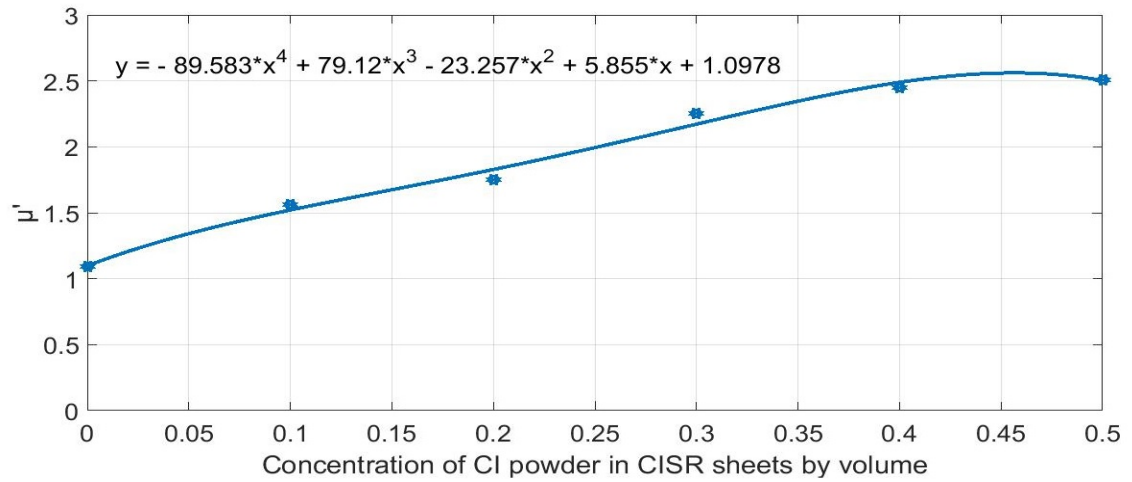


Figure 4.30: Polynomial approximation of  $\mu'$  at 2.5 GHz



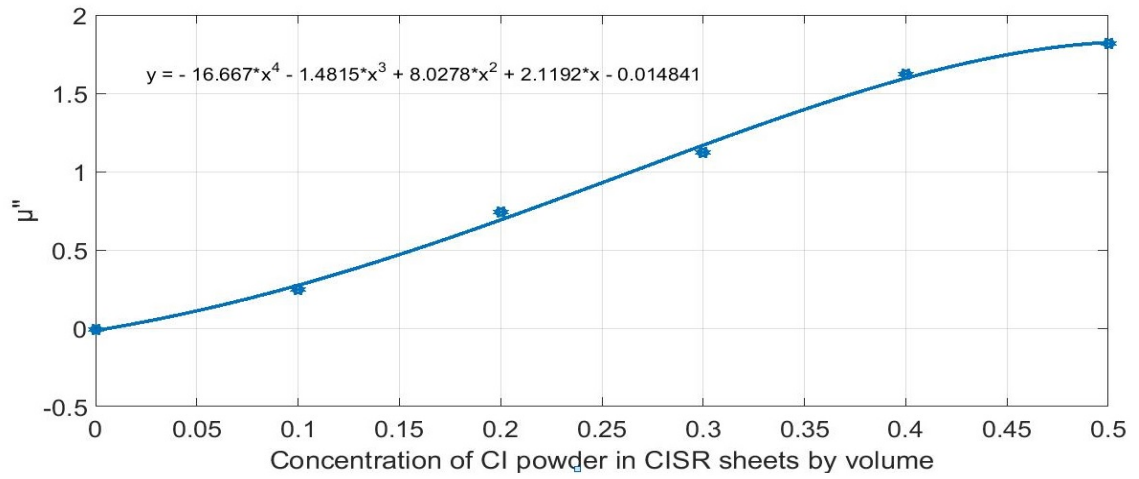


Figure 4.31: Polynomial approximation of  $\mu''$  at 2.5 GHz

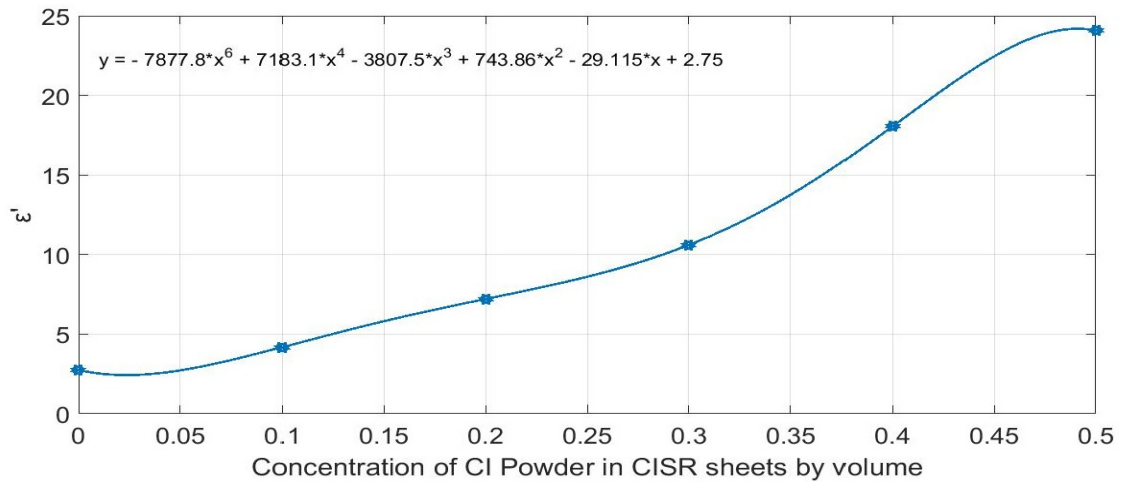


Figure 4.32: Polynomial approximation of  $\epsilon'$  at 6 GHz

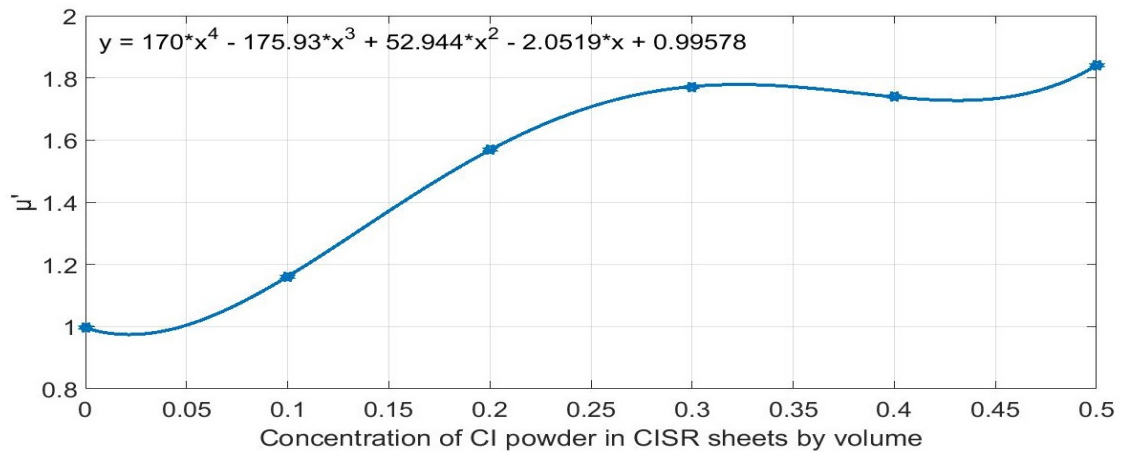


Figure 4.33: Polynomial approximation of  $\mu'$  at 6 GHz

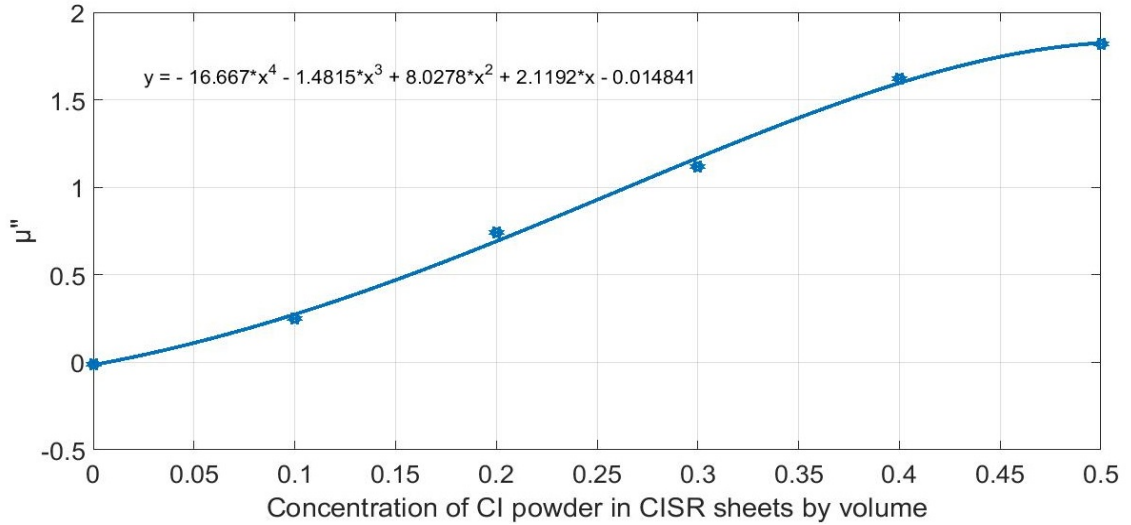


Figure 4.34: Polynomial approximation of  $\mu''$  at 6 GHz

## 4.6 Conclusions

Coaxial air line system is used for calculation of  $\epsilon_r$  and  $\mu_r$  of CISR sheets from measured S-parameters in the frequency range of 1 GHz to 4 GHz using NRW method. Corrected values for S parameters for toroidal-shaped CISR sleeves are obtained by E-cal kit, time domain gating in VNA and  $T_1$  and  $T_2$  estimation in coaxial air line by toroidal-shaped teflon sleeve.  $\epsilon_r$  and  $\mu_r$  values are calculated in 1 to 4 GHz frequency range from corrected value of S-parameter of toroidal-shaped CISR sleeves using NRW method.  $\epsilon_r$  and  $\mu_r$  values of CISR sheets are calculated accurately by using RDWG system by sandwiching CISR sheets between two quarter wavelength long Teflon sheets. For thin and flexible CISR sheets, RDWG system is specially suited because it is a non-destructive method. Polynomial approximation is used to get  $\epsilon_r$  and  $\mu_r$  values at intermediate concentration of CI powder in CISR sheets by volume. It is obtained by approximating the curves of  $\epsilon_r$  and  $\mu_r$ , with known values at 0%, 10%, 20%, 30%, 40% and 50% of CI powder.

## References

- [1] ASTM D7449 / D7449M-14, Standard Test Method for Measuring Relative Complex Permittivity and Relative Magnetic Permeability of Solid Materials at Microwave Frequencies Using Coaxial Air Line, *ASTM International*, West Conshohocken, PA, 2014, [www.astm.org](http://www.astm.org).
- [2] Raju, V. Seetha Rama, "Design of coaxial aircell fixture for the measurement of electromagnetic properties," *Journal Microwave Optoelectronic Electromagnetic Application*, vol.16, no.3, pp. 686-696, 2017.
- [3] N M Ridler, "Connectors, Air Lines and RF Impedance, " *The IEE Measurement, Sensors, Instrumentation and NDT Professional Network*, Printed and published by the IEE, Michael Faraday House, Six Hills Way, Stevenage, Herts SG1 ZAY, UK.
- [4] Kapil Sharma, "Wideband Dielectric Characterization of Triethylen Glycol Dimetharylate Ester Plastic, "MS Thesis in Department of Electrical Engineering, Pennsylvania State University, December 2013.
- [5] R. Vashisth, D. Ghodgaonkar and S. Gupta, "Design and Fabrication of Broadband Microwave Absorber using FSS embedded in CISR sheets," *2018 IEEE MTT-S International Microwave and RF Conference (IMaRC)*, pp. 1-4, Dec 2018.
- [6] R. Vashisth, D. Ghodgaonkar and S. Gupta, "Permittivity and Permeability Measurements of CISR sheets for Microwave Absorber Applications," *2018 IEEE International RF and Microwave Conference (RFM)*, Penang, Malaysia, pp. 359-362, 17-18 Dec 2018.

- [7] Z. Abbas, R. D. Pollard and R. W. Kelsall." Complex Permittivity Measurements at Ka-Band using Rectangular Dielectric Waveguide".*IEEE Transactions on Instrumentation and Measurement*. Volume 50, page No. 1334-1342. 2001
- [8] K Ismail, D. K. Ghodgaonkar, Z. Awang and A. Samsuri, C. M. S. Said and Mazlina Esa." Microwave detection of rubber filler using rectangular dielectric waveguide". *2005 Asia-Pacific Conference on Applied Electromagnetics, APACE 2005-Proceedings*. Page No.161-162, 2005;.
- [9] W. Hofmann, C. Bornkessel, A. Schwind and M. A. Hein, "Challenges of RF Absorber Characterization: Comparison Between RCS- and NRL-Arch-Methods," *2019 International Symposium on Electromagnetic Compatibility - EMC EUROPE*, 2019, pp. 370-375, doi: 10.1109/EMCEurope.2019.8871983
- [10] [https://www.datasheetarchive.com/whats\\_new/fa21ff8b670c362bb9daf90cd700f1a8.html](https://www.datasheetarchive.com/whats_new/fa21ff8b670c362bb9daf90cd700f1a8.html)
- [11] <https://www.keysight.com/in/en/product/N4690D/electronic-calibration-module-ecal-18-ghz-type-n-50-ohm-2-port.html>
- [12] D. K. Ghodgaonkar, V. V. Varadan and V. K. Varadan,"Free Space Measurement of Complex Permittivity and Complex Permeability of Magnetic Materials at Microwave Frequencies," *IEEE Transactions on Instrumentation and Measurements*, Vol. 39, pp. 398-394, April 1990.
- [13] D.K. Ghodgaonkar, V.K. Varadan and V.V. Varadan, "Microwave Dielectric and Magnetic Properties of Carbonyl Iron Powder Loaded Silicon Rubber Sheets," *Journal of Wave Material Interaction*, Vol. 8, pp.171-184,1994.
- [14] Yong Bao Feng, Tai Qiu, Chun-Ying Shen and Xiao-Yun Li,"Electromagnetic and absorption properties of carbonyl iron/rubber radar absorbing materials," *IEEE Transactions on Magnetism*, vol. 42, no. 3, pp. 363-368, March 2006.
- [15] A. H. Sihvola and E. Alanen,"Studies of Mixing Formula in the Complex Plane," *IEEE Transactions on Geoscience and Remote Sensing*, Vol. 39, pp. 679-687, 1991.

## Chapter 5

# Design of broadband microwave absorber using multilayer carbonyl iron filled silicone rubber sheets

### 5.1 Introduction

The multilayer microwave absorbers are designed to suppress unwanted external electromagnetic waves from various wireless sources. Multilayer microwave absorber are designed in 2.5 to 8.2 GHz ranges by stacking different layers of carbonyl iron filled silicone rubber (CISR) sheets by using genetic algorithm optimization. These CISR sheets are designed by different concentrations of CI in CISR sheets. For frequency 1.6 GHz to 2.6 GHz range, single layer microwave absorber of thickness 3 mm is designed by 50% of CI powder in CISR sheet by volume. The fabrication accuracies in thicknesses and concentrations of CISR sheets are  $\pm 0.5$  mm and  $\pm 2\%$  of CI by volume, respectively. These CISR sheets are fabricated by Ami Polymer Private Limited Silvassa, India. All multilayer microwave absorbers designed in this thesis have two layers because of inaccuracies in fabrication of CISR sheets.

Essentially, two important conditions are to be satisfied to suppress electromagnetic radiations [1]. Firstly, minimum reflection at the air-absorber interface and secondly, sufficient attenuation of the incident wave power within the absorber. Reduction of reflection at the interface can be obtained by taking the conditions of impedance matching at the air-absorber interface, and thereafter, attenuation within the absorber matrix using lossy material. These two conditions can be tailored by

appropriate values of  $\epsilon_r$  and  $\mu_r$  of the absorbing material at the desired frequency. The two main loss mechanisms for dielectric materials are conduction and dielectric losses. High conductivity leads to conduction losses and dipolar losses are due to polarization effects. On the other hand, magnetic composite absorption depends on magnetic hysteresis effect of the magnetic inclusions incorporated into the matrix materials as in case of CISR sheets.

In order to get both characteristics, it is preferred to have a multilayer microwave absorbers. The first layer should have matching characteristics with free space. So, its  $\mu'/\epsilon'$  should be close to 1. It should allow maximum power to pass through it. The second layer is used to have maximum attenuation characteristics.  $\epsilon''$  and  $\mu''$  of second layer should be as high as possible.

## 5.2 Theory of multilayer microwave absorbers

Transmission line model of multilayer microwave absorber is shown in Figure 5.1 [3,4,5].

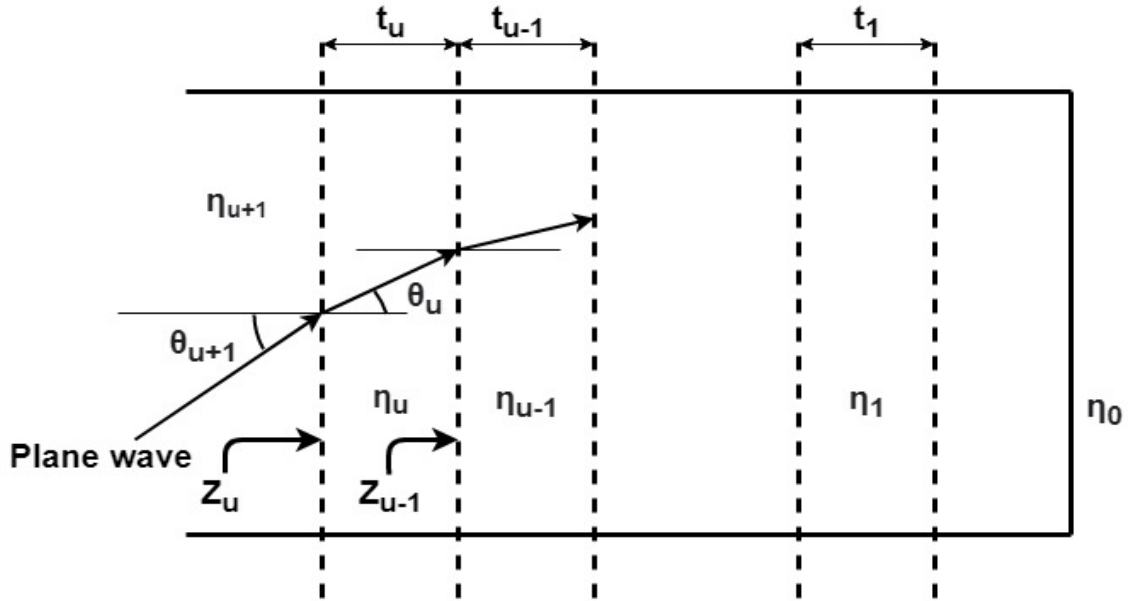


Figure 5.1: Transmission line model of multilayer microwave absorber

Where,  $\eta_0$  is the intrinsic impedance of metallic layer which is  $0 \Omega$ ,  $\eta_1$  is the intrinsic impedance of first layer with thickness  $t_1$  and  $\eta_u$  is the intrinsic impedance of  $u^{th}$  layer with thickness  $t_u$ .  $\eta_{u+1}$  is the intrinsic impedance of free space which

is  $377 \Omega$ .  $\theta_{u+1}$  is the angle of incidence from free space to  $u^{th}$  layer and  $\theta_u$  is angle of refraction in  $u^{th}$  layer.  $Z_u$  is the input impedance of the microwave absorber. Reflectivity of multilayer microwave absorber is given by following equations

$$Reflectivity (RC) = \frac{Z_u - \eta_{u+1}}{Z_u + \eta_{u+1}} \quad (5.1)$$

$$RC(dB) = 20 \log_{10}(RC)$$

Where RC can be expressed in linear form or in dB. Impedance of the microwave absorber from first layer ( $u = 1$ )  $Z_u$  can be found by following equations

$$Z_u = \eta_u \frac{Z_{u-1} + \eta_u \tanh(\gamma_u t_u)}{\eta_u + Z_{u-1} \tanh(\gamma_u t_u)} \quad (5.2)$$

Where,

$$\eta_u = 377 \sqrt{\frac{\mu_{ru}}{\epsilon_{ru}}} \quad (5.3)$$

$$\gamma_u = j2\pi f \sqrt{\epsilon_o \mu_o} \sqrt{\epsilon_{ru} \mu_{ru}} \cos(\theta_u) \quad (5.4)$$

$\epsilon_{ru}$  and  $\mu_{ru}$  are the complex permittivity and complex permeability of  $u^{th}$  layer. Equation 5.1 to 5.3 are successively applied from layer 1 to last layer ( $u^{th}$  layer) for calculation of input impedance of microwave absorber.

$\theta_u$  is given by following equation using Snell's law

$$\theta_u = \text{Sin}^{-1} \left( \frac{\mu_{ru+1} \eta_u \text{Sin}(\theta_{u+1})}{\mu_{ru} \eta_{u+1}} \right) \quad (5.5)$$

TE wave is referred as Transverse Electric Wave. Here, electric field is perpendicular to the plane of microwave absorber. TM wave is referred as Transverse Magnetic Wave. Here, magnetic field is perpendicular to the plane of microwave absorber.  $\eta_u^{TE}$  and  $\eta_u^{TM}$  are give by following equations

$$\eta_u^{TE} = \frac{\eta_u}{\text{Cos}(\theta_u)} \quad (5.6)$$

$$\eta_u^{TM} = \eta_u \text{Cos}(\theta_u) \quad (5.7)$$

Equation 5.4 to 5.6 are successively applied from last layer to first layer. Matlab code for calculation of reflectivity of multilayer microwave absorbers is given in appendix E.

### 5.3 Design of multilayer microwave absorbers using genetic optimization

Genetic Algorithms (GAs) [2] are adaptive heuristic search algorithms based on the evolutionary ideas of natural selection and genetics. There are different optimization techniques like particle swarm optimization, ant colony optimization, gravitational search optimization, etc. The main advantage of GA is that it is discrete in nature. GA is used to optimize multilayer microwave absorbers for maximum bandwidth (Reflectivity is better than  $< -10$  dB). It is required to take into consideration the tolerance of CISR sheets regarding thickness and concentration of CI powder by volume. The following steps are used.

1. Choosing the interested frequency band of operation from 1 to 3 GHz or 3 to 8.2 GHz.
2. Choose frequency step of 0.1 GHz or of your interest. This is needed to cover entire frequency range of interest.
3. For each frequency, it is required to randomly choose concentration of CI in CISR sheets by volume and thickness of all layers.  $\epsilon_r$  and  $\mu_r$  are calculated by using polynomial approximation based on concentration values as given in Section 4.5.
4. Two genes are required per layer which corresponds to concentration and thickness of CISR sheets. These genes form a chromosome. Each chromosome correspond to a solution of microwave absorber. In this thesis, the population of 15 chromosomes are used in calculations.
5. The preliminary reflectivity of microwave absorber are calculated by using impedance formula given in Section 5.2. So, each chromosome will produce



reflectivity ( $R_{sim}^{TE/TM}(f_i, \theta_i)$ ) over the chosen frequency, angle of incidence and polarization.

6. Fitness function is defined as

$$FitnessFunction = \sum_{\theta_i=0^\circ}^{\theta_{max}} \left( \sum_{f_i=f_{min}}^{f_{max}} (|R_{sim}^{TE/TM}(f_i, \theta_i)|_{dB} - |R_{dec}|_{dB}) \right) \quad (5.8)$$

Where the angle of incidence ( $\theta_i$ ) varies from  $0^\circ$  degrees to  $40^\circ$  ( $\theta_{max}$ ) with increment of  $10^\circ$ . The operating frequency ( $f_i$ ) varies over 1 to 3 GHz or 2.5 to 8.2.  $R_{des}$  (terminating condition) is the desired reflection coefficient in dB whose value is set at -10 dB.  $R_{sim}^{TE/TM}(f_i, \theta_i)$  are magnitude of simulated reflection coefficient under incident angle  $\theta_i$  at frequency  $f_i$  with TE and TM polarization in dB. If fitness criteria give a positive value which means the terminating condition has reached and the design of microwave absorber is complete. The chromosome which corresponds to the solution will give concentrations and thicknesses of designed multilayer microwave absorber. If terminating condition does not reach (fitness criteria gives negative results), then the best chromosome according to fitness function is kept and replacement of other chromosomes will be carried out by using recombination process.

7. Recombination consists of selection, crossover, mutation and replacement steps.

The first step is selection of chromosomes for recombination. The second step is the crossover. This process is similar to biological crossover. Two chromosomes breaks off at a certain point and break off portions are exchanged with each other. New chromosomes are produces. The mutation is a random change in an individual chromosome. This is the third step. If the rate of mutation is equal to 0% then the solution takes time and if it is 100%, GA becomes random optimization. The mutation rate is kept in the range of 3% to 5%. The last step of recombination is replacement. The replacement of old chromosomes with new chromosomes are carried out except best chromosome as shown in flow chart of Figure 5.2.

8. Then, again terminating condition is checked. If any chromosome meets the terminating condition then program terminates. If the terminating condition does not reach then program will go to step 7 till the terminating condition is reached.

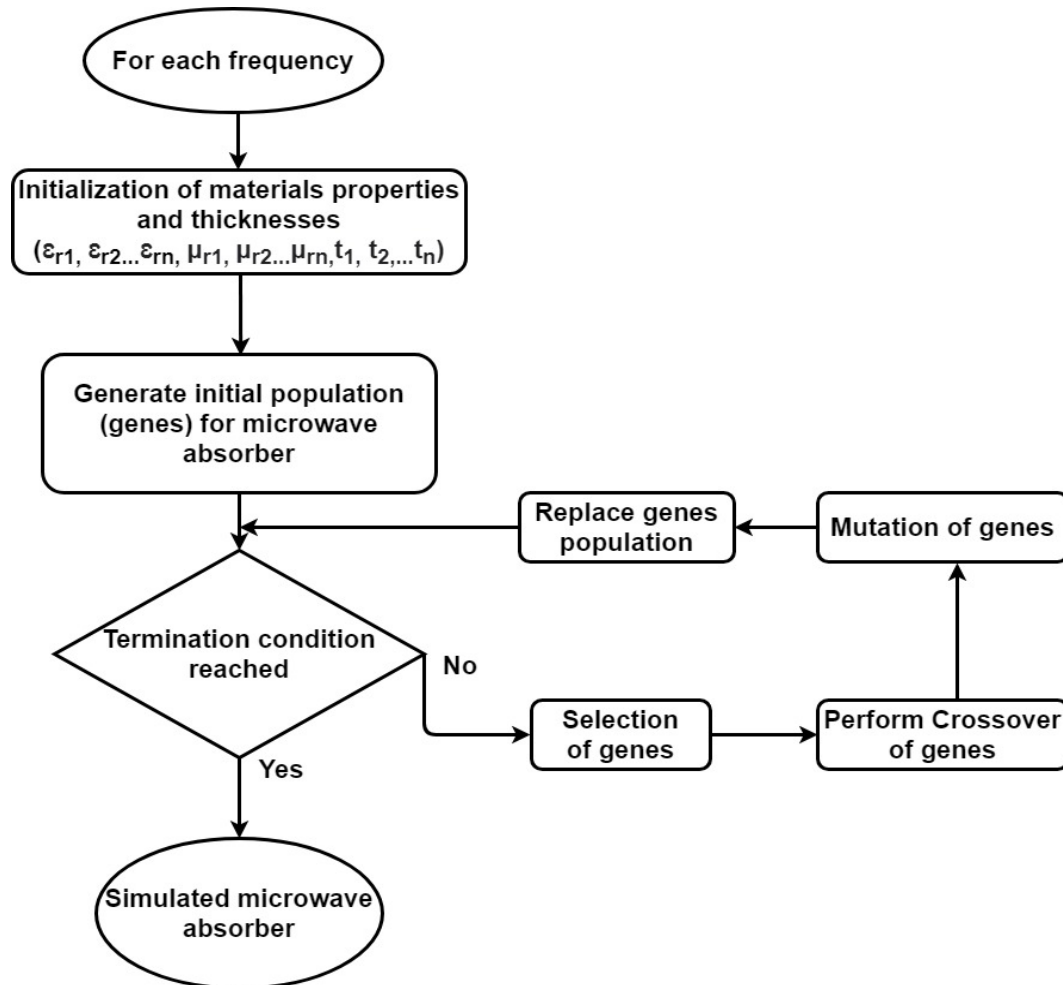


Figure 5.2: Flow Chart of Genetic Optimization

## 5.4 Measured and simulated results of multilayer microwave absorber in 1 to 8.2 GHz frequency range

### 5.4.1 Results for 2.5 to 8.2 GHz

Multilayer microwave absorber is designed as two layer absorber using genetic optimization. The two layer absorber consist of first layer of 0% CI powder by volume in CISR sheet and second layer of 50% CI powder by volume in CISR sheet. The thickness of first layer is 7.35 mm and second layer is 1.4 mm. It is analyzed by using equations 5.1 to 5.7 in Matlab. At normal incidences, the measured result of two layer absorber by RDWG method and NRL Arch method [Appendix C] are shown in Figure 5.3.

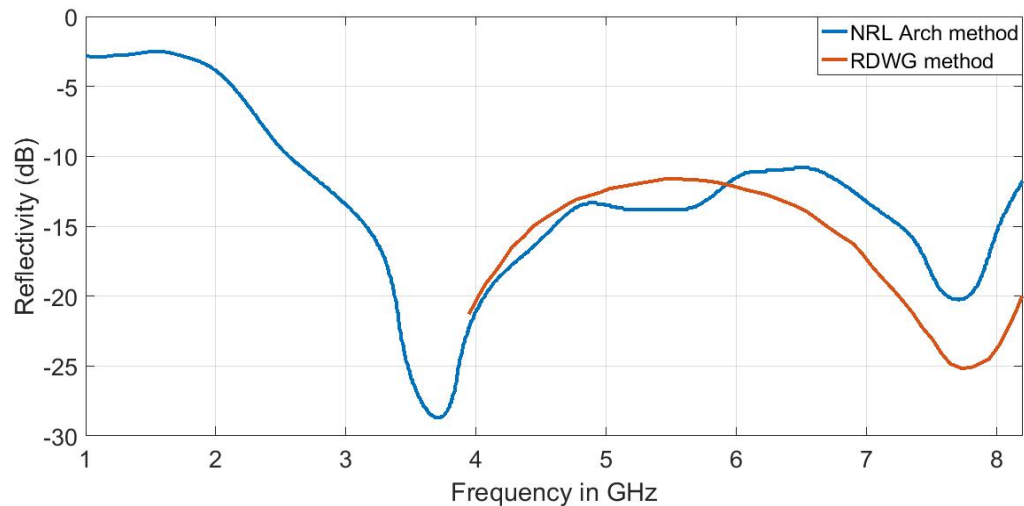


Figure 5.3: Measured results of two layer microwave absorber at normal incidence by NRL arch method and RDWG method

Measured reflectivity is found to be better than -10 dB in frequency range of 2.5 GHz to 8.2 GHz by NRL Arch method. Measured reflectivity is better than -11.8 dB in 3.95 to 8.2 GHz frequency range by RDWG method. Figure 5.4 shows the measured reflectivity of TE waves at various angle of incidences in frequency range of 1 to 8.2 GHz. Figure 5.5 shows the simulated reflectivity of TE waves at various

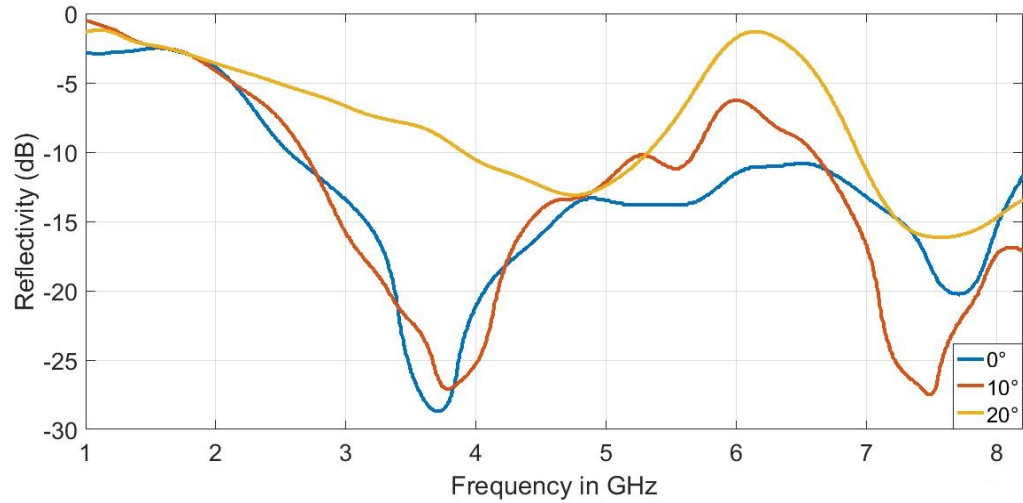


Figure 5.4: Measured reflectivity of two layer microwave absorber at angle of incidences ( $0^\circ$ ,  $10^\circ$  and  $20^\circ$ ) for TE waves in 1 to 8.2 GHz frequency range

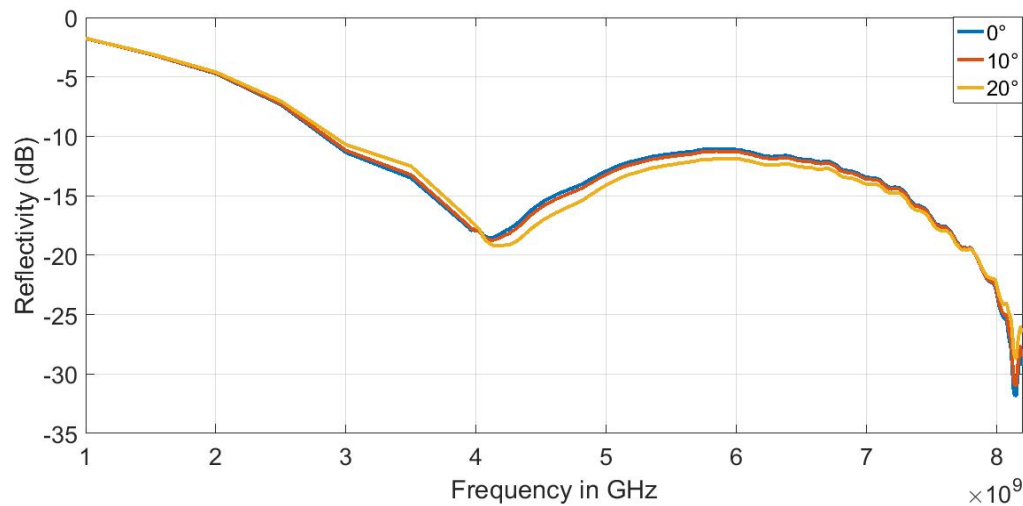


Figure 5.5: Simulated reflectivity of two layer microwave absorber at angle of incidences ( $0^\circ$ ,  $10^\circ$  and  $20^\circ$ ) for TE waves in 1 to 8.2 GHz frequency range

angle of incidences using equations 5.1 to 5.7 in the frequency range of 1 to 8.2 GHz. From Figure 5.3 to 5.5, it is observed that the simulation results are matching the measured results at normal incidence. The mismatch between simulated and measured results for TE waves at  $10^\circ$  and  $20^\circ$  are due to measurement errors. Figure 5.6 shows the measured reflectivity of TM waves at  $0^\circ$ ,  $10^\circ$  and  $20^\circ$  of incidences angles in frequency range of 1 to 8.2 GHz. Figure 5.7 shows the simulated reflectivity of TM waves at  $0^\circ$ ,  $10^\circ$  and  $20^\circ$  angle of incidences using equations 5.1 to 5.7 in the frequency range of 1 to 8.2 GHz. The measured results are matching with simulated

for TM waves at angles of incidence of  $0^\circ$  and  $10^\circ$ . The results are mismatching at  $20^\circ$  of incidence angle.

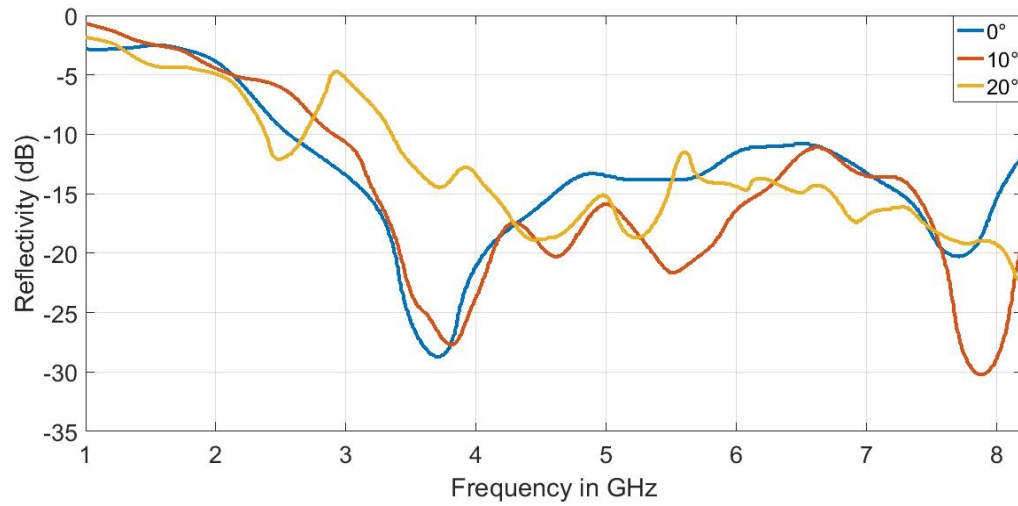


Figure 5.6: Measured reflectivity of two layer microwave absorber at angle of incidences ( $0^\circ$ ,  $10^\circ$  and  $20^\circ$ ) for TM waves in 1 to 8.2 GHz frequency range

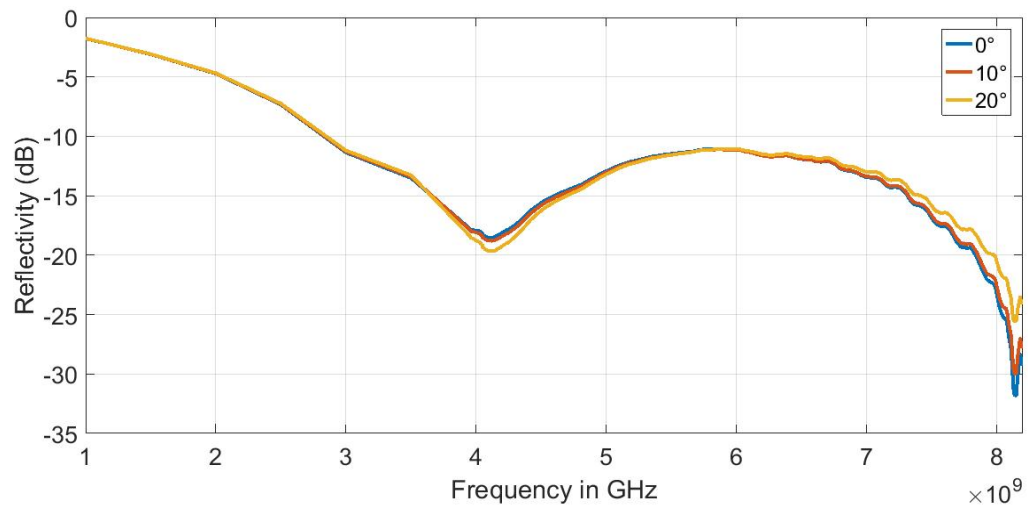


Figure 5.7: Simulated reflectivity of two layer microwave absorber at angle of incidences ( $0^\circ$ ,  $10^\circ$  and  $20^\circ$ .) for TM waves in 1 to 8.2 GHz frequency range

#### 5.4.2 Results for 1.6 to 2.6 GHz

For 1 to 3 GHz frequency range, two layer absorber was designed with first layer CISR sheets as 0% CI powder by volume and second CISR sheet as 50% CI powder by volume. Thickness of first layer is 20.5 mm and thickness of second layer is 22.2

mm. Because of the unavailability of small internal mixture for fabrication of CISR sheets and problem with manufacturing thick CISR sheets of 50% concentration, it was decided to use single layer quarter wavelength ( $\lambda/4$ ) resonant absorber of 3 mm CISR sheet of 50% CI powder by volume.

At normal incidence, the measured results of single layer absorber by NRL arch method and simulated result by using equation 5.3 to 5.7 are shown in Figure 5.8. Measured reflectivity is found to be better than -10 dB in frequency range of 1.6 GHz to 2.6 GHz. The bandwidth of simulated results are better from 1.7 to 3 GHz.

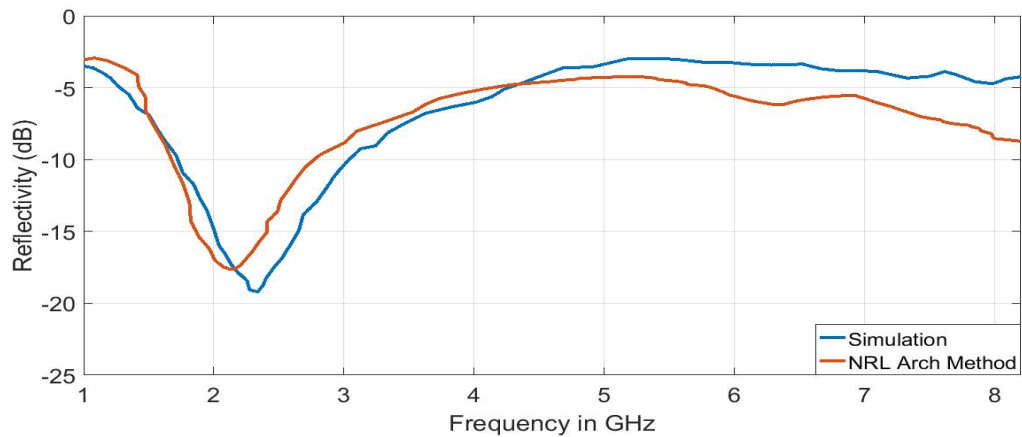


Figure 5.8: Measured and simulation result of single layer microwave absorber for normal incidence

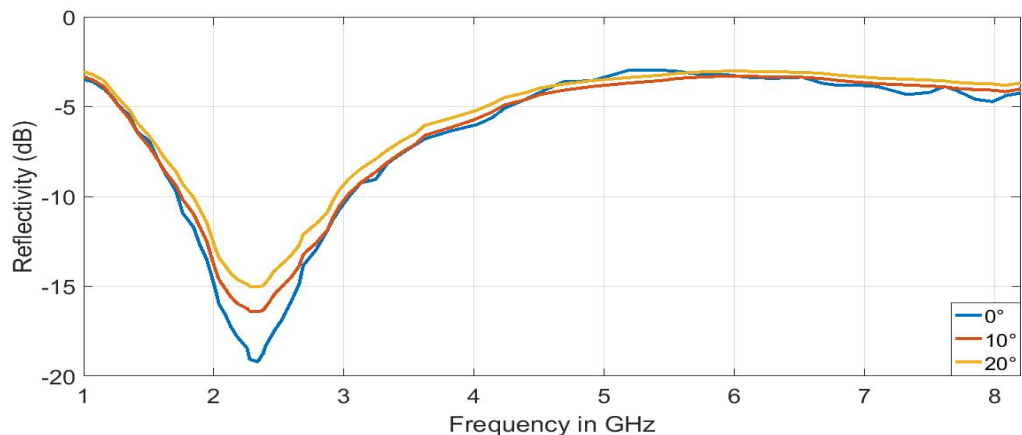


Figure 5.9: Simulation result of single layer microwave absorber at angle of incidences ( $0^\circ$ ,  $10^\circ$  and  $20^\circ$ ) for TE waves in 1 to 8.2 GHz frequency range

For single layer absorber, Figures 5.9 and 5.10 shows the simulated results of TE and TM polarizations for angle of incidences  $0^\circ$ ,  $10^\circ$  and  $20^\circ$ . The results shows the

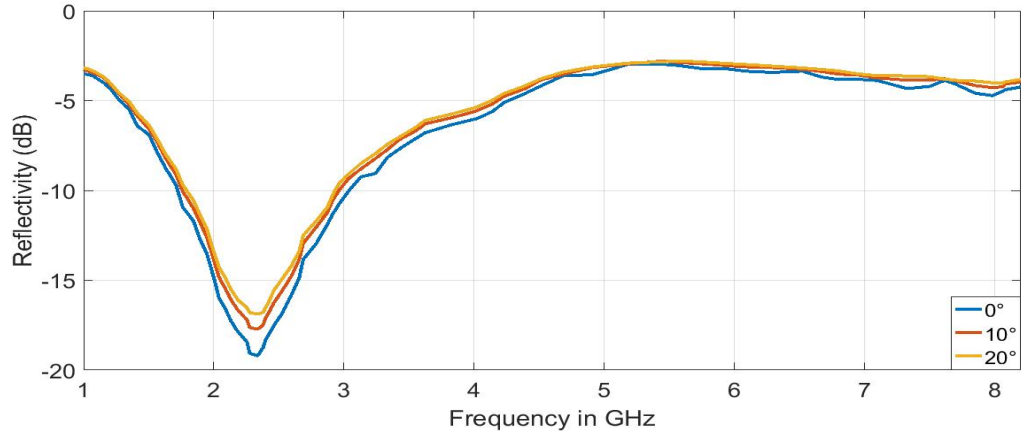


Figure 5.10: Simulation result of single layer microwave absorber at angle of incidences ( $0^\circ$ ,  $10^\circ$  and  $20^\circ$ , ) for TM waves in 1 to 8.2 GHz frequency range

behaviour of single layer microwave absorber does not change with incident angle in TE and TM polarizations.

## 5.5 Discussion and conclusions

Multilayer and single layer microwave absorbers are designed, fabricated and tested. All multilayer absorbers are designed as two layer absorbers because of fabrication inaccuracies in thickness and concentration of CI powder in CISR sheet. Genetic algorithm is used to optimize thickness and CI concentrations by volume in CISR sheets. Single layer absorber of thickness  $\lambda/4$  is designed as resonance absorber for 1.6 to 2.7 GHz frequency range. Two layer absorber is fabricated and tested by NRL arch method in the frequency range of 2.5 to 8.2 GHz. The simulated results are matching with measured results.

## References

- [1] Yong Bao Feng, Tai Qiu, Chun-Ying Shen and Xiao-Yun Li, "Electromagnetic and absorption properties of carbonyl iron/rubber radar absorbing materials," *IEEE Transactions on Magnetics*, vol. 42, no. 3, pp. 363-368, March 2006.
- [2] D.S.Weile, E. Michielssen and D.E. Goldberg, "Genetic algorithm design of Pareto optimal broadband microwave absorbers," *IEEE Transactions on Electromagnetic Compatibility*, vol.38, no.3, pp.518-525, August 1996.
- [3] Yonggang Xu, Liming Yuan, Xiaobing Wang, Deyuan Zhang, "Two-step milling on the carbonyl iron particles and optimizing on the composite absorption, " *Journal of Alloys and Compounds*, Vol 676, 2016, pp. 251-259.
- [4] X. Ren, H.Fan, Y.Cheng, "Microwave absorption properties of double-layer absorber based on carbonyl iron/barium hexaferrite composites," *Applied Physics A* 122, Article number 506, 2016. <https://link.springer.com/article/10.1007%2Fs00339-016-0041-8>.
- [5] Sung-Soo Kim, "Two-layered Microwave Absorber Laminated with Magnetic Composites for Intelligent Transport System, " *Applied Mechanics and Materials*, vol. 421, 2013, pp. 239-243.



## Chapter 6

# Design of broadband microwave absorbers using frequency selective surface embedded in carbonyl iron filled silicone rubber sheets

### 6.1 Introduction

In this chapter, broadband microwave absorbers are designed by using Frequency Selective Surface (FSS) embedded between two carbonyl iron filled silicone rubber sheets (CISR)[1,2]. Currently, there are two methods to design the geometry of FSS. First method is conventional type FSS [1,3-13] design by tailoring the geometry of the proposed structure such as length dipole, concentric ring, fractal shape, square loop etc. Second method is pixelated type FSS design by an optimization technique [2,14-18]. The former method is time-consuming and expensive because it requires human intuition, experience, and a large number of simulation experiments. However, the complex structure design of pixelated FSS makes it more difficult to obtain optimal structure parameters according to the desired frequency selective property. With the advantages of the latest binary version of various optimization techniques and the high computational power of computers, pixelated FSS design can be accomplished easily. The FSS design method based on pixelated unit cell structure provides a vast amount of flexibility in designing and achieving the desired geometry of the unit cell for various applications.

FSS is any thin, repetitive surface designed to reflect, transmit or absorb electromagnetic fields based on the frequency of the field. For thin and broadband microwave absorbers, conductive FSS [1] and resistive FSS [12] are used. The frequency response of FSS depends on various parameters such as thickness of substrate, dielectric and magnetic properties of materials, size of unit cell and geometry of FSS [1-23].

Figure 6.1 shows schematic diagram for broadband microwave absorber FSS layer embedded between layers 1 and layer 3. It is assumed that uniform plane wave of frequency  $f$  is incident at the broadband microwave absorber. Layer 1 and layer 3 can be realized by different concentration of carbonyl iron (CI) powder in CISR sheets by volume.  $t_a$ ,  $t_{fss}$  and  $t_b$  are thickness of layer 1, layer 2 and layer 3, respectively.  $\theta_i$  is the angle of incident and  $\theta_r$  is the angle of reflection. The layer

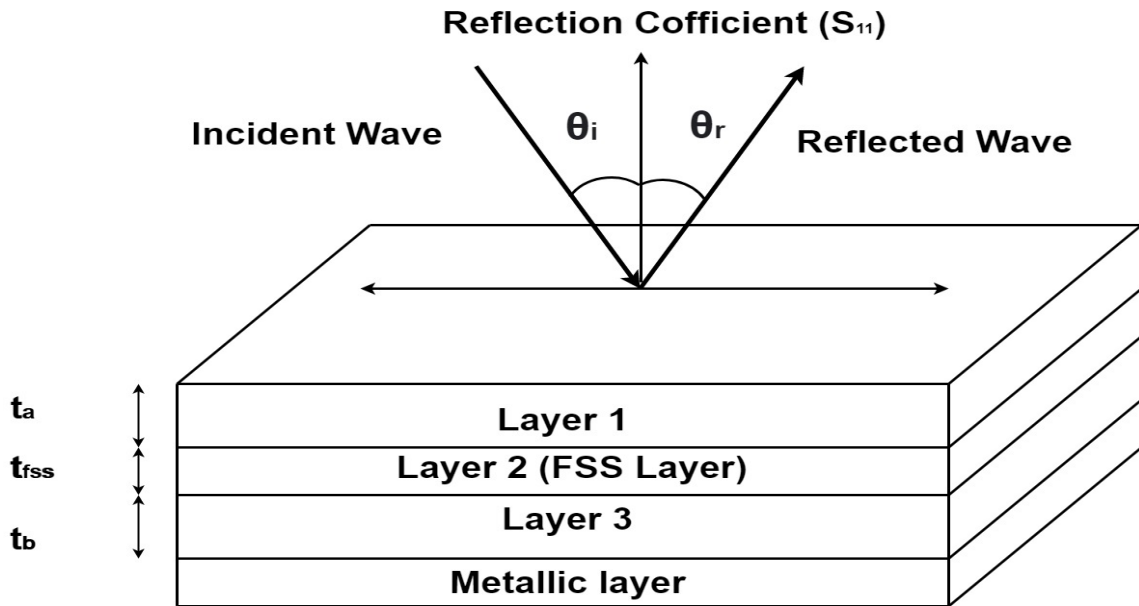


Figure 6.1: Schematic diagram of broadband microwave absorber

1 should have better matching characteristic ( $\mu'_r/\epsilon'_r = 1$ ) and layer 3 should have attenuation characteristic ( $\epsilon''_r$  and  $\mu''_r > 0$ ). FSS behave like a microwave filter. It is used to pass certain frequencies and block others. Using this property, broadband microwave absorption can be achieved.

## 6.2 Characterization of CISR sheets

Two CISR sheets with 24% of CI by volume as layer 1 and 33% of CI by volume as layer 2 are prepared [6]. These sheets are characterized in RDWG method. Thickness of each sheet is 2.7 mm. Figure 6.2 and 6.3 give values of  $\epsilon_r$  and  $\mu_r$  of CISR sheets. In case of 24% of CI by volume in CISR sheet,  $\mu''$  varies from 0.87 to 0.7 and  $\mu'$  varies from 1.85 to 1.23 from frequency range 3.95 to 8.2 GHz. In case of 33% of CI by volume in CISR sheets,  $\mu''$  varies from 0.9 to 1 and  $\mu'$  varies from 1.7 to 1.55 from frequency range 3.95 to 8.2 GHz.  $\epsilon''$  is approximately equal to zero in both cases.  $\epsilon'$  varies from 8.3 to 10.2 in 24% CI by volume in CISR sheets and from 11.8 to 11.9 in 33% CI by volume in CISR sheets in frequency range of 3.95 to 8.2 GHz.

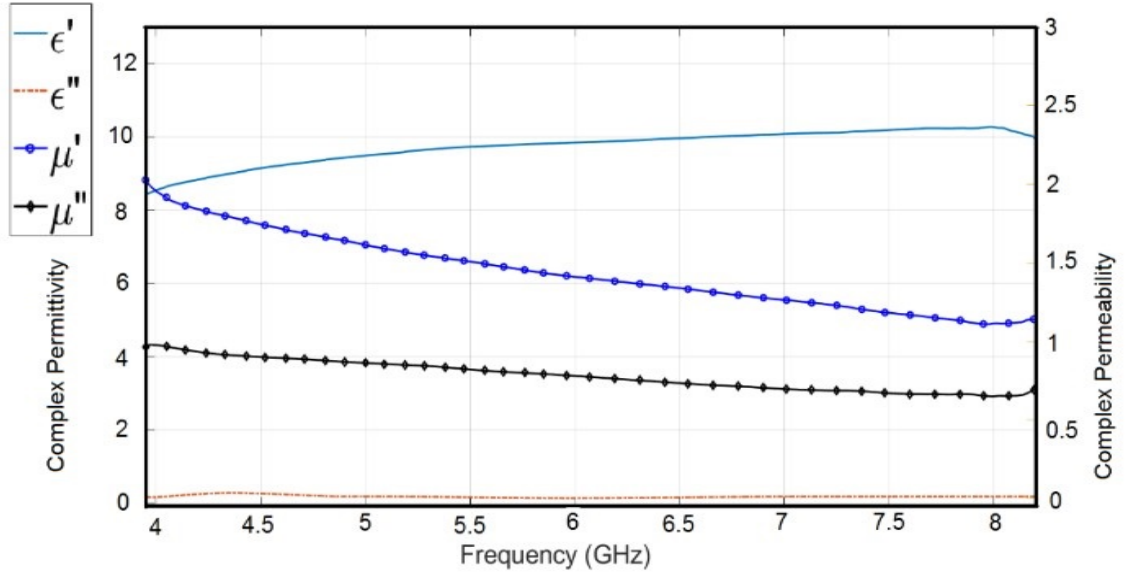


Figure 6.2: Measured  $\epsilon_r$  and  $\mu_r$  value for CISR sheets 24% of CI in CISR sheet by volume

## 6.3 Conventional Type FSS

For design of broadband microwave absorber in 3.95 to 8.2 GHz frequency range, the conventional type of FSS (layer 2) are designed by conductive concentric three square loops printed on FR4 dielectric substrate. Figure 6.4 shows the geometry of FSS unit cell. Measured dielectric constant and loss tangent of FR4 are 4.4 and 0.02,

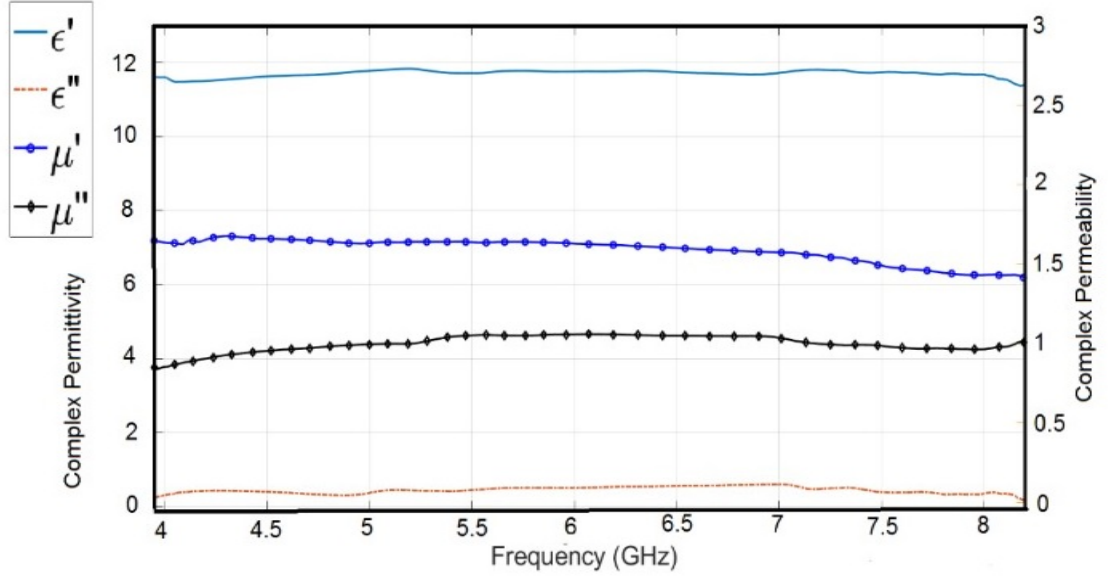


Figure 6.3: Measured  $\epsilon_r$  and  $\mu_r$  value for CISR sheets 33% of CI in CISR sheet by volume

respectively (books). The optimized FSS design for microwave absorber are  $a=15$  mm,  $b=13.6$  mm,  $c=9.6$  mm,  $d=5.2$  mm,  $e=0.8$  mm,  $f=1$  mm,  $g=0.8$  mm,  $t_d=0.9$  mm and  $t_{cu}=0.02$  mm, which is obtained by performing large number of simulation in CST microwave studio.  $t_d$  and  $t_{cu}$  are thickness of FR4 and thickness of printed copper, respectively. Equivalent circuit of FSS consist of three parallel LC circuits which correspond to three squares[24].

The fabrication is carried out in a PCB company. Printed photograph of FSS is shown in Figure 6.5.  $10 \times 10$  FSS unit cell are fabricated on single FR4 substrate of size  $15 \text{ cm} \times 15 \text{ cm}$ .

For FSS layer (layer 2 in Figure 6.1), Measurement of  $S_{11}$  and  $S_{21}$  is carried out by using RDWG method. NRW method (Appendix 1) is used to extract  $\epsilon_r$  and  $\mu_r$  from measured  $S_{11}$  and  $S_{21}$  values. Calculated  $\epsilon_r$  and  $\mu_r$  values of FSS layer are shown in Figure 6.6.  $\epsilon'$  value is near -80 at 3.95 GHz and reaches to 125 at 6.6 GHz. Then, the value of  $\epsilon'$  suddenly fall to again -80 at 6.8 GHz and rises to near -20 at 8.2 GHz. The value of  $\epsilon'$  is 0 at 6.75 GHz. The value of  $\epsilon''$  is always positive. The value of  $\epsilon''$  varies from near 40 at 3.95 GHz to 0 at 6 GHz, then it start rising and reaches to 220 at 6.75 GHz. The value of  $\epsilon''$  falls again from 220 at 6.75 GHz to near 0 at 8.2 GHz. The value of  $\mu'$  rises from -0.8 at 3.95 GHz to 1.8 at 8.2 GHz and the

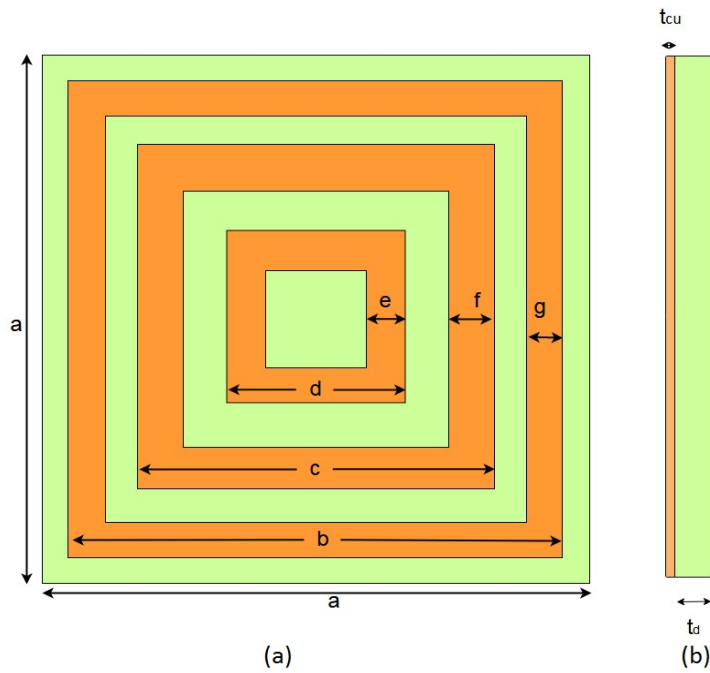


Figure 6.4: Geometry of FSS unit cell (a) Top view (b) Side view

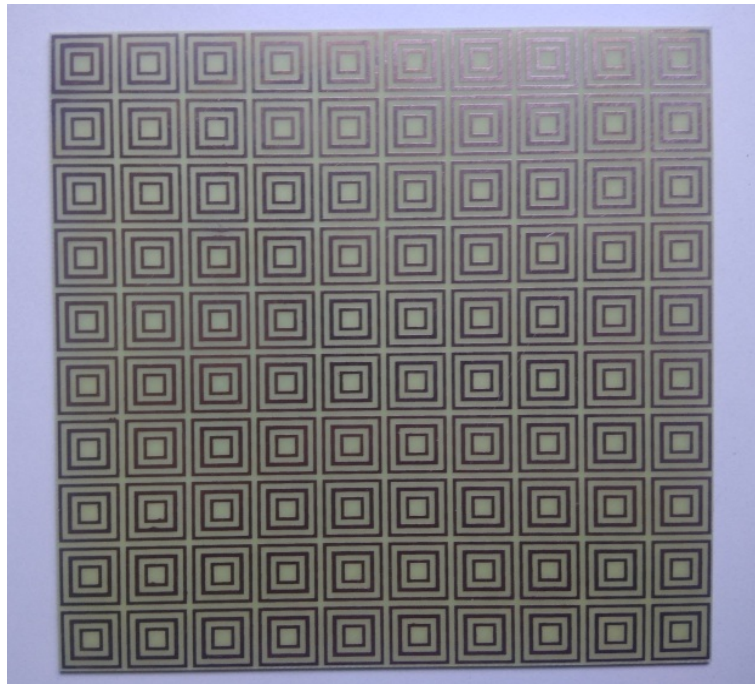


Figure 6.5: Photograph of Fabricated FSS

value of  $\mu''$  is -1 at 3.95 GHz to -1.2 at 8.2 GHz. This behaviour shows that it is a metamaterial. Calculated impedance of FSS layer is shown in Figure 6.7. At 5.2 GHz, FSS layer behaves like free-space. At 4.2 GHz and 7.6 GHz, FSS behave like a short circuit . Theses properties help in getting broadband absorption.

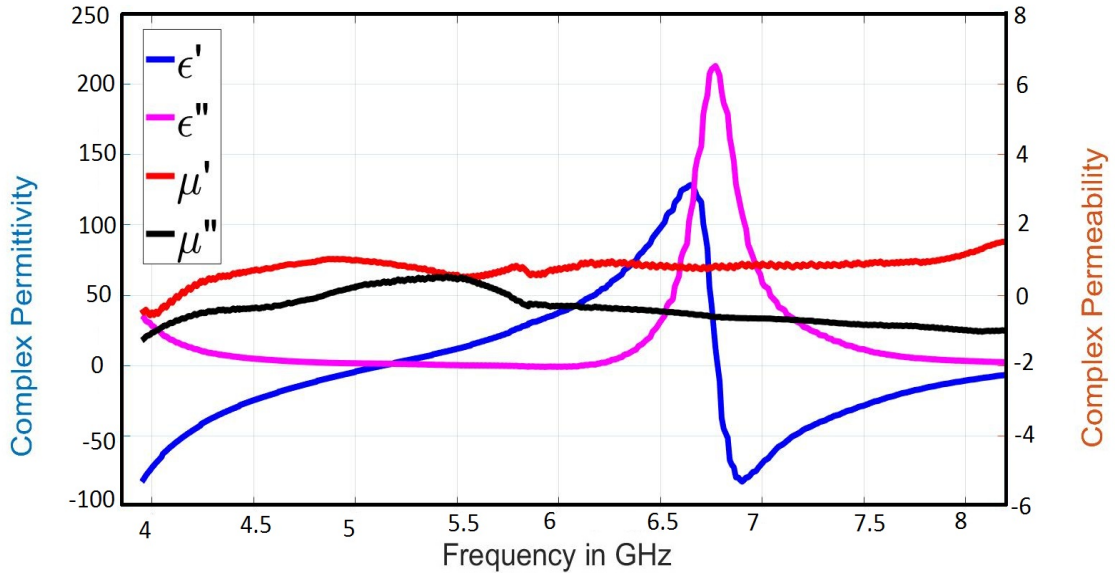


Figure 6.6:  $\epsilon_r$  and  $\mu_r$  value of FSS

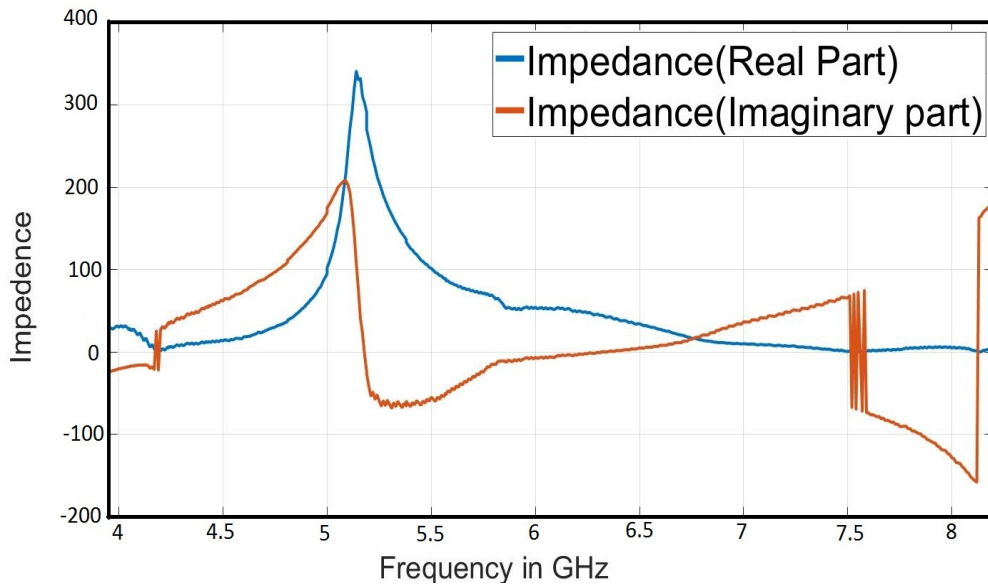


Figure 6.7: Calculated impedance of FSS

Using RDWG system, the measured reflectivity of broadband microwave absorber and two-layer absorber (without FSS layer) are shown in Figure 6.8. Simulated reflectivity of broadband microwave absorber are also shown in Figure 6.8. The two layer absorber (without FSS layer) reflectivity is not better than -6 dB in 3.95 to 8.2 GHz frequency range. Broadband microwave absorbers gives reflectivity better than -11 dB in 3.95 to 8.2 GHz frequency range. FSS layer is light in weight, invariable in thickness and easy to fabrication. These measured results are slightly different

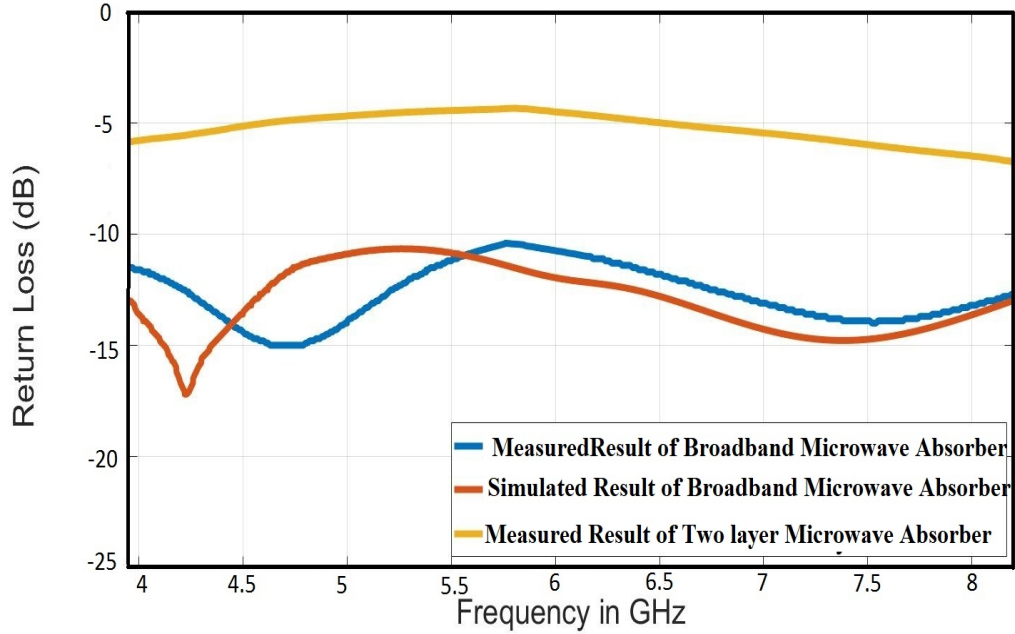


Figure 6.8: Simulated and measured results of microwave absorbers

from simulated results because of dimension tolerance of FSS unit cell, dimension tolerance of CISR sheets and glue used for pasting. It is observed that broadband microwave absorber has two absorption peaks at 4.2 GHz and 7.6 GHz in simulated results. At these frequency, FSS layer behave like a short circuit as shown in Figure 6.7. Maximum power get absorbed in layer 1 at 4.2 GHz and 7.6 GHz. At 5.2 GHz, simulated reflectivity of microwave absorber is minimum (-11 dB). At this frequency, FSS behave like free space which is embedded in two CISR layers.

CST Microwave Studio is used to study the reflectivity of broadband microwave absorber for normal and oblique incident in TE and TM polarizations as shown in Figure 6.9 and 6.10. For TM polarization, reflectivity are better then -10 dB for all angles. In case of TE polarization, reflectivity are greater then -10 dB for 30° to 60° angles. Due to changes in propagation of electric and magnetic fields in broadband microwave absorber for TE and TM polarizations absorption characteristics are different. [9,15]



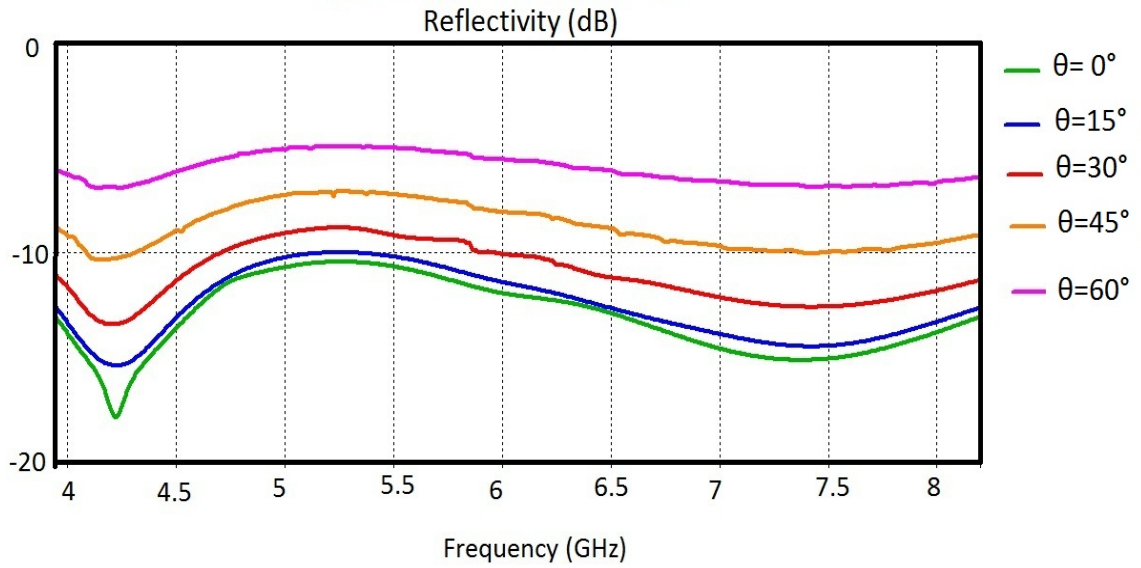


Figure 6.9: TE polarization of broadband microwave absorber at various incidence angles

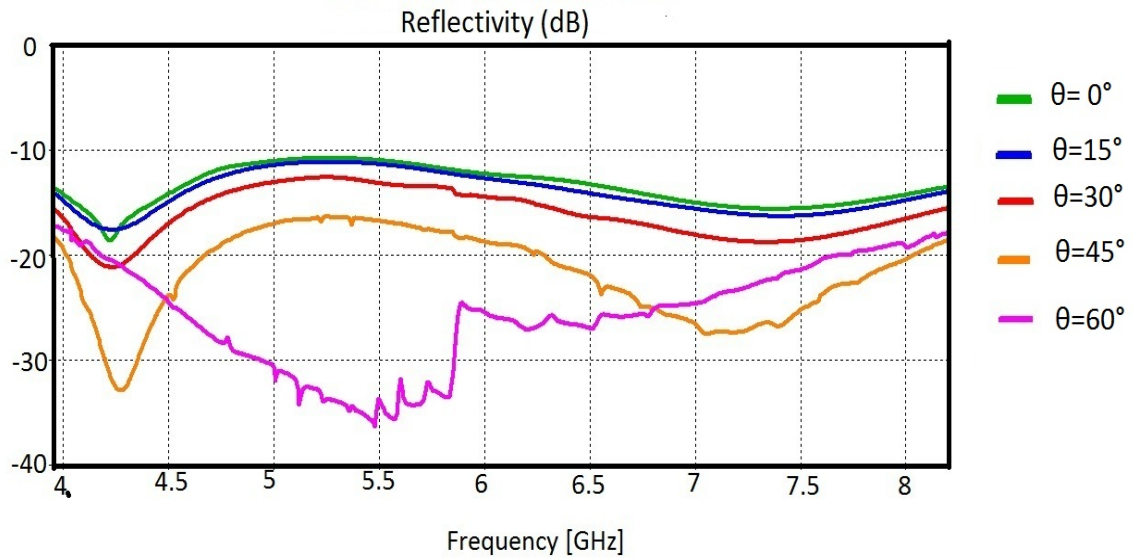


Figure 6.10: TM polarization of broadband microwave absorber at various incidence angles

## 6.4 Pixelated FSS

Pixelated FSS (layer 2 of Figure 6.1) is designed using Geometry-Refinement Method (GRM) and Genetic Algorithm (GA) optimization [25]. GA optimization was used in the placement of pixels in unit cell of optimized pixelated FSS as shown in Figure



6.11. GRM technique is used to avoid the lattice point that was placed during the GA

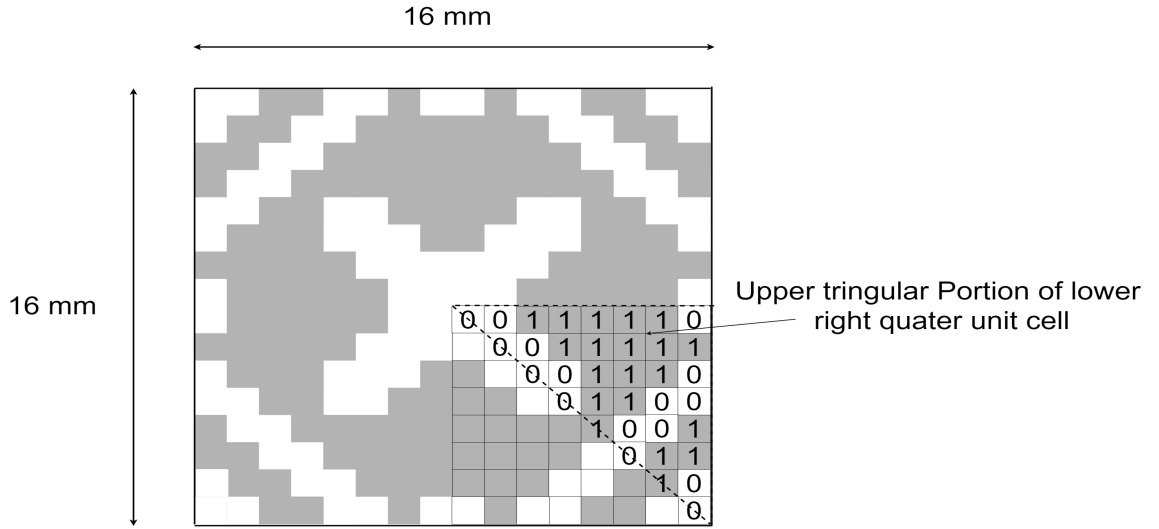


Figure 6.11: Flow chart of optimized pixelated FSS layer

optimization. GA and GRM operation is performed in Matlab. The simulation of broadband microwave absorber is performed in CST Microwave Studio (Figure 6.1). The pixels are arranged with eight fold symmetry as shown in Figure 6.11 (from 256 to 36 bit) which help in reducing computation time and make pixelated structure polarization insensitive [15]. The flowchart of our design of optimized pixelated FSS layer is shown in Figure 6.12. Initial population of 15 different genes are produced for GA optimization.

GA may probably put point contact  $\begin{pmatrix} 1 & 0 \\ 0 & 1 \end{pmatrix}$  and  $\begin{pmatrix} 0 & 1 \\ 1 & 0 \end{pmatrix}$  of conductor in the unit cell in the genes. These points are called the lattice point [25]. Lattice point give rise to a problem as these point does not touch analytically but physically does. This causes a change in resonance frequency because the electrical length can change due to contact at these lattice points. After generating 1st population, GRM technique has to find a 2D array of  $\begin{pmatrix} 1 & 0 \\ 0 & 1 \end{pmatrix}$  and  $\begin{pmatrix} 0 & 1 \\ 1 & 0 \end{pmatrix}$  (critical point) one after another and replace them with  $\begin{pmatrix} 1 & 0 \\ 1 & 1 \end{pmatrix}$  and  $\begin{pmatrix} 0 & 1 \\ 1 & 1 \end{pmatrix}$ , respectively [25]. This method takes the connectivity condition of the elements into consideration, thereby resulting in an easy fabrication which is far better than the pixel-overlap technique [26].

The evaluation criterion of the broadband microwave absorber performance has been chosen as the difference between the computed and desired reflection coeffi-

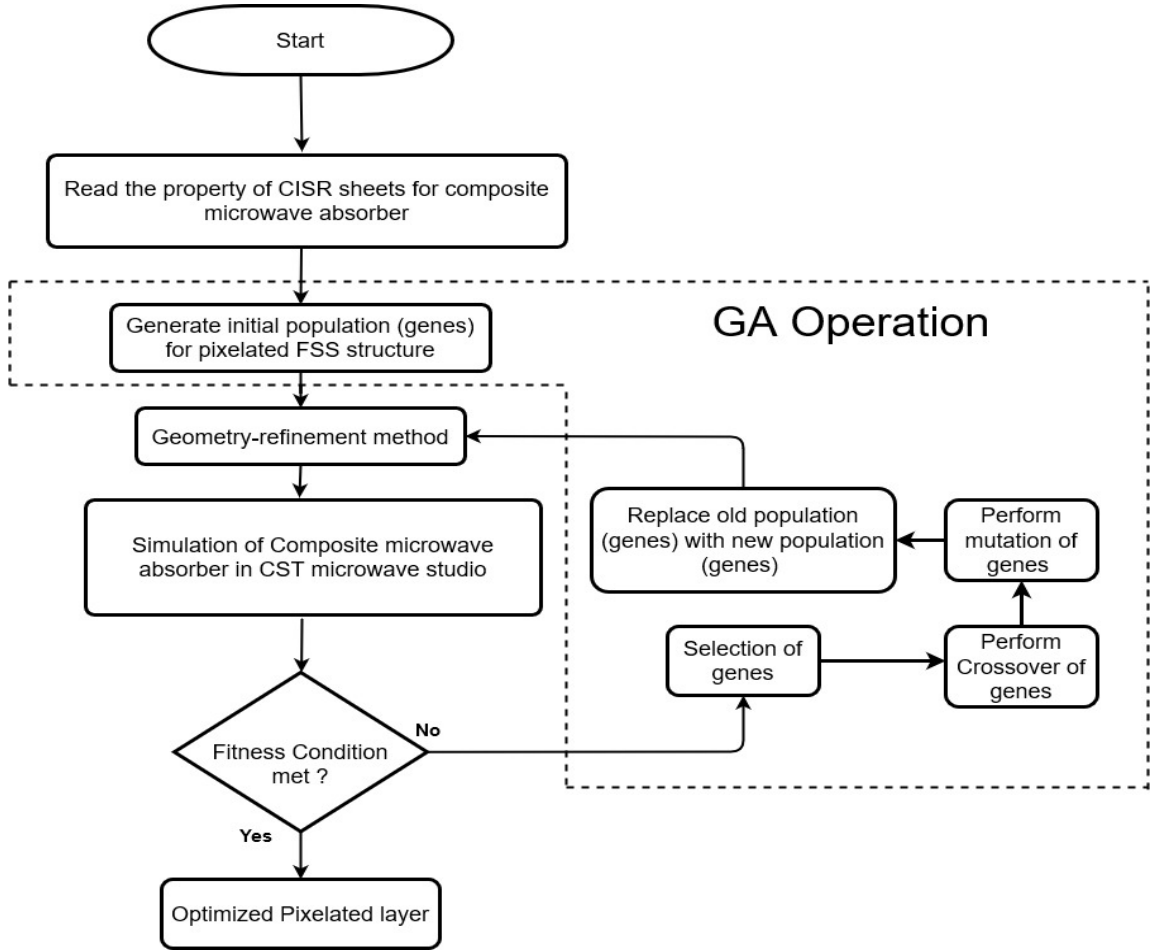


Figure 6.12: Flow chart of optimized pixelated FSS layer

cient. To improve the incident angle stability and polarization stability, reflection coefficients under different incident angles and polarization have been taken into consideration.

Broadband microwave absorber Fitness Function (F) is given in equation 6.1.

$$F = \sum_{\theta_i=0^\circ}^{\theta_{max}} \left( \sum_{f_i=f_{min}}^{f_{max}} (|R_{sim}^{TE/TM}(f_i, \theta_i)|_{dB} - |R_{des}|_{dB}) \right) \quad (6.1)$$

Where the angle of incidence ( $\theta_i$ ) varies from  $0^\circ$  degrees to  $40^\circ$  ( $\theta_{max}$ ) with increment of  $10^\circ$ . The operating frequency ( $f_i$ ) varies from 3.95 GHz ( $f_{min}$ ) to 8.2 GHz ( $f_{max}$ ) in step of 0.01 GHz.  $R_{des}$  is the desired reflection coefficient in dB whose value is set to -10 dB.  $R_{sim}^{TE/TM}(f_i, \theta_i)$  are magnitude of simulated reflection coefficient under incident angle  $\theta_i$  at frequency  $f_i$  with TE and TM polarization in dB. After generating reflection coefficient for each genes, it is checked for fitness function

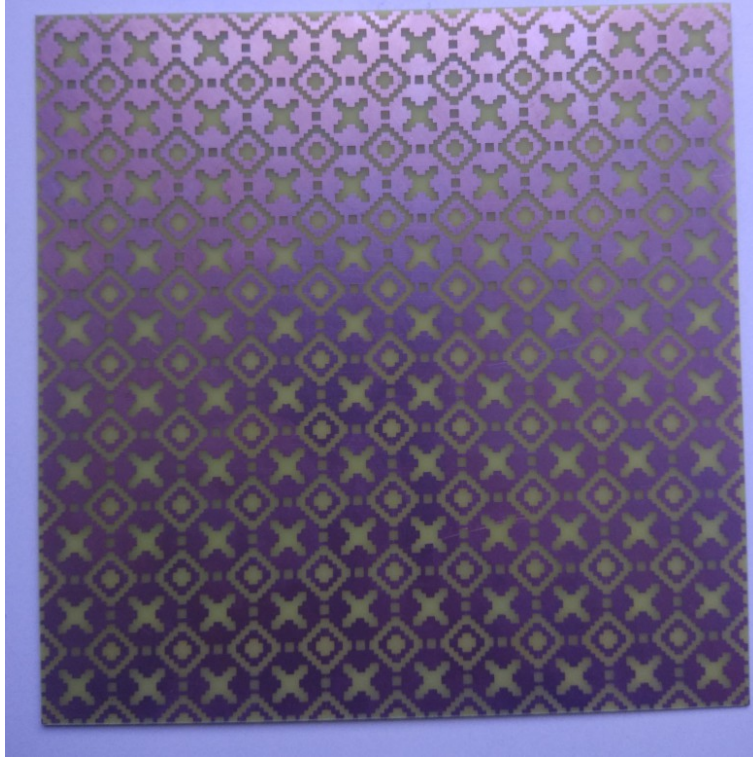


Figure 6.13: Photograph of optimized pixelated FSS layer

(termination condition). If any genes meet the fitness function then that genes is best gens and corresponding structure is the optimize pixelated FSS layer. If fitness condition does not meet then, best solution genes is kept and other genes are given to GA optimization as a feedback. New genes are produced after selection, crossover and mutation of other genes and similarly iteration was carried out until desired reflection coefficient is obtained.

The dimension of each pixel is 1 mm x 1 mm making 256 pixels per unit cell. A total of 10 x 10 unit cells (160 x160 mm) are printed on single side of FR4 with thickness of 0.035 mm. The thickness of FR4 is 0.9 mm. The total thickness of optimized pixelated FSS layer with FR4 is 0.935mm ( $t_{fss}$ ). It is having pixels of 1 and 0 which correspond to the copper (metallic pixels) and free space (blank pixels), respectively. The photograph of optimized pixelated FSS is shown in Figure 6.13. Its fabrication is carried out by using photoresist solder mask technique. RDWG system was used to measure reflection ( $S_{11}$ ) and transmission ( $S_{21}$ ) coefficients after calibration. The measured and simulated transmission and reflection coefficients of optimized pixelated FSS at normal incidence are shown in Figure 6.14 (magnitude)

and Figure 6.15 (phase) which shows the validity of our optimized design.

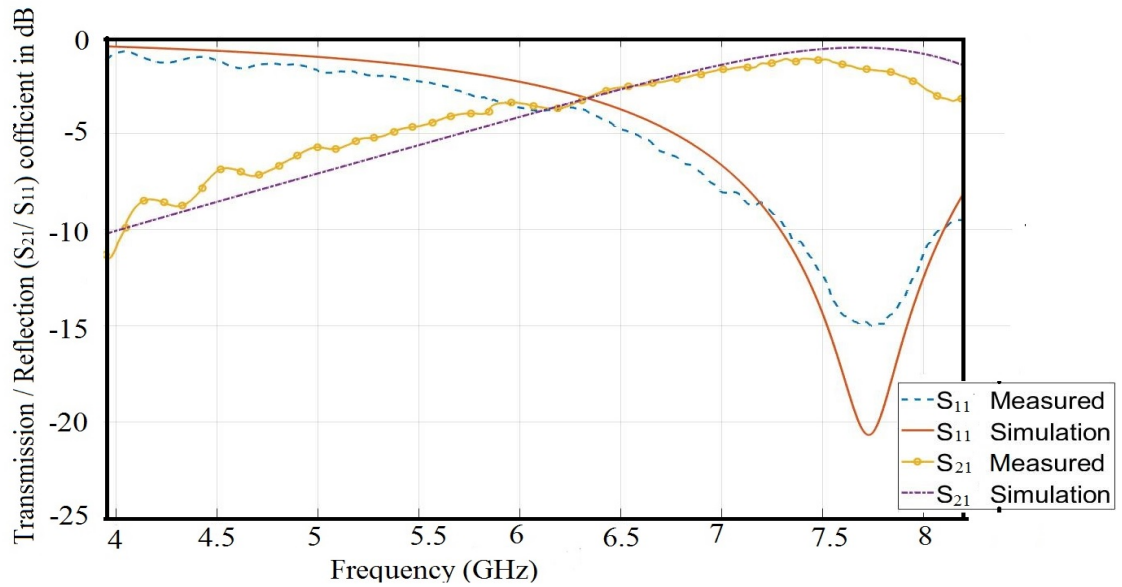


Figure 6.14: Reflection and Transmission of optimized pixelated FSS layer (Magnitude)

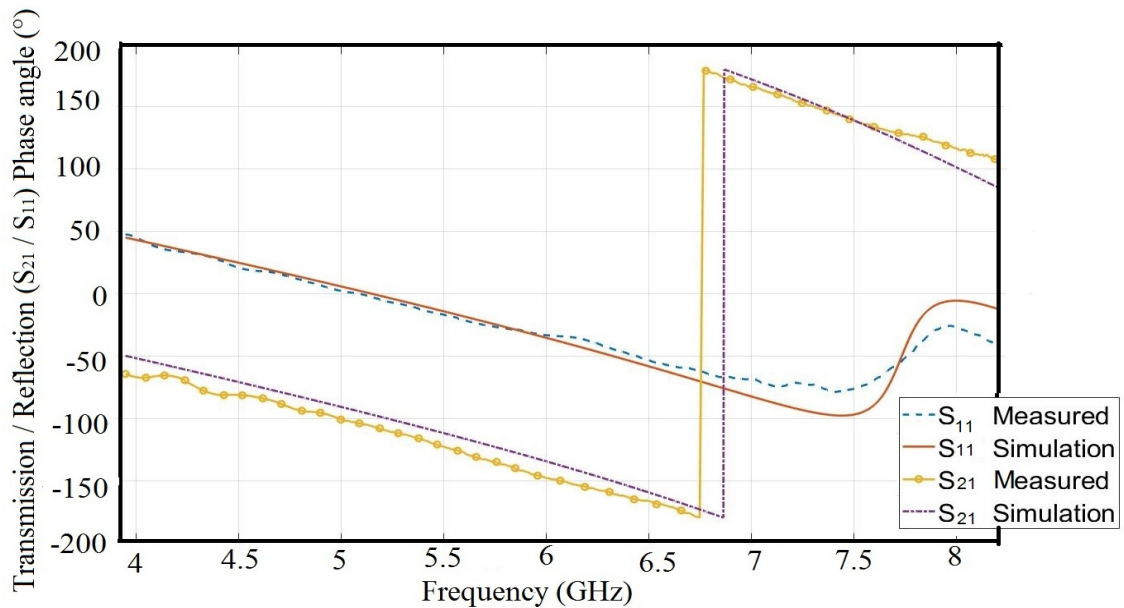


Figure 6.15: Reflection and Transmission of optimized pixelated FSS layer (Phase)

Optimized pixelated FSS layer behave like a filter which will pass the signal from 7.3 to 8.1 GHz frequency band ( $S_{11}$  is below -10 dB) and block the signal from 3.95 to 4.1 GHz frequency band ( $S_{21}$  is below -10 dB). The 4.1 GHz to 7.3 GHz band is the transition band of the signal from block to passband.

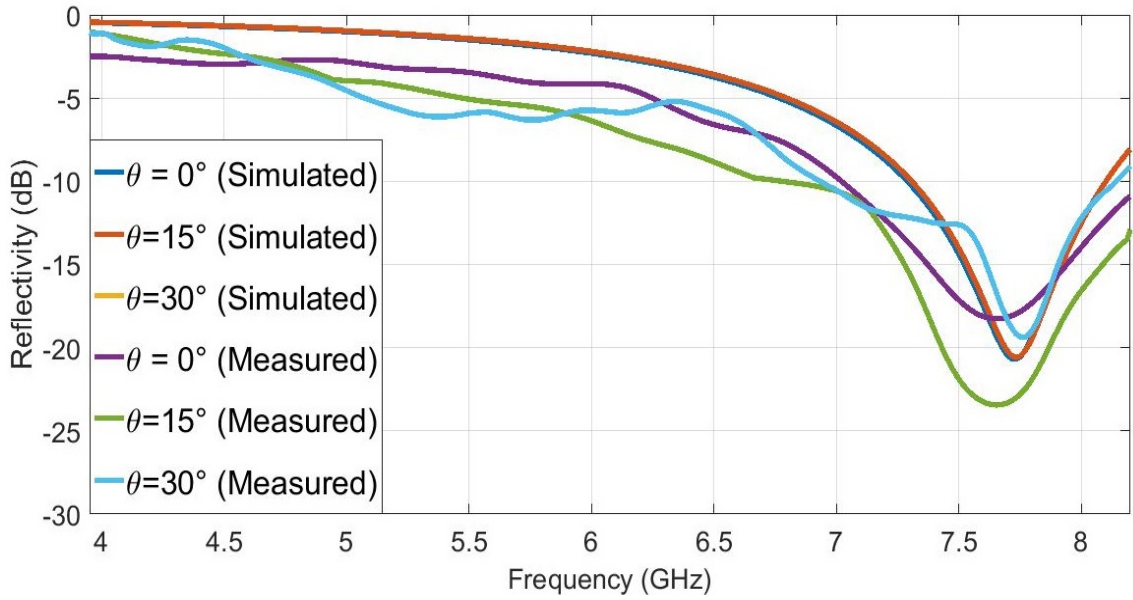


Figure 6.16: Reflectivity of optimized pixelated FSS layer in TE polarization

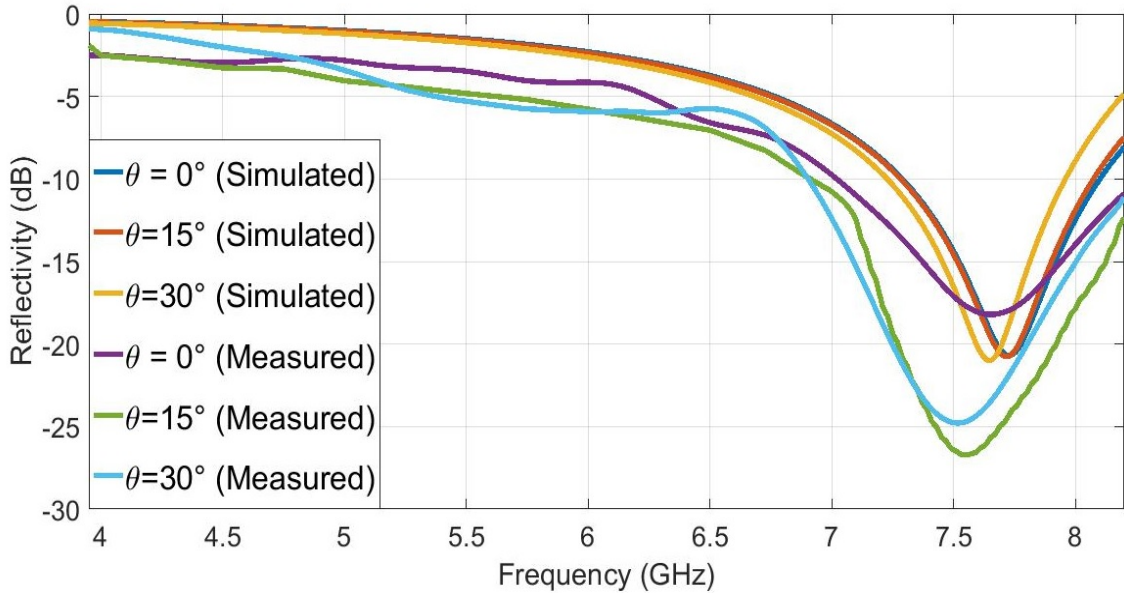


Figure 6.17: Reflectivity of optimized pixelated FSS layer in TM polarization

In order to know polarization insensitivity of optimized pixelated FSS for TE and TM polarizations, the simulated and measured reflectivity at different incidence angles are shown in Figures 6.16 and 6.17, respectively. The measurement of reflectivity ( $S_{11}$ ) at various oblique incidence angles are performed by NRL arch method [27]. Simulated results for different incident angles are close to each other for TE and TM polarizations except at 30° angle of incidence. For 30° angle of incidence, the resonance frequency for TE and TM polarizations are 7.75 GHz and 7.65 GHz,

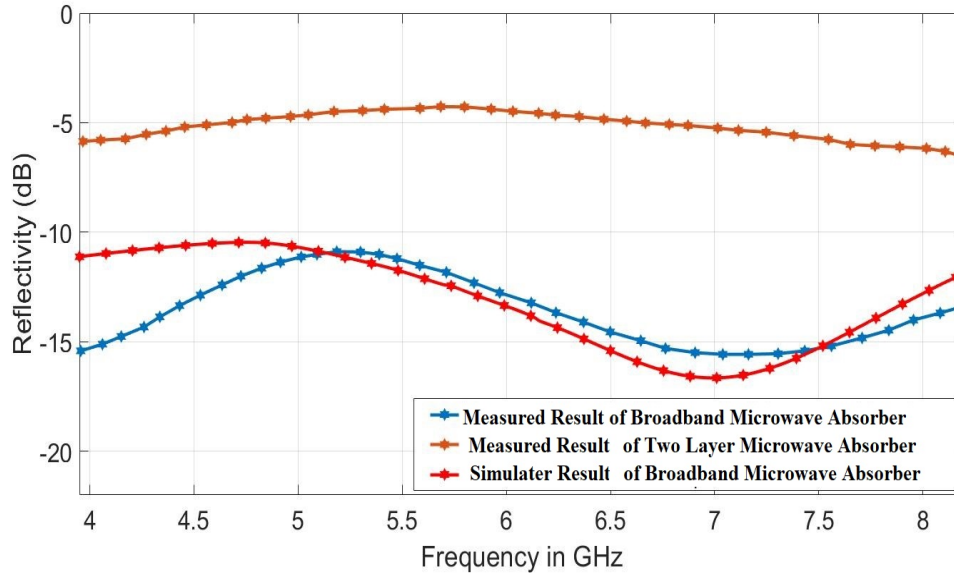


Figure 6.18: Measured reflectivity of broadband microwave absorber by RDWG system

respectively. In case of measured reflectivity in Figure 6.16 and 6.17, the results are same for TE and TM polarization at  $0^\circ$  and  $15^\circ$  of incidence angles. But, at  $30^\circ$  incident angle, the resonance frequency for TE and TM polarizations are 7.75 GHz and 7.5 GHz, respectively. These differences between measured and simulated values are due to dimension tolerance (0.05 mm) during manufacturing and measurement errors. Hence, the characteristic of polarized-insensitivity were exhibited for the optimized pixelated FSS layer.

RDWG measurement system is used to measure reflectivity of broadband microwave absorber. It is measured by placing a metal layer at the other end in the overall microwave absorber. Figure 6.18 shows simulated (using CST Microwave Studio) and measured reflectivity of broadband microwave absorber. It is observed that measured as well as simulated reflectivity are better than -10 dB. Measured reflectivity of two layer microwave absorber (broadband absorber without optimized pixelated FSS layer 2) is not better than -6 dB. By introducing optimized pixelated FSS layer in between two CISR sheets, reflectivity less than -10 dB is obtained which is light in weight, invariable in thickness and easy in fabrication. These measured results are slightly different from simulated results because of dimension tolerance of FSS unit cell, and glue used for pasting. It has two resonant absorption bands



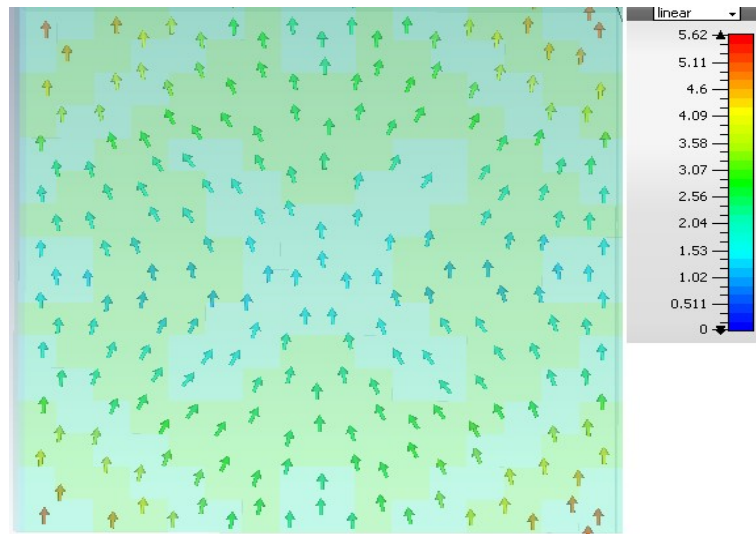


Figure 6.19: Vector plot of the surface current density in metallic plate at resonance frequency of 4 GHz

around 4 GHz and 7.5 GHz. Near 4 GHz, broadband microwave absorber behave like layer 1 backed by metallic sheet (because  $S_{21}$  is less than -10 dB). So, maximum microwave energy gets absorbed in the layer 1 as compare to layer 3. broadband microwave absorber at frequencies around 7.5 GHz consists of two CISR sheets with a free space of 0.935 mm (because pixelated FSS layer behaves like free space) in between. This type of arrangement is used to achieve absorption near 7.5 GHz as the maximum energy is absorbed in layer 3. For region between near 4 GHz to near 7.5 GHz, the behavior of optimized pixelated FSS layer change from stop-band to pass-band so maximum energy absorption will change from layer 1 to layer 3.

The same phenomena can be explained by using surface current density diagram through multiple resonance. Resonant frequencies of 4 and 7.5 GHz have been investigated by using vector plots of surface current density in the metallic plate and optimized pixelated FSS layer. The reason for the multiple resonance are shown in Figures 6.19, 6.20, 6.21, 6.22. The color and arrows indicate the magnitude and direction of vector currents, respectively. Also, as shown in the scale on the right side of above Figures, the rainbow color in which the red color indicates the maximum magnitude and blue color indicates the minimum magnitude.

At 4 GHz, the surface current density distribution in the metallic plate mainly focus on outer four edges of the conductor as shown in Figure 6.19. Its maximum

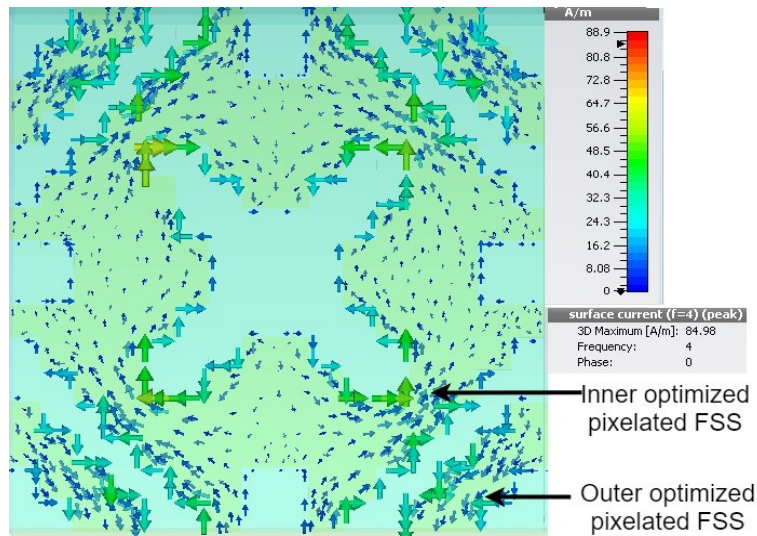


Figure 6.20: Vector plot of the surface current density in pixelated FSS layer at resonance frequency of 4 GHz

magnitude is 5.41 A/m going upward direction as indicated by red arrow. 0.5 A/m is the minimum surface current density at center as shown by blue arrow. The surface current density distribution in optimized pixelated FSS layer is shown in Figure 6.20. The direction of surface current in inner optimized pixelated FSS is upward and in outer optimized pixelated FSS is downward. Over all direction of surface current is upward and its maximum magnitude is 84.98 A/m as indicated by red arrow. 5.54 A/m is the minimum surface current density as shown by blue arrow. For resonance at 4 GHz, incident microwave induces currents in optimized pixelated layer and metal plate around which induced microwaves are produced and it causes absorption in CISR sheets (layers 1 and 3).

At 7.5 GHz, the surface current density is mainly concentrated towards center of the metal plate shown in Figure 6.21. It has a maximum magnitude of 2.6 A/m at the center and a minimum of 0.221 A/m at the outer edge. The maximum magnitude of optimized pixelated FSS is 67.86 A/m and minimum magnitude is 5.1 A/m as shown in Figure 6.22. The direction of surface current is downwards in metal plate and upward in optimized pixelated layer. The antiparallel currents causes magnetic resonance [28,29] which results in induced magnetic field and confined mainly to layer 3. Then, microwave power is absorbed by layer 3.

The analysis of different incident angles and polarization are shown in Figure 6.23



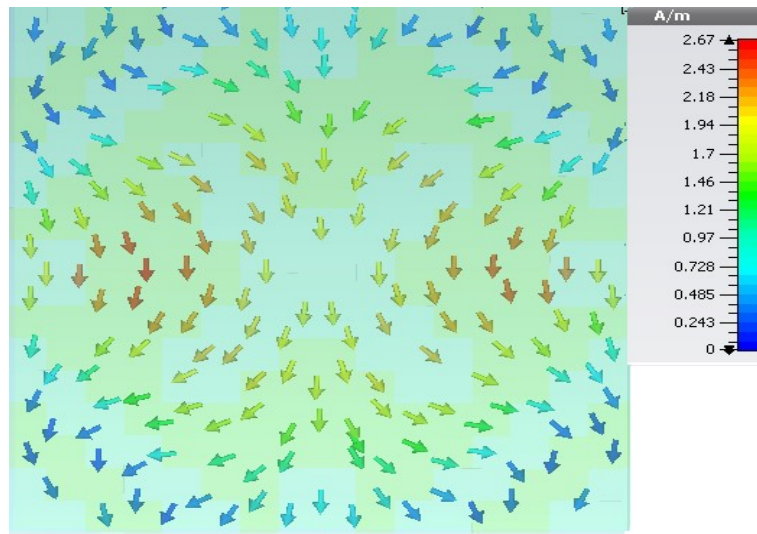


Figure 6.21: Vector plot of the surface current density in metallic layer at resonance frequency of 7.5 GHz

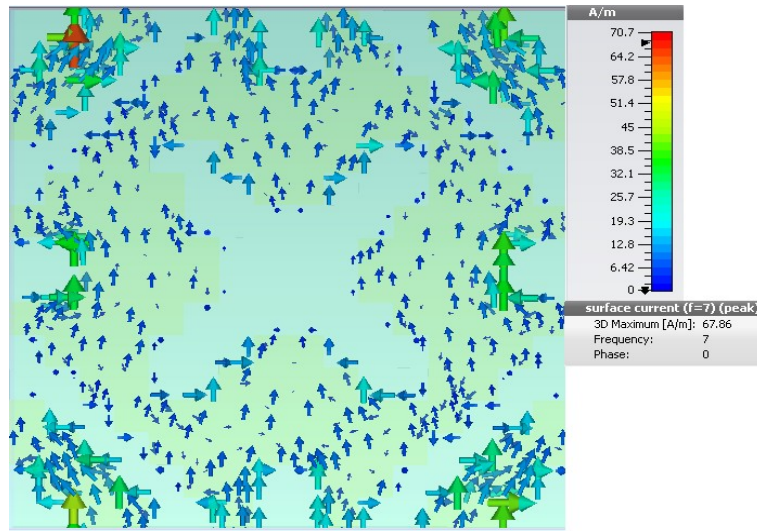


Figure 6.22: Vector plot of the surface current density in pixelated FSS layer at resonance frequency of 7.5 GHz

and 6.24. The reflectivity of the TE-polarized wave slightly increases with increases in incidence angles, while in case of TM-polarized wave it decreases smoothly with increasing incidence angles. The reflectivity is generally insensitive to the incidence angles from  $0^\circ$  to  $20^\circ$ . Due to the use of magnetic materials in layer 1 and layer 3 of broadband microwave absorber, the propagation of electric and magnetic fields are different for TE and TM polarizations [9][15]. These differences are increases at higher angle of incidences because of large changes in characteristics impedance of TE and TM polarizations [30].

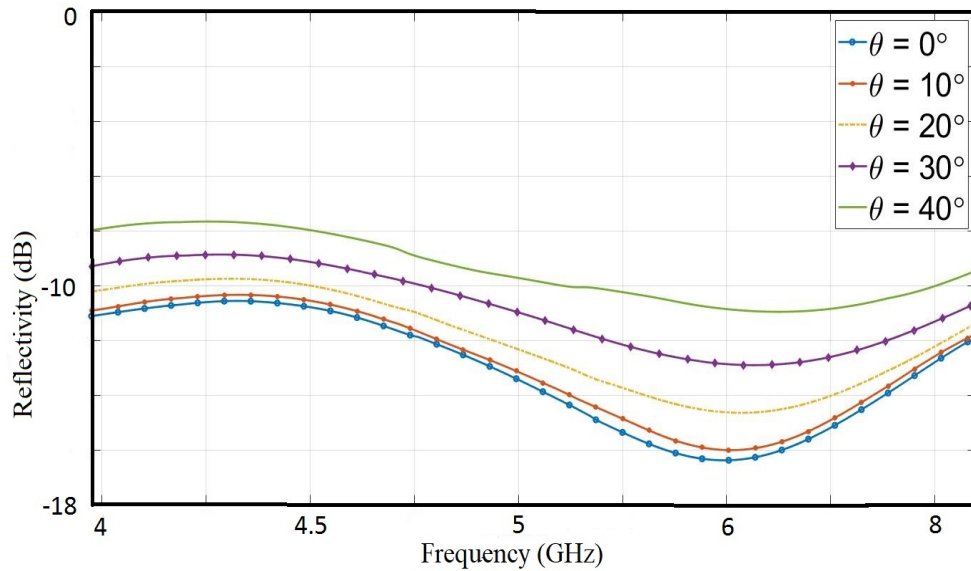


Figure 6.23: Reflectivity in TE-polarization at different incident angle

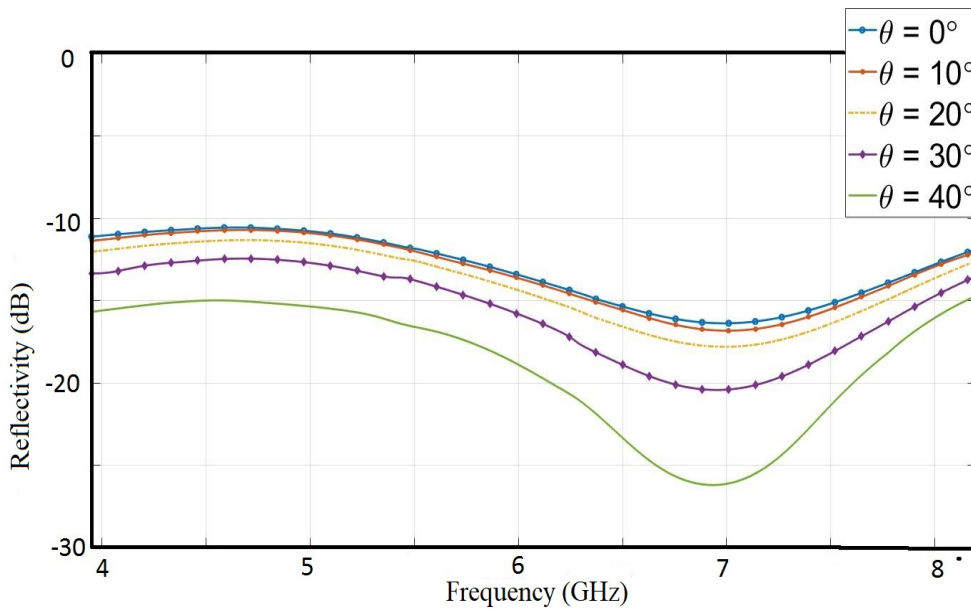


Figure 6.24: Reflectivity in TM-polarization at different incident angle

## 6.5 Comparison with other broadband microwave absorbers

The broadband microwave absorber is compared with already reported broadband absorbers as given in Table 6.1. The comparison is done in terms of bandwidth, reflectivity, thickness, number of layers and design methodology.

Table 6.1: Broadband microwave absorber are compared with other broadband microwave absorbers

Sr. No	Microwave Absorber	Bandwidth	Thickness	No. of layer	Design methodology
1	Rahul Vashisth et al[2]	3.95 to 8.2 GHz	6.335 mm	3	Pixelated Structure
2	Rahul Vashisth et al[1]	3.95 to 8.2 GHz	6.32 mm	3	FSS structure hit and trial
3	Wei Yuan et al[19]	4 to 18 GHz	2.2 mm	3	FSS structure hit and trial
4	Zilong Zhang[30]	2.2 to 9.5 GHz	4 mm	7	FSS structure hit and trial
5	Mengyun Zhao et al[14]	3 to 6 GHz	4 mm	2	Pixelated Structure
6	Linbo Zhang et al [21]	6.3 to 17.3 GHz	2.4 mm	3	FSS structure hit and trial
7	Hai-Yan Chen et al [22]	1.19 to 2.89 GHz	2 mm	5	FSS structure hit and trial

R. Vashisth et al [2] designed and fabricated broadband microwave absorber having reflectivity better than -10 dB in the frequency range of 3.95 to 8.2 GHz. They has designed and fabricated microwave absorber by using pixelated FSS embedded in two CISR sheets. R Vashisth et al [1] realized microwave absorber by embedding the conductive concentric square loops FSS layer between two CISR sheets. Wei Yuan et al[19] has designed microwave absorber in 4 to 18 GHz frequency range with edge-split square- loop FSS embedded in two rubber CI sheets. Zilong Zhang et al[30] also designed 2.2 to 9.5 GHz microwave absorber by using 3 layers of square patch FSS in four rubber CI sheets. M. Zhao et al [14] have fabricated and measured performance of metallic pixelated FSS with resistor (100 $\Omega$ ). They observed two strong absorption peaks below -6 dB in pixelated FSS in 3.08 to 6 GHz range. Linbo Zhang et al [21] has designed microwave absorber in 6.3 to 17.3 GHz range. This broadband microwave

absorber is based on two perforated magnetic polymer composites layers embedded with a FSS layer. Hai-Yan Chen et al [22] designed a microwave absorber with bandwidth of 1.19 to 2.89 GHz with two FSS layers and three magnetic composite layers.

## 6.6 Conclusion

Broadband microwave absorbers using conventional type FSS and pixelated type FSS are designed fabricated and tested by embedding them between two CISR sheets (24% and 33% of CI in CISR sheets by volume) Conventional type FSS layer were designed in CST microwave studio after performing large number of simulations. Pixelated FSS layer is designed with GA optimization and GRM technique. The fabricated FSS layer is tested with simulation results to validate the design. The reflectivity of both broadband microwave absorbers are tested in RDWG and found to be better than -11 dB at normal incidence in the frequency range of 3.95 to 8.2 GHz. The two layer microwave absorber (without FSS layer) reflectivity is around -6 dB. But by embedding FSS layer between two CISR layers increases its reflectivity to -11 dB which is low cost, light in weight. The broadband microwave absorber using pixelated FFS layer has better design methodology as it does not require human intuition, experience and a large number of simulations required in hit and trail metholodgy of conventional type FSS absorber. The analysis is performed at different incidence angle and TE / TM polarizations which shows reflectivity is generally insensitive to the incidence angles from 0° to 20°.

## References

- [1] R. Vashisth, D. Ghodgaonkar and S. Gupta, "Design and Fabrication of Broadband Microwave Absorber using FSS embedded in CISR sheets," *2018 IEEE MTT-S International Microwave and RF Conference (IMaRC)*, Kolkatta, India, 2018, pp. 1-4, doi: 10.1109/IMaRC.2018.8877271
- [2] Vashisth Rahul, Ghodgaonkar Deepak, Gupta Sanjeev, " Broadband Microwave Absorber using Pixelated FSS Embedded in CISR Sheets in Frequency Range of 3.95 to 8.2 GHz". *Journal of Electromagnetic Waves and Applications*, Taylor & Francis, 1569-3937. doi: 10.1080/09205071.2021.1947899 .
- [3] M. Li, S. Xiao, Y. Bai and B. Wang, "An Ultrathin and Broadband Radar Absorber Using Resistive FSS," *IEEE Antennas and Wireless Propagation Letters*, vol. 11, pp. 748-751, 2012, doi: 10.1109/LAWP.2012.2206361.
- [4] Wenwen Lai, Yan Wang, Junkun He." Effects of Carbonyl Iron Powder (CIP) Content on the Electromagnetic Wave Absorption and Mechanical Properties of CIP/ABS broadbands". *Polymers (Basel)*, Vol 12(8), Aug 2020.
- [5] B. S. Zhang, Y. Feng, H. Xiong, Y. Yang, and H. X. Lu. "Microwave-absorbing properties of De-aggregated flake-shaped carbonyl-iron particle broadbands at 2-18 GHz". *IEEE Transaction On Magnetism* vol. 42, no. 7, pp. 1778-1781, July 2006, doi: 10.1109/TMAG.2006.874188..
- [6] R. Vashisth, D. Ghodgaonkar and S. Gupta. "Permittivity and Permeability Measurements of CISR sheets for Microwave Absorber Applications". *2018 IEEE International RF and Microwave Conference (RFM)*, Penang, Malysis, 2018, pp. 359-362, doi: 10.1109/RFM.2018.8846539.

- [7] Eric Michielssen, Jean-Michel Sajer, S. Ranjithan, and Raj Mittra. "Design of lightweight, broad-band microwave absorbers using genetic algorithms". *IEEE Transactions on Microwave Theory and Techniques*. vol. 41, no. 6, pp. 1024-1031, June-July 1993, doi: 10.1109/22.238519.
- [8] F. Costa and A. Monorchio. "A Frequency Selective Radome With Wideband Absorbing Properties". *IEEE Transactions on Antennas and Propagation*, vol. 60, no. 6, pp. 2740-2747, June 2012, doi: 10.1109/TAP.2012.2194640.
- [9] A. H. Panaretos, D. E. Brocker, and D. H. Werner. "Ultra-Thin Absorbers Comprised by Cascaded High-Impedance and Frequency Selective Surfaces". *IEEE Antennas and Wireless Propagation Letters*, vol. 14, pp. 1089-1092, Dec. 2015, doi: 10.1109/LAWP.2015.2390145.
- [10] Y. P. Shang, Z. X. Shen, and S. Q. Xiao. "Frequency-Selective Resorber Based on Square-Loop and Cross-Dipole Arrays". *IEEE Transaction on Antennas and Propagation*, vol. 62, no. 11, pp. 5581-5589, Nov. 2014, doi: 10.1109/TAP.2014.2357427.
- [11] Y. N. Kazantsev, A. V. Lopatin, N. E. Kazantseva, A. D. Shatrov, V. P. Mal'tsev, J. Vilcakova, et al.. "Broadening of Operating Frequency Band of Magnetic-Type Radio Absorbers by FSS Incorporation". *IEEE Transaction on Antennas and Propagation*, vol. 58, no. 4, pp. 1227-1235, April 2010, doi: 10.1109/TAP.2010.2041316.
- [12] L. Sun, H. Cheng, Y. Zhou, and J. Wang. "Design of a lightweight magnetic radar absorber embedded with resistive FSS". *IEEE Antennas and Wireless Propagation Letters*, vol. 11, pp. 675-677, 2012, doi: 10.1109/LAWP.2012.2203292.
- [13] K. N. Rozanov. "Ultimate thickness to bandwidth ratio of radar absorbers". *IEEE Transaction on Antennas and Propagation*, vol. 48, no. 8, pp. 1230-1234, Aug. 2000, doi: 10.1109/8.884491.
- [14] Mengyun Zhao, Xiaowei Yu, Qiao Wang, Peng Kong, Yun He, Ling Miao, and Jianjun Jiang. "Novel Absorber Based on Pixelated Frequency Selec-

- tive Surface Using Estimation of Distribution Algorithm". *IEEE Antennas and Wireless Propagation Letters*, vol. 14, pp. 1467-1470, 2015, doi: 10.1109/LAWP.2015.2411692.
- [15] D. G. Holtby, K. L. Ford and B. Chambers. "Geometric transition radar absorbing material loaded with a binary frequency selective surface". *Radar Sonar Navigation*. Vol. 5, Iss. 4, (Apr 2011): pp. 483-488. doi: 10.1049/jet-rsn.2010.0213
- [16] S. Chakravarty and R. Mittra. "Design of a frequency selective surface (FSS) with very low cross-polarization discrimination via the parallel micro-genetic algorithm (PMGA)". *IEEE Transactions on Antennas and Propagation*, vol. 51, no. 7, pp. 1664-1668, July 2003, doi: 10.1109/TAP.2003.813637.
- [17] M. M. Tirkey and N. Gupta. "Design Simulation and Analysis of a Polarization-Independent Ultrathin Pixelated Metasurface Absorber". *2019 IEEE MTT-S International Microwave and RF Conference (IMaRC)*, pp. 1-4, doi: 10.1109/IMaRC45935.2019.9118698.
- [18] Ghaderi, B., Nayyeri, V., Soleimani, M. et al. "Pixelated Metasurface for Dual-Band and Multi-Polarization Electromagnetic Energy Harvesting". *Sci Rep* 8 , 13227 (2018). <https://doi.org/10.1038/s41598-018-31661-6>
- [19] W. Yuan, Q. Chen, Y. Xu, H. Xu, S. Bie and J. Jiang. "Broadband Microwave Absorption Properties of Ultrathin broadbands Containing Edge-Split Square-Loop FSS Embedded in Magnetic Sheets". *IEEE Antennas and Wireless Propagation Letters*, Vol. 11, 2015, pp. 447-451. <https://doi.org/10.1007/s13391-015-4358-9>
- [20] P. Ranjan, A. Choubey, Santosh Kumar Mahto, Rashmi Sinha. "A six-band ultra-thin polarization-insensitive pixelated metamaterial absorber using a novel binary wind driven optimization algorithm". *Journal of Electromagnetic Waves and Applications*. 2018;32:2367-2385. DOI: 10.1080/09205071.2018.1510344
- [21] Linbo Zhang, Peiheng Zhou, Huibin Zhang, Lijuan Lu, Guorui Zhang, Haiyan Chen, Haipeng Lu, Jianliang Xie, and Longjiang Deng. "A Broadband Radar

- Absorber Based on Perforated Magnetic Polymer Composites Embedded With FSS". *IEEE Transactions on Magnetics*, vol. 50, no. 5, pp. 1-5, May 2014, Art no. 4004305, doi: 10.1109/TMAG.2013.2293129.
- [22] H. Chen, H. Zhang and L. Deng. "Design of an Ultra-Thin Magnetic-Type Radar Absorber Embedded With FSS". *IEEE Antennas and Wireless Propagation Letters*, vol. 9, pp. 899-901, 2010, doi: 10.1109/LAWP.2010.2076344.
- [23] Haibing Xu, Shaowei Bie and Jianjun Jiang. "Ultra-broadband and polarization insensitive metamaterial absorber based on frequency selective surface". *2016 10th International Congress on Advanced Electromagnetic Materials in Microwaves and Optics (METAMATERIALS) 2016*, pp. 400-402, doi: 10.1109/MetaMaterials.2016.7746414.
- [24] Langley, Richard J. and Edward A. Parker. "Double-square frequency-selective surfaces and their equivalent circuit." *Electronics Letters* 19, 1983, pp- 675-677.
- [25] M. Ohira, H. Deguchi, M. Tsuji and H. Shigesawa. "Multiband single-layer frequency selective surface designed by combination of genetic algorithm and geometry-refinement technique". *IEEE Transactions on Antennas and Propagation*, vol. 52, no. 11, pp. 2925-2931, November 2004, doi: 10.1109/TAP.2004.835289.
- [26] Ning Liu, Xianjun Sheng, Chunbo Zhang, Jingjing Fan and Dongming Guo. "Design of FSS radome using binary particle swarm algorithm combined with pixel-overlap technique". *Journal of Electromagnetic Waves and Applications*, Vol 31(5), 2017, pp.522-531. DOI: 10.1080/09205071.2017.1294506
- [27] W. Hofmann, C. Bornkessel, A. Schwind and M. A. Hein. "Challenges of RF Absorber Characterization: Comparison Between RCS- and NRL-Arch-Methods". *2019 International Symposium on Electromagnetic Compatibility- EMC EUROPE*, 2019, pp. 370-375, doi: 10.1109/EMCEurope.2019.8871983.
- [28] H. Tao, N. I. Landy, C. M. Bingham, X. Zhang, R. D. Averitt, and W. J. Padilla. "A metamaterial absorber for the terahertz regime: design, fabrication



and characterization". *Optics Express*, Vol. 16, Issue 10, 2008, pp. 7181-7188.  
<https://doi.org/10.1364/OE.16.007181>

[29] J. Zhou, E. N. Economou, T. Koschny, and C. M. Soukoulis. "Unifying approach to left-handed material design". *Optics Letter*. Vol. 31, Issue 24, 2006, pp. 3620-3622 ,<https://doi.org/10.1364/OL.31.003620>

[30] Zilong Zhang, Lei Zhang, Xiqiao Chen, Zhuang Wu, Yaoyi He, Yangyang Lv, Yanhong Zou. "Broadband metamaterial absorber for low-frequency microwave absorption in the S-band and C-band". *Journal of Magnetism and Magnetic Materials*, Vol 497, 2020, 166075, ISSN 0304-8853, <https://doi.org/10.1016/j.jmmm.2019.166075>.

## Chapter 7

# Conclusions and suggestions for future work

Two rectangular dielectric waveguide (RDWG) systems have been designed, namely, WR-137 for 5.85 to 8.2 GHz and WR-187 for 3.95 to 5.85 GHz, for non-destructive testing of  $\epsilon_r$ ,  $\mu_r$  of carbonyl iron silicone rubber (CISR) sheets. S-parameter measurements are carried out by sandwiching CISR sheets between two Teflon sheets. These Teflon sheets provide impedance matching and prevent sagging of CISR sheets. Coaxial air line system and RDWG system were used for calculation of  $\epsilon_r$  and  $\mu_r$  of CISR sheets from measured S-parameters in the frequency range of 1 GHz to 8.2 GHz using Nicolson-Ross-Weir method. 0%, 10%, 20%, 30%, 40% , 50% of CI powder by volume in CISR sheets were fabricated and tested. Polynomial approximation is used to get  $\epsilon_r$  and  $\mu_r$  values at intermediate concentrations of CI powder in CISR sheets by volume.

Multilayer microwave absorbers were designed by using genetic algorithm for finding concentrations of CI powder in CISR sheets and thicknesses of different layers. Two layer absorber is fabricated and tested by NRL arch method in the frequency range of 2.5 to 8.2 GHz. Single layer absorber of thickness  $\lambda/4$  is designed as resonance absorber for 1.6 to 2.7 GHz range.

Broadband microwave absorbers are design and fabricated by using conventional type FSS and pixelated type FSS embedded between two CISR sheets (24% and 33% of CI in CISR sheets by volume). The design of conventional type FSS layer was carried out after performing large number of simulations. Pixelated FSS layer was designed with genetic optimization and geometry refinement method which has better design methodology with high computational power of computers. The reflectivity of pixelated type microwave absorbers as well as conventional type FSS

microwave absorber are better than -10 dB in the 3.95 to 8.2 GHz frequency band for normal incidence. For TE/TM polarizations, the reflectivity of FSS microwave absorbers were insensitive to angle of incidences from 0° to 20°.

For CISR sheets, CI powder is a commonly used filler material in silicon rubber because of the high value of attenuation coefficients (50.56 dB/cm), high Curie temperature, and the higher specific saturation magnetization intensity. Silicon rubber is preferred as the host material in CISR sheets because of excellent weathering resistance, resistance to aging, chemical resistance, insulating properties and compatibility with many kinds of fillers.

Literature survey was carried out for characterization of CISR sheets, multilayer microwave absorber and FSS microwave absorbers. Yong-Bao Feng et al characterization results matches with  $\epsilon_r$  and  $\mu_r$  results of CISR sheets reported in this thesis. Yong-Bao Feng et al reported for  $\epsilon_r$  and  $\mu_r$  values for different CI powder in rubber (Ethylene–Propylene–Diene Monomer) which matches with CISR sheets (0% to 50% CI powder concentration in CISR sheets by volume) used in this thesis.

The work presented here may be extended as follows:

- Other filler materials in CISR sheets.

For design of multilayer microwave absorbers, filler materials (like graphite powder, carbon nano tube, ferrites, etc) other than CI powder can be investigated because resonance frequency of CI powder is at 2 GHz.

- Pixelated FSS design.

Pixelated FSS design by using smaller pixel can be explored as it gives more frequency flexibility. Optimization of complete pixelated FSS microwave absorber can be tried.



# Appendix A

## FGM-40, FGM-125 and AN-series Data sheet

[1,2]



### Eccosorb® FGM

Thin, Flexible, Broadband Microwave Absorber



#### THIN FLEXIBLE BROADBAND ABSORBER

Eccosorb FGM is a thin, flexible, magnetically loaded, silicone absorber. Silicone absorbers have high service temperature capabilities and offer advantages for high power and low outgassing applications. They can be subjected to high altitudes, including space, with no adverse effects.

#### FEATURES AND BENEFITS

- High power performance
- High magnetic loss
- Low outgassing properties

#### MARKETS

- Commercial Telecom
- Security and Defense

#### SPECIFICATIONS

TYPICAL PROPERTIES	ECCOSORB FGM-40	ECCOSORB FGM-125
Frequency Range (GHz)	4 - 18	2 - 12
Max Service Temperature °C (°F)	170 (338)	170 (338)
Hardness (Shore A)	94	85
Weight kg/m <sup>2</sup> (lb/ft <sup>2</sup> )	5.0 (1.0)	10.8 (2.2)
Outgassing (%TML) (%CVCM)*	0.16/0.06	0.31/0.10

*Data for design engineer guidance only. Observed performance varies in application.*

*Engineers are reminded to test the material in application.*

\* Outgassing data per ASTM E595-07; criteria for acceptability is 1.00% TML and 0.10% CVCM.

#### APPLICATIONS

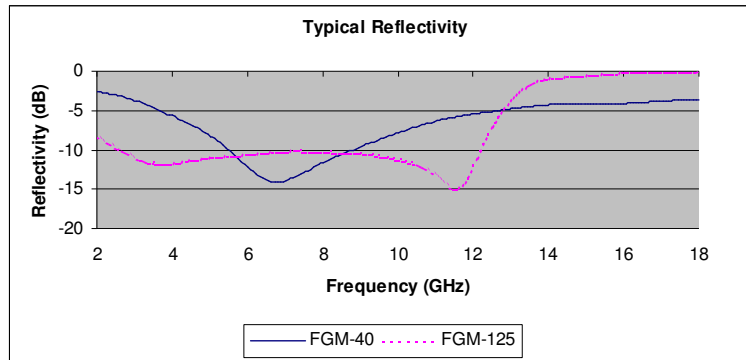
- Eccosorb FGM is used to line cavities in which antennas operate. It may be applied to surfaces to improve radar performance, reduce radar cross section or backscattering.
- Eccosorb FGM is effective even at high power in reducing specular reflections as well as surface currents due to the high magnetic loss properties.
- When bonded to a metal surface Eccosorb FGM will significantly reduce the reflectivity of metal objects or structures due to the flow of microwave currents on that surface.
- It can be applied to antenna elements, microwave dishes, the inner or outer surfaces of waveguides for isolation, attenuation or modification of radiating patterns.
- Applications include power amplifiers, oscillators, down/up converters and LNB's. It is also utilized to modify antenna patterns, cover antenna feed supports, line antenna caps to reduce reflections and improve the isolation of sensitive RF devices.

#### AVAILABILITY

- Standard sheets are 305 x 305mm (12"x12").
- Standard thicknesses are 1.0mm (.040") and 3.2mm (.125").
- On request Eccosorb FGM can be supplied with a Pressure Sensitive Adhesive.
- The product is also available in other sizes, thicknesses and customer specified configurations upon request.

**INSTRUCTIONS FOR USE**

- To obtain low reflectivity, the absorber must be mounted on a metal surface.
- The material can be bonded by use of an RTV silicone based adhesive in conjunction with a suitable primer. To obtain a strong bond, the metallic surface should be thoroughly cleaned with a degreasing solvent.
- Eccosorb FGM can be readily cut with a sharp knife and template. It is a very flexible material and conforms to contoured surfaces.



RFP-DS-FGM 092515

Any information furnished by Laird Technologies, Inc. and its agents is believed to be accurate and reliable. All specifications are subject to change without notice. Responsibility for the use and application of Laird Technologies materials rests with the end user. Laird Technologies makes no warranties as to the fitness, merchantability, suitability or non-infringement of any Laird Technologies materials or products for any specific or general uses. Laird Technologies shall not be liable for incidental or consequential damages of any kind. All Laird Technologies products are sold pursuant to the Laird Technologies' Terms and Conditions of sale in effect from time to time, a copy of which will be furnished upon request. © Copyright 2015 Laird Technologies, Inc. All Rights Reserved. Laird, Laird Technologies, the Laird Technologies Logo, and other marks are trademarks or registered trademarks of Laird Technologies, Inc. or an affiliate company thereof. Other product or service names may be the property of third parties. Nothing herein provides a license under any Laird Technologies or any third party intellectual property rights.

2

Flexible Foam Sheet Broadband Microwave Absorber



**FLEXIBLE FOAM SHEET BROADBAND MICROWAVE ABSORBER:**

Eccosorb AN is a lightweight, flexible, polyurethane foam sheet broadband microwave absorber. It is designed to reflect less than -17 dB of normal incident energy above specified frequencies and relative to a metal plate.

**FEATURES AND BENEFITS**

- Carbon loaded, multilayer absorber
- Broadband free space absorber
- Low weight
- RoHS/Reach compliant

**MARKETS**

- Commercial Telecom
- Security and Defense
- Test & Measurement

**SPECIFICATIONS**

TYPICAL PROPERTIES	ECCOSORB AN
Front surface color (facing oncoming EMI)	White
Back surface color	Black
Max. Service Temperature °C (°F)	90 (194)
Power Handling, W/cm <sup>2</sup>	0.15
Fire Retardancy	UL94-HBF

*Data for design engineer guidance only. Observed performance varies in application. Engineers are reminded to test the material in application.*

**APPLICATIONS**

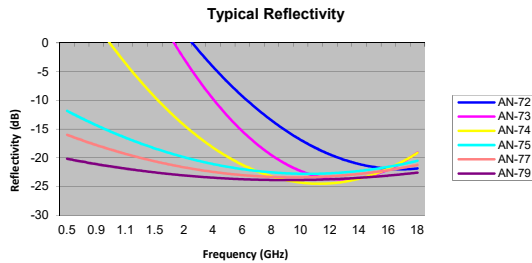
- Eccosorb AN is commonly used for the lining of small test chambers to reduce reflections.
- Eccosorb AN is being used for reducing crosstalk between adjacent antennas, shrouding antennas to improve the antenna patterns and undesired backlobes, as well as selective shadowing of parts of a target for RCS measurements.
- Shadowing of posts and supports in anechoic chambers, and as absorbing blankets for testing radar systems without harm to personnel.
- For isolation of components or antennas by means of insertion loss, it can be used without a metal backing.

**AVAILABILITY**

- Eccosorb AN is available in six standard grades depending upon the lowest desired frequency of operation, starting from 600 MHz.
- Standard sheets are 61 cm X 61 cm (24" x 24")
- Eccosorb AN is available in other sizes and customer specified configurations, incorporating miter cuts or attachment to metal parts.
- It can be manufactured, on special order, on a mandrel, to take a contoured shape.

Americas: +1.866.928.8181  
Europe: +49.(0).8031.2460.0  
Asia: +86.755.2714.1166

[www.lairdtech.com](http://www.lairdtech.com)



	Reflectivity range (>17 dB)	Nominal Thickness cm (inch)	Nominal Weight kg/piece (lb/piece)
<b>AN-72</b>	>20 GHz	0.6 (0.24)	0.25 (0.6)
<b>AN-73</b>	>7.5 GHz	1.0 (0.39)	0.50 (1.1)
<b>AN-74</b>	>3.5 GHz	1.9 (0.75)	0.70 (1.5)
<b>AN-75</b>	>2.4 GHz	2.9 (1.14)	0.80 (1.8)
<b>AN-77</b>	>1.2 GHz	5.7 (2.24)	1.50 (3.3)
<b>AN-79</b>	>600 MHz	11.4 (4.49)	2.95 (6.5)

### ENVIRONMENTAL PROPERTIES

- Eccosorb AN is not waterproof and will not operate correctly when wet. Since there is no washout, it will function as expected after being allowed to dry.
- A special CERSEAL coating to prevent moisture uptake in high humidity to moderately wet environments is available on special request.
- For high humidity to moderately wet environments, sealed versions of Eccosorb AN are available. They are essentially the same material as Eccosorb AN but the absorber is sealed to provide improved outdoor properties.  
The available types are :  
Eccosorb AN-xx-W :sealed with neoprene coated nylon fabric, color olive green.  
Eccosorb AN-xx-WPC : sealed with a poly-urethane coating, different colors available on request  
Eccosorb AN-xx-WPVC :sealed with a PVC plastic, different colors are available on request and can be provided with eye-lets for fixing
- Reflectivity performance is similar to the standard Eccosorb AN product;

### INSTRUCTIONS FOR USE

- To obtain low reflectivity, the absorbers must be mounted on a metal surface. If a metal surface is not available, Eccosorb AN can be supplied metal backed with aluminum foil (ML).
- For correct operation, Eccosorb AN must have the white (front) face towards the signal to be attenuated.
- Layering of multiple pieces or slicing off part of the thickness will degrade the overall performance.
- Reflectivity performance also degrades for off-normal bistatic incidence and at different rates for different polarizations.
- Eccosorb AN can be securely bonded to itself or to other materials such as metal, wood, and common plastic composites. Our specific Eccostock® foam adhesive is recommended.

RFP-DS-AN 081215

Any information furnished by Laird Technologies, Inc. and its agents is believed to be accurate and reliable. All specifications are subject to change without notice. Responsibility for the use and application of Laird Technologies materials rests with the end user. Laird Technologies makes no warranties as to the fitness, merchantability, suitability or non-infringement of any Laird Technologies materials or products for any specific or general uses. Laird Technologies shall not be liable for incidental or consequential damages of any kind. All Laird Technologies products are sold pursuant to the Laird Technologies Terms and Conditions of sale in effect from time to time, a copy of which will be furnished upon request. © Copyright 2015 Laird Technologies, Inc. All Rights Reserved. Laird, Laird Technologies, the Laird Technologies Logo, and other marks are trademarks or registered trademarks of Laird Technologies, Inc. or an affiliate company thereof. Other product or service names may be the property of third parties. Nothing herein provides a license under any Laird Technologies or any third party intellectual property rights.



## References

- [1] <https://www.laird.com/products/microwave-absorbers/microwave-absorbing-elastomers-and-films/eccosorb-fgm>.
- [2] <https://www.laird.com/products/microwave-absorbers/microwave-absorbing-foams/eccosorb-an>

## Appendix B

### NRW Method

Figure B.1 shows a CISR sheets of thickness  $d$  placed in free space [1]. The complex permittivity ( $\epsilon_r$ ) and complex permeability ( $\mu_r$ ), relative to free space, are defined as,

$$\epsilon_r = \epsilon' - j\epsilon'' = \epsilon'(1 - j \tan\delta_\epsilon) \quad (\text{B.1})$$

$$\mu_r = \mu' - j\mu'' = \mu'(1 - j \tan\delta_\mu) \quad (\text{B.2})$$

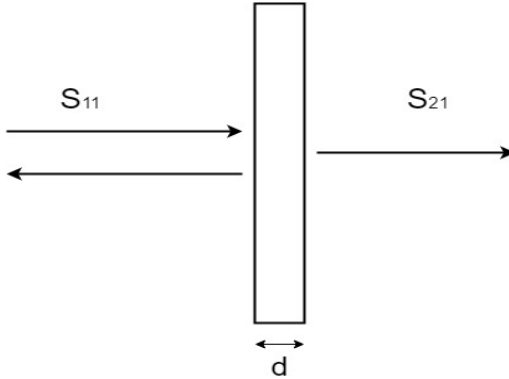


Figure B.1: Schematic diagram of CISR sheet

It is assumed that the CISR sheet is of infinite extent literally so that diffraction effects at the edges can be neglected. A linearly polarized, uniform plane wave of frequency  $f$  is normally incident on the sample. The reflection and transmission coefficients  $S_{11}$  and  $S_{21}$  are measured in free space for the normally incident plane wave. By applying boundary condition at the air sample interface in Figure B.1, it can be shown that  $S_{11}$  and  $S_{21}$  parameters are related to the parameters  $\Gamma$  (Reflection

Coefficient) and T (Transmission Coefficient) by the following equations.

$$S_{11} = \frac{\Gamma(1 - T^2)}{1 - \Gamma^2 T^2} \quad (\text{B.3})$$

$$S_{21} = \frac{T(1 - \Gamma^2)}{1 - \Gamma^2 T^2} \quad (\text{B.4})$$

$$\Gamma = \frac{Z_{sn} - 1}{Z_{sn} + 1} \quad (\text{B.5})$$

$$T = e^{-\gamma d} \quad (\text{B.6})$$

In equations B.7 and B.8,  $Z_{sn}$  and  $\gamma$  are the normalized characteristic impedance and propagation constant of the CISR sheet. They are related to  $\epsilon_r$  and  $\mu_r$  by following relationships.

$$Z_{sn} = \sqrt{\frac{\mu_r}{\epsilon_r}} \quad (\text{B.7})$$

$$\gamma = \gamma_0 \sqrt{\epsilon_r \mu_r} \quad (\text{B.8})$$

Where  $\gamma_0 = (j 2\pi/\lambda_0)$  represents the propagation constant of free space and  $\lambda_0$  is the free-space wavelength. From equations B.3 and B.4,  $\Gamma$  and T are given by following equation.

$$\Gamma = K \pm \sqrt{K^2 - 1} \quad (\text{B.9})$$

Where,

$$K = \frac{S_{11}^2 - S_{21}^2 + 1}{2S_{11}} \quad (\text{B.10})$$

$$T = \frac{S_{11} - S_{21} - \Gamma}{1 - (S_{11} + S_{21})\Gamma} \quad (\text{B.11})$$

In equation B.9, the plus or minus sign is chosen such that  $|\Gamma| < 1$ . Using equation

B.10, the complex propagation constant  $\gamma$  is given by following equation.

$$\gamma = [\log_e(1/T)]/d \quad (\text{B.12})$$

From equations B.5 and B.8, we get following equation.

$$\sqrt{\frac{\mu_r}{\epsilon_r}} = \frac{1 + \Gamma}{1 - \Gamma} \quad (\text{B.13})$$

From equations B.7 and B.13, we get following equations.

$$\epsilon_r = \frac{\gamma}{\gamma_0} \left( \frac{1 - \Gamma}{1 + \Gamma} \right) \quad (\text{B.14})$$

$$\mu_r = \frac{\gamma}{\gamma_0} \left( \frac{1 + \Gamma}{1 - \Gamma} \right) \quad (\text{B.15})$$

Since the parameter T in equation B.12 is a complex number, there are multiple values for  $\gamma$ . If T is defined by the following equation.

$$T = |T|e^{j\phi} \quad (\text{B.16})$$

Then,  $\gamma$  is given by;

$$\gamma = [\log_e(1/|T|)]/d + j \left[ \frac{2\pi n - \phi}{d} \right] \quad (\text{B.17})$$

Where  $n = 0 \pm 1, \pm 2 \dots$

The real part of  $\gamma$  is unique and single valued, but the imaginary part of  $\gamma$  has multiple values. So, equation B.14 and equation B.15 will give multiple values of  $\epsilon_r$  and  $\mu_r$ . The phase constant  $\beta$  is as given below.

$$\beta = (2\lambda/\lambda_m) = \text{imaginary part}(\gamma) \quad (\text{B.18})$$

Where  $\lambda_m$  is the wavelength in CISR sheet. From equations B.17 and B.18,

$$d/\lambda_m = n - \frac{\phi}{2\pi} \quad (\text{B.19})$$

For  $n = 0$  and  $-2\pi < \phi < 0$ ,  $(d/\lambda_m)$  is between 0 and 1. If the CISR sheet thickness  $d$  is chosen such that it is less than  $\lambda_m$ , then equation B.9 - B.15 will give a unique value of  $\epsilon_r$  and  $\mu_r$  which corresponds to  $n = 0$ . For  $d > \lambda_m$ , ambiguity in  $\epsilon_r$  and  $\mu_r$  can be resolved by making measurements on two different thicknesses of CISR sheets. In case of flexible CISR sheets, the accuracy of free-space measurement of  $S_{11}$  and  $S_{21}$  is poor because of sagging. For thin and flexible CISR sheets, they are sandwiched between two Teflon sheets. These Teflon sheets are quarter wavelength at mid-band for impedance matching. Thickness of Teflon sheets ( $d_q$ ) are 7.4 mm and 10.3 mm for WR-137 and WR-187 waveguide bands, respectively [2,3]. Schematic diagram of Teflon sheet-CISR sheet-Teflon sheet assembly is shown in Figures B.2.

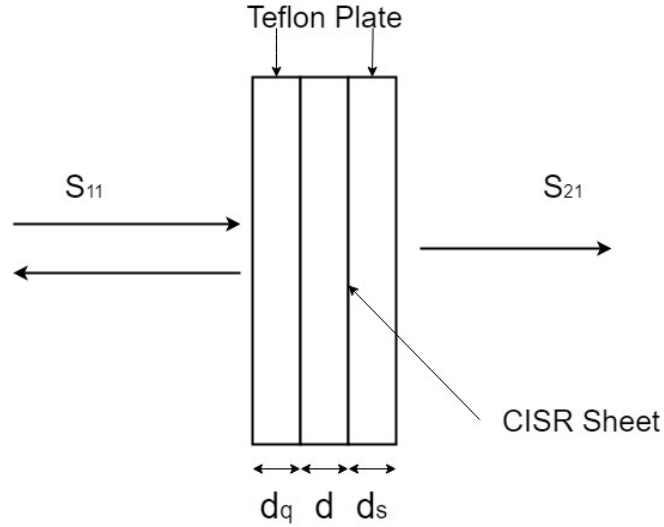


Figure B.2: Schematic diagram of Teflon sheet-CISR sheet-Teflon sheet assembly

Parameters  $S_{11a}$  and  $S_{21a}$  of the Teflon sheet-CISR sheet-Teflon sheet assembly are measured in free space.  $S_{11}$  and  $S_{21}$  of the CISR sheet can be calculated from  $S_{11a}$  and  $S_{21a}$  of assembly. Because of symmetry of the assembly and the reciprocal nature of the CISR sheet,  $S_{11a} = S_{22a}$  and  $S_{21a} = S_{12a}$ . The ABCD matrix  $[A^a]$  of the assembly is given by following equation.

$$[A^a] = \begin{bmatrix} A^a & B^a \\ C^a & D^a \end{bmatrix} = \begin{bmatrix} (1 - S_{11a}^2) + S_{21a}^2 & (1 + S_{11a})^2 - S_{21a}^2 \\ (1 - S_{11a})^2 - S_{21a}^2 & (1 - S_{11a}^2) + S_{21a}^2 \end{bmatrix} \frac{1}{S_{21a}} \quad (\text{B.20})$$

From  $\epsilon_r$ , and  $d_q$  of Teflon sheets, the ABCD matrix is given by the following equation.

$$[A^q] = \begin{bmatrix} A^q & B^q \\ C^q & D^q \end{bmatrix} = \begin{bmatrix} \cosh(\gamma_q d_q) & Z_q \sinh(\gamma_q d_q) \\ \sinh(\gamma_q d_q) / Z_q & \cosh(\gamma_q d_q) \end{bmatrix} \quad (\text{B.21})$$

where  $\gamma_q$  is the propagation constant in Teflon sheet which is defined as,

$$\gamma_q = j(2\pi\sqrt{\epsilon_r\mu_r}) / \lambda_0 \quad (\text{B.22})$$

Where  $\lambda_0$  represents the free-space wavelength and  $Z_q$  is the normalized characteristic impedance of Teflon sheet.

If the ABCD matrix of the CISR sheet is denoted by  $[A^s]$ , then the relationship between  $[A^a]$  and  $[A^s]$  is given by the following matrix equations.

$$[A^a] = [A^q][A^s][A^q] \quad (\text{B.23})$$

or

$$[A^s] = [A^q]^{-1}[A^a][A^q]^{-1} \quad (\text{B.24})$$

Parameters  $S_{11}$  and  $S_{21}$ , of the CISR sheet are given by following expressions.

$$S_{11} = \frac{A^s + B^s - C^s - D^s}{A^s + B^s + C^s + D^s} \quad (\text{B.25})$$

$$S_{21} = \frac{2}{A^s + B^s + C^s + D^s} \quad (\text{B.26})$$

## Matlab Code the for NRW method

```
1  clc;
2  clear all;
3  close all;
4  t=input('Thickness in mm');
5  d=t.*1e-3;
6  cvs1=csvread('magnitude.CSV');
7  fr0=cvs1(:,1);
8  S11_dB=-cvs1(:,2);
9  S11_phase=cvs1(:,3);
10 cvs2=csvread('MAGNITUDES21.CSV');
11 S21_dB=-cvs2(:,2);
12 S21_phase=cvs2(:,3);
13 fr0=fr0.*1e9;
14 c=3e8;
15 lambda_0=c./fr0;
16 gamma_0=0+j*2.*pi./lambda_0;
17 %% Convert db and phase to magnitude and radian
18
19 mag_S11=db2mag(S11_dB);
20 pha_S11=deg2rad(S11_phase);
21 S11_ABS=mag_S11.*exp(j.*pha_S11);
22 mag_S21=db2mag(S21_dB);
23 pha_S21=deg2rad(S21_phase);
24 S21_ABS=mag_S21.*exp(j.*pha_S21);
25 S12=S21_ABS;
26 S22=S11_ABS;
27 %% Convert magnitude and radian into complex number
28 [x,y]=pol2cart(pha_S11,mag_S11);
29 Com_S11=x+j*y;
```

```

30 [a,b]=pol2cart(pha_S21,mag_S21);
31 Com_S21=a+j*b;
32 %% Calculate K
33 S11_2=Com_S11.^2;
34 S21_2=Com_S21.^2;
35 K=((S11_2-S21_2+1)./(2*Com_S11));
36 %% Calculate Gamma
37 K_2=K.^2;
38 GM_1=K+sqrt(K_2-1);
39 GM_2=K-sqrt(K_2-1);
40 if abs(GM_1)<1
41     GM_1=GM_1;
42 else
43     GM_1=GM_2;
44 end
45 %% Calculate Tee
46 Tee=((Com_S11+Com_S21-GM_1)./(1-((Com_S11+Com_S21).*GM_1)));
47 Tee_mag=abs(Tee);
48 Tee_ang=angle(Tee);
49 %% Calculate propogation constant
50 gamma=((log(1./Tee_mag))-j*(Tee_ang));
51 gamma=gamma./d;
52 s=((1-GM_1)./(1+GM_1));
53 epsilon=(gamma./gamma_0).*s;
54 mu=(gamma./gamma_0)./s;
55 input=[fr0/1e9 real(epsilon) -imag(epsilon) real(mu) ...
        -imag(mu)];
56 csvwrite('FSS_DATA.csv',input)
57 %% Plot Comman
58 figure(1)
59 q=plot(fr0,real(epsilon),'linewidth',2,'color','r')

```



```

60 xlabel('Frequency')
61 ylabel('Real part of Permittivity')
62 axis ([3.95e9 8.2e9 -200 200]);
63 grid on;
64 saveas(gcf, 'FSS_er.jpg')
65 figure(2)
66 r=plot(fr0,-imag(epsilon),'linewidth',2,'color','b')
67 xlabel('Frequency')
68 ylabel('Imaginary part of Permittivity')
69 axis([3.95e9 8.2e9 -200 300])
70 grid on;
71 saveas(gcf, 'FSS_er2.jpg')
72 figure(3)
73 s=plot(fr0,real(mu),'linewidth',2,'color','g')
74 xlabel('Frequency')
75 ylabel('Real part of Permeability')
76 axis([3.95e9 8.2e9 -10 10]);
77 grid on;
78 saveas(gcf, 'FSS_mu.jpg');
79 figure(4)
80 t=plot(fr0,-imag(mu),'linewidth',2,'color','black')
81 xlabel('Frequency')
82 ylabel('Imaginary part of Permeability')
83 axis([3.95e9 8.2e9 -10 10]);
84 grid on;
85 saveas(gcf, 'FSS_mu2.jpg');
86 t=plot(fr0,real(epsilon),fr0,-imag(epsilon),fr0,real(mu),fr0,-imag(m

```

## References

- [1] D. K. Ghodgaonkar, V. V. Varadan and V. K. Varadan, "Free-space measurement of complex permittivity and complex permeability of magnetic materials at microwave frequencies," *IEEE Transactions on Instrumentation and Measurement*, vol. 39, no. 2, pp. 387-394, April 1990, doi: 10.1109/19.52520.
- [2] R. Vashisth, D. Ghodgaonkar and S. Gupta, "Permittivity and Permeability Measurements of CISR sheets for Microwave Absorber Applications," *2018 IEEE International RF and Microwave Conference (RFM)*, Penang, Malaysia, 2018, pp. 359-362.
- [3] R. Vashisth, D. Ghodgaonkar and S. Gupta, "Design and Fabrication of Broadband Microwave Absorber using FSS embedded in CISR sheets," *2018 IEEE MTT-S International Microwave and RF Conference (IMaRC)*, Kolkata, India, 2018, pp. 1-4.

## Appendix C

### NRL Arch Method (1 to 8.2 GHz)

NRL arch method is the industry standard for testing the reflectivity of materials [1,2]. Originally designed at the Naval Research Laboratory, the NRL Arch method, allows for quick, repeatable non-destructive testing of microwave absorbent materials over a wide frequency range. Reflectivity is defined as the reduction in reflected power caused by the introduction of an absorbent material. This reduction in power is compared to a ‘perfect’ reflection which is approximated very well by the reflection off a flat metallic plate [1].

The measurement system for NRL arch method consists of two double ridge horn antennas, coaxial cables, wooden board, two stands and vector network analyser (Rohde & Schwarz ZVA 40 with operating frequency range from 40 MHz to 40 GHz) [3]. These double ridge horn antenna are ETS-Lindgren, Model No. 3115 [4]. The bandwidth of antennas is 750 MHz to 18 GHz, with gains of 5 dB, 7.5 dB and 8.2 dB at 1 GHz, 4 GHz and 8 GHz, respectively. The half power beam widths in E-plane are 90°, 40° and 47° at 1 GHz, 4 GHz and 8 GHz, respectively. The half power beam widths in H-plane are 70°, 60° and 34° at 1 GHz, 4 GHz and 8 GHz, respectively. The aperture dimensions of the antenna are 15.9 *cm* × 24.4 *cm*. The wooden boards are used to hold microwave absorber sheets of cross sections 1 *foot* × 1 *foot* and 2 *feet* × 2 *feet*. The height of wooden boards are 4 *feet*. The distance between double ridge horn antenna and wooden board is 2.5 meter which will ensure far field operation in 1 to 8.2 GHz range. The measurement system is located in anechoic chamber to avoid multiple reflections as shown in Figure C.1. The measurement procedure is as follows.

1. Perform SOLT calibration of network analyzer till ends of two coaxial cables.

2. After connecting coaxial cables to two horn antennas, height of antenna on tripods are adjusted to 4 feet.
3. The angle between two antenna beams of horn antennas are kept close to  $0^\circ$  for normal incidence.
4. Time domain gating on VNA is used to eliminate multiple reflections and cross talk between antennas.
5. Mount  $1 \text{ foot} \times 1 \text{ foot}$  or  $2 \text{ feet} \times 2 \text{ feet}$  metallic plate on the wooden board. Record  $S_{21}$  in dB of metal plate as shown in Figure C.2.
6. Mount microwave absorber on the metallic plate. Record  $S_{21}$  in dB as shown in Figure C.2.
7. Reflectivity of microwave absorber at normal incidences (or oblique incidence) is calculated by subtracting microwave absorber readings from metallic plate readings.
8. Angle between two horn antennas are adjusted to  $10^\circ$  or  $20^\circ$  for oblique incident measurement. Perform step 4 to 7 for oblique incidence.

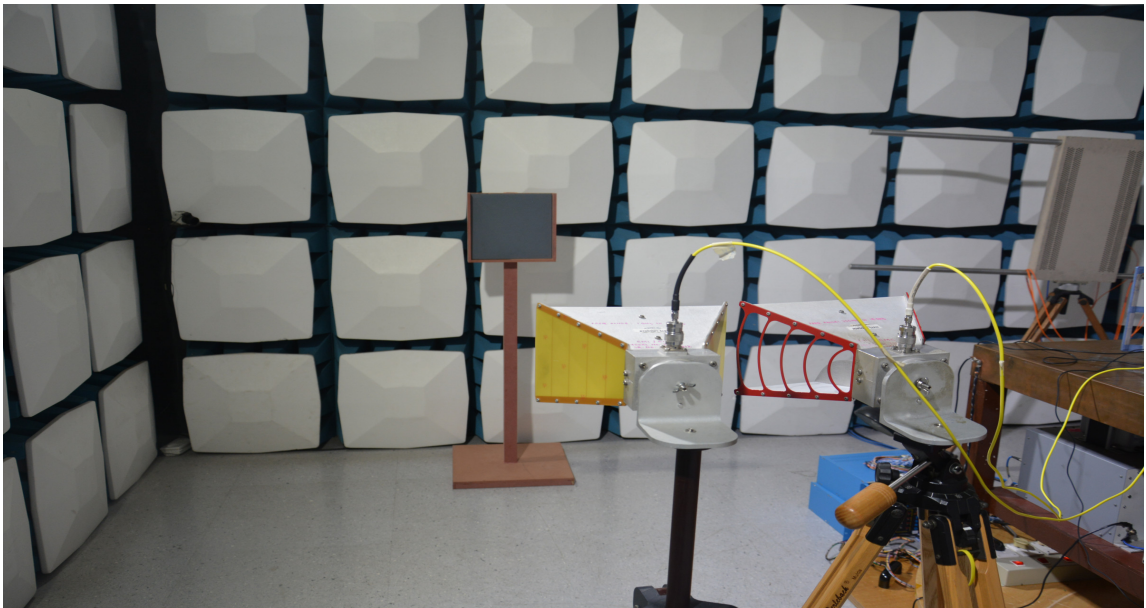


Figure C.1: Measurement system for NRL arch method

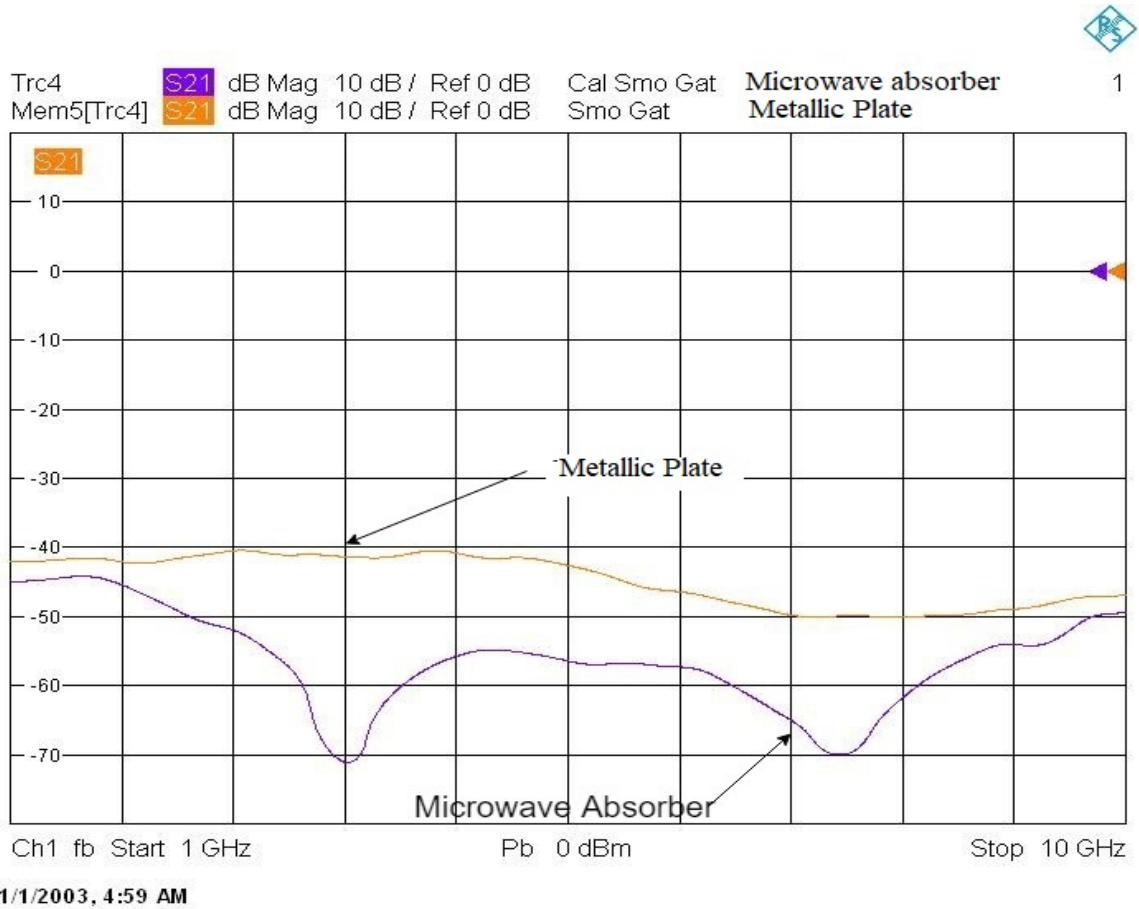



Figure C.2:  $S_{21}$  of metallic plate and microwave absorber.

## References

- [1] W. Hofmann, C. Bornkessel, A. Schwind and M. A. Hein, "Challenges of RF Absorber Characterization: Comparison Between RCS- and NRL-Arch-Methods," *2019 International Symposium on Electromagnetic Compatibility-EMC EUROPE.2019*:pp. 370-375.
- [2] M. Franchitto, R. Faez, A. J. F. Orlando, M. C. Rezende and I. M. Martin, "Electromagnetic behavior of radar absorbing materials based on conducting polymers," *Proceedings of the 2001 SBMO/IEEE MTT-S International Microwave and Optoelectronics Conference. (Cat. No.01TH8568)*, 2001, pp. 137-140 vol.1, doi: 10.1109/SBMOMO.2001.1008736.
- [3] <https://www.rohde-schwarz.com/us/products/test-and-measurement/network-analyzers/rs-zva-vector-network-analyzer63493-9660.html>.
- [4] <http://www.ets-lindgren.com/datasheet/antennas/double-ridged-guide/4002/400203>.

# Appendix D

## BASF CN Germany

Product specification		Inorganic Specialities	 The Chemical Company
CAS-CEPCN-E Revision 3	2005-02-18 Page 1 of 1		
supersedes:RCA-CEPCN-E, Rev.2	dated 2000-04-13		
© = registered trademark of BASF Aktiengesellschaft			

### CARBONYL IRON POWDER CN

PRD-No.: 30042255

#### 1. General

This product is produced and marketed by BASF AG, Ludwigshafen, Germany. The units producing and marketing this product are certified according to ISO 9001:2000.

Appearance: grey, fine grained powder, with mechanically soft, spherical particles  
 Description: Iron, Fe  
 CAS-Nr: 7439-89-6  
 EINECS-Nr: 231-096-4

#### 2. Properties

Property	Unit	Limit	Test Method
Fe	g / 100 g	min. 99.5	calculated
C	g / 100 g	max. 0.04	IRS (RCA/Q-C 296)
N	g / 100 g	max. 0.01	TCD (RCA/Q-C295)
O	g / 100 g	max. 0.3	IRS (RCA/Q-C 295)
Tap density	g / cm <sup>3</sup>	3.5 – 4.1	ASTM B 527 (analog)
Particle size distribution:			
D <sub>10</sub>	µm	max. 4.0	Microtrac X100
D <sub>50</sub>	µm	max. 8.0	Microtrac X100
D <sub>90</sub>	µm	max. 25	Microtrac X100

The aforementioned data shall constitute the agreed contractual quality of the product at the time of passing of risk. The data are controlled at regular intervals as part of our quality assurance program. Neither these data nor the properties of product specimens shall imply any legally binding guarantee of certain properties or of fitness for a specific purpose. No liability of ours can be derived therefrom.

more information? Please visit us at [www.carbonylironpowder.com](http://www.carbonylironpowder.com)

## References

- [1] <https://aerospace.basf.com/carbonyl-iron-powder.html>



## Appendix E

# Matlab Code for Calculation of Reflectivity of Multilayer Microwave Absorbers

```
1 clear all;
2 clc;
3 a1=csvread('50IIW_DATA.csv');
4 a2=csvread('0%.csv');
5 freq=a1(:,1).*1e9;
6 theta(:,1)=[0;10;20;30;40];
7 t1=1.4e-3;
8 t2=7.35e-3;
9
10 %%
11 er(:,1)=a1(:,2)-j.*a1(:,3);
12 mu(:,1)=a1(:,4)-j.*a1(:,5);
13 mu(:,2)=a2(:,4)-j.*a2(:,5);
14 er(:,2)=a2(:,2)-j.*a2(:,3);
15 er(:,3)=1-j.*0;
16 mu(:,3)=1-j.*0;
17 %%
18 z(:,1)=120.*pi.*sqrt(mu(:,1)./er(:,1));
19 z(:,2)=120.*pi.*sqrt(mu(:,2)./er(:,2));
20
```

```

21 c0=3e8;
22 z(:,3)=120.*pi;
23 %%
24
25 gamma1(:,3)=...
26     j.*2.*pi.*freq.*sqrt(er(:,3).*mu(:,3)).*cosd(0)./c0;
27
28 %%
29 for k=2:-1:1;
30 thet1(:,k)= ...
31     asind((mu(:,k+1).*z(:,k)).*sind(0)./(mu(:,k).*z(:,k+1))));
32
33 thet2(:,k)= ...
34     asind((mu(:,k+1).*z(:,k)).*sind(10)./(mu(:,k).*z(:,k+1))));
35
36 thet3(:,k)= ...
37     asind((mu(:,k+1).*z(:,k)).*sind(20)./(mu(:,k).*z(:,k+1))));
38
39 thet4(:,k)= ...
40     asind((mu(:,k+1).*z(:,k)).*sind(30)./(mu(:,k).*z(:,k+1))));
41
42 thet5(:,k)= ...
43     asind((mu(:,k+1).*z(:,k)).*sind(40)./(mu(:,k).*z(:,k+1))));
44
45 %% TE
46 zout1(:,k)=z(:,k)./cosd(thet1(:,k));

```

```

47 zout2(:,k)=z(:,k)./cosd(thet2(:,k));
48 zout3(:,k)=z(:,k)./cosd(thet3(:,k));
49 zout4(:,k)=z(:,k)./cosd(thet4(:,k));
50 zout5(:,k)=z(:,k)./cosd(thet5(:,k));
51
52 %% TM
53 zout6(:,k)=z(:,k).*cosd(thet1(:,k));
54 zout7(:,k)=z(:,k).*cosd(thet2(:,k));
55 zout8(:,k)=z(:,k).*cosd(thet3(:,k));
56 zout9(:,k)=z(:,k).*cosd(thet4(:,k));
57 zout10(:,k)=z(:,k).*cosd(thet5(:,k));
58
59
60 gamma1(:,k)=j.*2.*pi.*freq.*sqrt(er(:,k).*mu(:,k))./c0;
61 gamma1(:,k)=gamma1(:,k).*cosd(thet1(:,k));
62 gamma2(:,k)=j.*2.*pi.*freq.*sqrt(er(:,k).*mu(:,k))./c0;
63 gamma2(:,k)=gamma2(:,k).*cosd(thet2(:,k));
64 gamma3(:,k)=j.*2.*pi.*freq.*sqrt(er(:,k).*mu(:,k))./c0;
65 gamma3(:,k)=gamma3(:,k).*cosd(thet3(:,k));
66 gamma4(:,k)=j.*2.*pi.*freq.*sqrt(er(:,k).*mu(:,k))./c0;
67 gamma4(:,k)=gamma4(:,k).*cosd(thet4(:,k));
68 gamma5(:,k)=j.*2.*pi.*freq.*sqrt(er(:,k).*mu(:,k))./c0;
69 gamma5(:,k)=gamma5(:,k).*cosd(thet5(:,1));
70 end
71
72 zin1=zout1(:,1).*tanh(gamma1(:,1)*t1);
73 zin2=zout1(:,2).*((zin1+zout1(:,2).*tanh(gamma1(:,2).*t2))....
74 ./(zout1(:,2)+zin1.*tanh(gamma1(:,2).*t2)));
75
76 zin=(zin2-377)./(zin2+377);
77 zin=abs(zin);

```

```

78         db_1=20.*(log10(zin));
79
80
81 zin1=zout2(:,1).*tanh(gamma2(:,1)*t1);
82 zin2=zout2(:,2).*((zin1+zout2(:,2).*tanh(gamma2(:,2).*t2))...
83         ./(zout2(:,2)+zin1.*tanh(gamma2(:,2).*t2)));
84
85         zin=(zin2-377)./(zin2+377);
86         zin=abs(zin);
87         db_2=20.*(log10(zin));
88
89
90
91 zin1=zout3(:,1).*tanh(gamma3(:,1)*t1);
92 zin2=zout3(:,2).*((zin1+zout3(:,2).*tanh(gamma3(:,2).*t2))...
93         ./(zout3(:,2)+zin1.*tanh(gamma3(:,2).*t2)));
94
95         zin=(zin2-377)./(zin2+377);
96         zin=abs(zin);
97         db_3=20.*(log10(zin));
98
99
100
101 zin1=zout4(:,1).*tanh(gamma4(:,1)*t1);
102 zin2=zout4(:,2).*((zin1+zout4(:,2).*tanh(gamma4(:,2).*t2))...
103         ./(zout4(:,2)+zin1.*tanh(gamma4(:,2).*t2)));
104
105         zin=(zin2-377)./(zin2+377);
106         zin=abs(zin);
107         db_4=20.*(log10(zin));
108

```

```

109 zin1=zout5(:,1).*tanh(gamma5(:,1)*t1);
110 zin2=zout5(:,2).*((zin1+zout5(:,2).*tanh(gamma5(:,2).*t2))...
111         ./(zout5(:,2)+zin1.*tanh(gamma5(:,2).*t2)));
112
113         zin=(zin2-377)./(zin2+377);
114         zin=abs(zin);
115         db_5=20.*(log10(zin));
116
117 zin1=zout6(:,1).*tanh(gamma1(:,1)*t1);
118 zin2=zout6(:,2).*((zin1+zout1(:,2).*tanh(gamma1(:,2).*t2))...
119         ./(zout6(:,2)+zin1.*tanh(gamma1(:,2).*t2)));
120
121         zin=(zin2-377)./(zin2+377);
122         zin=abs(zin);
123         db_6=20.*(log10(zin));
124
125 zin1=zout7(:,1).*tanh(gamma2(:,1)*t1);
126 zin2=zout7(:,2).*((zin1+zout2(:,2).*tanh(gamma2(:,2).*t2))...
127         ./(zout7(:,2)+zin1.*tanh(gamma2(:,2).*t2)));
128
129         zin=(zin2-377)./(zin2+377);
130         zin=abs(zin);
131         db_7=20.*(log10(zin));
132
133 zin1=zout8(:,1).*tanh(gamma3(:,1)*t1);
134 zin2=zout8(:,2).*((zin1+zout8(:,2).*tanh(gamma3(:,2).*t2))...
135         ./(zout8(:,2)+zin1.*tanh(gamma3(:,2).*t2)));
136
137         zin=(zin2-377)./(zin2+377);
138         zin=abs(zin);
139         db_8=20.*(log10(zin));

```

```

140 zin1=zout9(:,1).*tanh(gamma4(:,1)*t1);
141 zin2=zout9(:,2).*((zin1+zout9(:,2).*tanh(gamma4(:,2).*t2))...
142         ./(zout9(:,2)+zin1.*tanh(gamma4(:,2).*t2)));
143
144         zin=(zin2-377)./(zin2+377);
145         zin=abs(zin);
146         db_9=20.*(log10(zin));
147
148 zin1=zout10(:,1).*tanh(gamma5(:,1)*t1);
149 zin2=zout10(:,2).*((zin1+zout5(:,2).*tanh(gamma5(:,2).*t2))...
150         ./(zout10(:,2)+zin1.*tanh(gamma5(:,2).*t2)));
151
152         zin=(zin2-377)./(zin2+377);
153         zin=abs(zin);
154         db_10=20.*(log10(zin));
155
156
157 figure(1)
158 plot(freq./1e9,db_1,freq./1e9,db_2,freq./1e9,...
159       db_3,freq./1e9,db_4,freq./1e9,db_5,'linewidth',3);
160 grid on;
161 figure(2)
162
163 plot(freq./1e9,db_6,freq./1e9,db_7,freq./1e9,...
164       db_8,freq./1e9,db_9,freq./1e9,db_10,'linewidth',3);
165 grid on;

```

# List of Publications

## International Journal

1. Vashisth Rahul, Ghodgaonkar Deepak, Gupta Sanjeev, " Broadband Microwave Absorber using Pixelated FSS Embedded in CISR Sheets in Frequency Range of 3.95 to 8.2 GHz". *Journal of Electromagnetic Waves and Applications*, Taylor & Francis, 1569-3937. doi: 10.1080/09205071.2021.1947899

## International Conference Proceedings

1. R. Vashisth, D. Ghodgaonkar and S. Gupta, "Permittivity and Permeability Measurements of CISR sheets for Microwave Absorber Applications," 2018 IEEE International RF and Microwave Conference (RFM), Penang, Malaysia, 2018, pp. 359-362.
2. R. Vashisth, D. Ghodgaonkar and S. Gupta, "Design and Fabrication of Broadband Microwave Absorber using FSS embedded in CISR sheets," 2018 IEEE MTT-S International Microwave and RF Conference (IMaRC), Kolkata, India, 2018, pp. 1-4.

## Articles under preparation

- Rahul Vashisth, Deepak Ghodgaonkar and Sanjeev Gupta, "Design and fabrication of broadband microwave absorber using CISR sheets in 2.5 to 8.2 GHz range," Submitted to Wireless, Antenna and Microwave Symposium, 2022 Conference, NIT Raurkela, India.